PROBABILISTIC SEISMIC DEMAND ANALYSIS

FOR THE NEAR-FAULT ZONE

By

REZA SEHHATI

A dissertation submitted in partial fulfillment of

the requirements for the degree of

DOCTOR OF PHILOSOPHY

WASHINGTON STATE UNIVERSITY

Department of Civil & Environmental Engineering

DECEMBER 2008

To the Faculty of Washington State University:

The members of the Committee appointed to examine the dissertation of REZA SEHHATI find it satisfactory and recommend that it be accepted.

_____
Chair

_____

_____

_____

ACKNOWLEDGMENTS

This research was performed in the Department of Civil and Environmental Engineering at Washington State University, Pullman, Washington. Support for this work was provided by the United States DOT RITA UTC Program (contract number 07-G-0010) through Transportation Northwest (TRANSNOW) under budget number 430846.

Sincere thanks to Dr. Adrian Rodriguez-Marek, the chair of my committee, for his invaluable guidance and financial support through this research efforts. Special thanks go to Dr. William F. Cofer, co-chair of the committee, for his helpful suggestions and supportive manner. I would also like to thank Dr. David McLean and Dr. Mohamed ElGawady for their participation and assistance by serving on my committee. I am also grateful for feedback from Dr. Daniel Dolan and Dr. David Pollock.

Probabilistic Seismic Demand Analysis for the Near-Fault Zone

Abstract

by Reza Sehhati, Ph.D.

Washington State University

December 2008

Chair: Dr. Adrian Rodriguez-Marek

Ground motions close to a fault can be significantly influenced by rupture directivity effects. In particular, the effects of forward-directivity may cause severe damage to buildings. These effects have not been clearly addressed in current building codes and engineers still lack specific guidelines as to how to account for forward-directivity effects when determining the seismic hazard for structures. A methodology for probabilistic seismic demand analysis that includes the effects of forward directivity through time domain analysis is proposed in this work. First, the characteristics of forward-directivity ground motions and the structural response to these motions are studied and simplified mathematical representations for pulse-type forward-directivity ground motions are proposed. Intensity Measures for forward directivity ground motions are then proposed based on the simplified pulses. For this purpose, the non-linear dynamic response of three generic multi-story shear buildings to near-fault and ordinary ground motion ensembles was studied using Incremental Dynamic Analysis. Results show that whenever the pulse period of forward-directivity ground motions is close to the first-mode structural period, structural response is controlled

by forward-directivity pulses. For these cases, structural response can be predicted using pulse-period and pulse-amplitude as intensity measures.

The principles of Probabilistic Seismic Demand Analysis are then extended to consider the effect of forward-directivity within a probabilistic framework. Structural response to pulse-type forward-directivity ground motions is quantified by means of time-domain analysis of simplified pulses that comprehensively represent all possible pulse-type ground motion scenarios. The hazard due to pulse-type motions is then coupled with conventional spectral domain seismic demand analyses for non-pulse-type ground motions. Results show that the proposed methodology captures more accurately the structural response to pulse-type ground motions than with current methods, leading to the prediction of greater hazard for near-fault scenarios. In addition, the proposed method provides a clear guide for the selection of time histories for the design of near-fault structures.

TABLE OF CONTENTS

LIST OF TABLES

LIST OF FIGURES

Dedication

This dissertation is dedicated to my mother who gave me guidelines for life.

"In generosity and helping others be like a river.

In compassion and grace be like sun.

In concealing others' faults be like night

In anger and fury be like dead.

In modesty and humility be like earth.

In tolerance be like a sea.

Either exist as you are or be as you look."

Maulana Jalalud-din Rumi

CHAPTER ONE

INTRODUCTION

1.1. Problem Statement

Modern seismic design philosophy as expressed in Performance-Based Seismic Design (PBSD) (SEAOC Vision 2000) targets a broader set of design objectives than those historically considered for structural systems. PBSD introduces a framework by which the owner of a structure may select from a range of target behavior levels and performance objectives and provides the means to confirm that a proposed structural design meets those objectives. As a result, the PBSD framework permits the design of civil structures for predictable and definable seismic performance within established risk levels. The Earthquake Performance Levels (or damage states) that PBSD considers range from "Fully Operational" to "Near Collapse"; the levels of risk it considers by means of Earthquake Design Levels range from "Frequent" to "Very Rare". To meet these performance targets at high risk levels, structures are allowed to deform nonlinearly. Hence, direct estimates of the inelastic response of structures are required. Moreover, it becomes necessary to provide alternative analysis and design procedures to achieve the prescribed seismic performance objectives. A tool that can aid engineers in assessing various analysis and design schemes is Probabilistic Seismic Demand Analysis. PSDA is built upon the more traditional Probabilistic Seismic Hazard Analysis and couples the probabilistic description of future ground motions from PSHA with their random dynamic effects on the structure. Results of PSDA provide the annual

likelihood of exceedance of engineering demand parameters, which in turn can be correlated to the annual probability of exceedance of different Performance Levels, which in turn are correlated to Earthquake Design Levels considered by PBSD.

This dissertation addresses the problem of incorporating PSDA principles to analysis of structures located in the vicinity of active faults. Near-fault ground motions are largely affected by finite source effects. In particular, ground motions in the near-fault affected by forward-directivity effects exhibit distinct velocity pulses at the beginning of time history records. These pulses, in turn, may result in high seismic demands; hence, the design or retrofit of structures that are in the proximity of an active fault must consider the effects of forward-directivity pulses. Recent research has addressed the seismological aspects of fault mechanisms leading to forward-directivity, the characteristics of pulse-like ground motions (Somerville et al. 1997; Spudich and Chiou 2008), and structural response to these motions (Hall 1998; Mylonakis and Reinhorn 2001; Zhang and Iwan 2002). However, designers still lack specific guidelines as to how to account for forward-directivity effects when determining the seismic hazard for a given structure. The overall goal of this research project is to develop PSDA for structures in near-fault zones and include the effects of forward-directivity into the determination of seismic demand for a structure. This work will improve seismic hazard analyses and design of near-fault structures by introducing effective IMs, and by proposing a rigorous method to link the IMs to Engineering Demand Parameters (EDP) for structures affected by near-fault ground motions.

1.2. Background

Near-fault ground motions, defined as those recorded within a distance of about 20 km from the ruptured fault, may be significantly different from those observed further away from the seismic source. In particular, near-fault ground motions affected by rupture directivity effects are characterized by large, long-period pulses at the beginning of the time history. These forward-directivity pulses are observed more clearly in the velocity time history. Pulse-like ground motions impose significant demand to structures and cause large inelastic drift, resulting in significant permanent deformations (Hall et al. 1995; Bertero et al. 1978; Hall 1998; Alavi and Krawinkler 2004a).

During an earthquake, fault rupture propagates at a relatively constant velocity, and as rupture progresses it generates a shear wave front, (Figure 1-1). If the velocity of rupture propagation approaches the shear wave velocity, the shear waves traveling ahead of the rupture are reinforced and their amplitude increases rapidly (see Figure 1-2). This is the case for most earthquakes, where the rupture velocity is usually 70 to 80% of the shear wave velocity (an exception would be earthquakes where super-shear rupture was observed, as discussed by Bouchon and Vallee (2003). Overlapping of pulses can lead to strong directivity pulses at sites toward which the fault ruptures (Figures 1-1 and 1-2). This phenomenon, called forward rupture directivity or simply forward-directivity, occurs when the direction of slip on the fault is aligned with the site and the rupture front propagates toward the site. When forward rupture directivity conditions are met, the propagation of fault rupture toward a site at a velocity close to shear wave velocity causes most of the seismic energy from the

rupture to arrive in a large long-period pulse of motion that occurs at the beginning of the record (Somerville et al. 1997). The radiation pattern of the shear dislocation on the fault causes this large pulse of motion to be oriented in the direction perpendicular to the fault, causing the strike-normal ground motions to be larger than the strike-parallel ground motions at periods longer than about 0.5 sec (Somerville 2003). If the rupture propagates away from the site, backward directivity occurs. Backward directivity ground motions have lower amplitude and larger duration than their forward-directivity counterparts. Neutral-directivity occurs when the site is in front of the epicenter.

When forward-directivity effects are present, the fault-normal and fault-parallel components must be treated separately. In forward-directivity ground motions, strike-normal ground motions are associated with a reversing displacement in the direction normal to the fault. In contrast, strike-parallel ground motions are associated with permanent displacement in the direction parallel to the fault which sometimes is called the "Fling-step". The Fling-step is the result of residual ground displacement due to tectonic deformation associated with the rupture mechanism. The Fling-step occurs in the direction of fault slip (Somerville et al. 1997). In strike-slip faults, the Fling-step occurs in the strike-parallel direction, as in the Kocaeli and Duzce earthquakes (Kalkan and Kunnath 2006). On the other hand, in dip-slip faults a component of the Fling-step is observed in the strike-normal direction of the horizontal component, as in the Chi-Chi earthquake (Mavroeidis and Papageorgiou 2003). The permanent displacements resulting from the Fling Step are generally of little consequence to structures because they occur slowly, the exception being if a structure

straddles the fault (Hall et al. 1995) or the structure has an extremely long fundamental period.

In the case of a strike-slip fault, forward-directivity occurs in regions away from the hypocenter and is stronger near the end of the fault that is located away from the hypocenter. On the other hand, in dip-slip faults the alignment of both the rupture direction and the slip direction up-dip on the fault plane produces rupture directivity effects at sites located around the surface exposure of the fault (or its up-dip projection if it does not break the surface). Unlike the case for strike-slip faulting, where forward rupture directivity effects occur at all locations along the fault away from the hypocenter, dip-slip faulting produces directivity effects on the ground surface that are most concentrated in a limited region up-dip from the hypocenter (Somerville et al. 1997).

In brief, the differences between pulse-like forward-directivity and ordinary ground motions can be summarized as the followings:

- The velocity-time histories of pulse-like ground motions initiate with long period pulses.
- Near-fault ground motions containing forward-directivity pulses have higher Peak Ground Velocity (PGV).

- The spectral accelerations of pulse-like ground motions are higher within a period band centered on the period of the forward-directivity pulses (ranging from 0.6 sec to upwards of 5 sec).

- Duration of near-fault ground motions is shorter.

With the exception of the last item, all other particularities of pulse-like ground motions imply that they are more destructive and impose a larger demand on structures when compared to ordinary ground motions. Structures with the fundamental period close to the period of the forward-directivity pulse are more vulnerable to pulse-like ground motions. The forward-directivity pulse period has been found to be proportional to the earthquake magnitude, lengthening as the earthquake magnitude increases. Therefore, smaller magnitude earthquakes generate pulses with shorter period that normally are closer to the fundamental period of typical structures. The implication is that typical structures may be more vulnerable to forward-directivity pulses caused by smaller magnitude earthquakes. This contradicts conventional engineering intuition that directly correlates damage potential with earthquake magnitude.

Even though there is a consensus on the importance of forward-directivity effects, there are still questions about how they should be included into predictions of seismic hazard (e.g., see Travasarou et al. 2006). The current state of practice accounts for forward-directivity effects either by modifying response spectra or by the use of equivalent pulse models. The use of equivalent pulses is driven by research that indicates that structural response is

significantly influenced by the characteristics of the velocity-time history (Anderson and Bertero 1987; Hall et al. 1995; Alavi and Krawinkler 2000; Sasani and Bertero 2000; Mylonakis and Reinhorn 2001; Zhang and Iwan 2002) and equivalent pulse models are acceptable proxy for pulse-like motions. However, some researchers (Malhotra 1999; Chopra and Chintanapakdee 2001) indicate that modifications to the linear and nonlinear design spectra are enough to capture structural response to pulse-like ground motions.

In this study, the traditional approach to PSDA is modified to include the use of simplified pulses in the prediction of the EDPs. The proposed PSDA considers separately the contribution to hazard of ground motions with pulses and those without pulses, using a recently proposed model to predict the probability of pulse occurrence (Iervolino and Cornell 2008). Traditional analysis methodologies using response-spectra based fragility curves are used for ground motions without pulses. For ground motions that have a pulse an equivalent pulse model along with time-domain analyses are used to predict structural response. The parameters of the equivalent pulse model are determined using predictive relationships for pulse period and amplitude. The seismic hazard computed using the proposed PSDA is generally higher than that computed using traditional PSDA analysis, highlighting the importance of considering forward-directivity pulses for design.

1.3. Objectives

The goal of this study is to obtain explicit estimates of seismic demand for structures subjected to near-fault ground motions and explore the effect of forward-directivity on

seismic hazard. Probabilistic methods are utilized to include the effects of pulse-like ground motions on Intensity Measures (IMs) and Engineering Demand Parameters (EDPs). The novelty of the proposed approach lies on the use of equivalent pulses and time-domain analyses within the PSDA methodology. The outcome of the proposed methodology is a seismic hazard curve for an arbitrary EDP. The curve includes the effects of forward-directivity. This is achieved through a PSDA method that incorporates forward-directivity effects. The overall goal can be divided into the following objectives:

1. Define appropriate IMs for near-fault ground motion.

2. Develop an equivalent pulse model to represent the characteristics of pulse-like ground motions.

3. Use the equivalent pulse model to evaluate EDPs through Incremental Dynamic Analysis (IDA) for near-fault ground motions with dominant forward-directivity pulses.

4. Use statistical methods to correlate structural response obtained from the nonlinear time-history dynamic analyses to EDPs.

5. Incorporate the use of equivalent pulses into Probabilistic Seismic Demand Analysis for the selected EDPs.

6. Investigate shortcomings of the design of structures in near-fault zones based on the International Building Code (IBC 2006) and subsequently provide

recommendations to improve the design of structures subjected to pulse-like ground motions.

1.4. Dissertation Outline

This dissertation is divided into 5 chapters. Chapter 2 presents an extended review of Performance-Based Seismic Design, Intensity Measures, Engineering Demand Parameters, current literature on Forward-Directivity Ground Motions (FDGMs), and the use of simplified pulse representations for FDGMs. Chapter 2 also discusses available statistical methodologies to correlate EDPs to IMs.

In Chapter 3, the effects of forward-directivity near-fault ground motions on the response of three multi-story structures are studied and an equivalent pulse model to represent pulse-like ground motions is developed. Once it is proven that simplified pulse representations capture structural response accurately, these representations are used to compute EDPs as a function of pulse parameters.

In Chapter 4, a new PSDA model to include forward-directivity effects through time-domain analysis of structures is proposed. Chapter 4 is followed by an example which illustrates the procedure and shows the applicability and limitations of the proposed methodology. Finally, Chapter 5 addresses the shortcoming of the design procedures provided by building codes and recommends methods to improve design of structures subjected to near-fault ground motions.

1.5. Figures

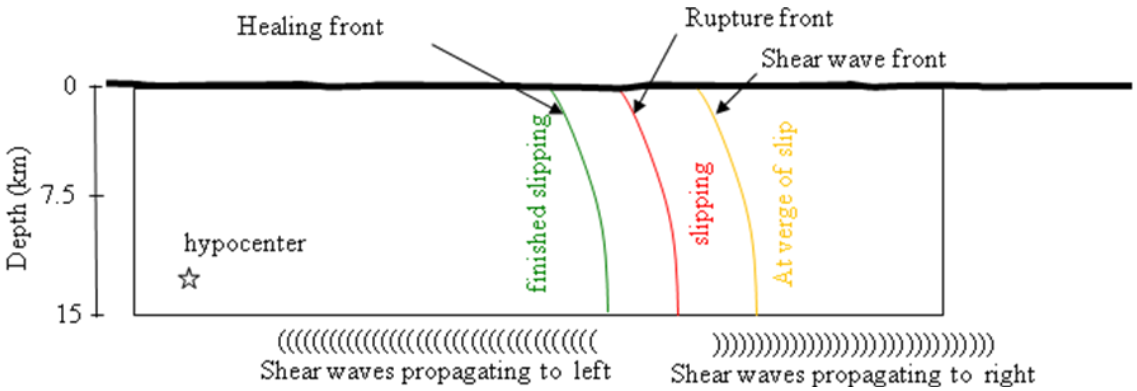

Figure 1-1: Schematic diagram of rupture directivity effects for a vertical strike-slip fault. The rupture begins at the hypocenter and spreads circularly at a speed that is about 80% of the shear wave velocity (modified from Somerville et al. 1997)

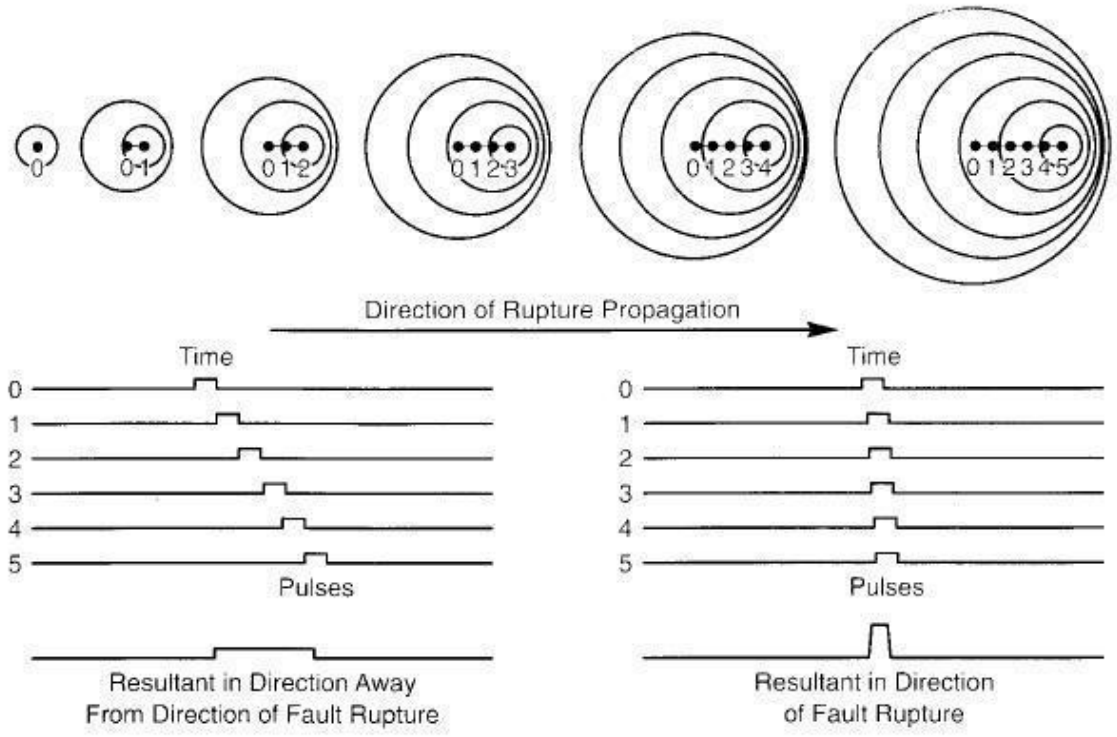

Figure 1-2: Schematic illustration of directivity effect on ground motions at sites toward and away from direction of fault rupture (Kramer 1996).

CHAPTER TWO

CURRENT STATE OF THE PRACTICE

Various methods have been proposed to include the effects of forward-directivity in seismic analysis. Most of these methods increase the level of the conventional Intensity Measure (e.g. elastic response spectra) to account for forward-directivity effects. This raises a fundamental question: Is the conventional Intensity Measure a proper representation of the near-fault ground motion with forward-directivity pulses? The following sections introduce the current state of practice in order to consider this question in context.

2.1. Performance-Based Earthquake Engineering

Current codes do not evaluate a building's performance after the onset of damage. Instead, they require compliance with a minimum safety standard by specifying a design which historically has protected life safety in earthquakes. Conversely, what is called Performance-Based Earthquake Engineering in the Pacific Earthquake Engineering Research Center (PEER 1999) and Performance-Based Seismic Design in FEMA-273 (1997) is a methodology that provides a means to more reliably predict seismic risk in all buildings in terms more useful to building users. PBSD employs the concept of performance objectives, which is the specification of an acceptable level of damage to a building if it experiences an earthquake of a given severity. Therefore, the specific objectives of engineering assessment analyses are in effect quantities such as the mean annual frequency (MAF) of the loss exceeding x dollars, or such as the MAF of collapse or any other variables. These can only be estimated probabilistically. Once hazard curves for structural response are provided, the results can be used to make decisions about the adequacy of a design or the need to retrofit.

The first generation of performance-based earthquake engineering (PBEE-1) assessment and design procedures for buildings in the United States (ATC-40 1996; FEMA-274 and Agency 1997) made important steps toward the implementation of performance-based earthquake engineering. These procedures, developed in the early to mid 1990s, conceptualized the problem that is illustrated in part of Figure 2-1. In this figure, a building is loaded by earthquake-induced lateral forces that produce nonlinear response (damage) in structural components. Relationships were established between structural response indices (inter-story drifts, plastic rotation demands, and member forces) and performance-oriented descriptions such as Immediate Occupancy (IO), Life Safety (LS) and Collapse Prevention (CP). Subsequently, performance evaluation of the structure can be associated with variables such as monetary losses, downtime, and casualty rate. Hamburger (2003) identified several well-accepted shortcomings with these first generation procedures, namely,

1. engineering demands were based on simplified analysis techniques, including static and linear analysis methods. Where dynamic or nonlinear methods were used, calibrations between calculated demands and component performance were largely lacking;

2. the defined relations between engineering demand and component performance were based somewhat inconsistently on relations measured in laboratory tests, calculated by analytical models, or assumed on the basis of engineering judgment. Consistent approaches based on relevant data are needed to produce reliable outcomes; and

3. structural performance was defined on the basis of component performance states. Structural system performance was assumed to be equal to the worst performance calculated for any component in the building.

The second generation of performance-based earthquake engineering assessment and design procedures (PBEE-2) were formed based on probability-based performance assessment tools (Cornell et al. 2002). The PBEE-2 process, illustrated in Figure 2-2, begins with the definition of one (or more) ground motion Intensity Measures that should capture the important characteristic(s) of earthquake ground motion that affect the response of the structural framing and nonstructural components and building contents. For building structures, the second step of the PBEE-2 process is to determine Engineering Demand Parameters that describe the response of the structure as a whole and of its individual structural components. This is accomplished by structural response simulations using earthquake ground motions scaled to predetermined IM levels. However, as described in Section 2.10, statistical methods can alternatively be used to accomplish the second step of the PBEE-2.

Next, the EDPs for the structural and nonstructural components and building contents are linked to Damage Measures (DMs) that describe the physical condition of those components and contents (such as permanent deformation, toppling of equipment, or cracking or spalling of material in structural components and architectural finishes). Damage Measures include effective descriptions of the damage state or condition, which are then used to estimate the effects on functionality, occupancy-readiness, life safety consequences and necessary repairs of or to the building including nonstructural components and systems. The

product of this step is a set of conditional probabilities, P[DM|EDP], which are then integrated with P[EDP] to calculate the occurrence frequency of DM, P[DM]. Thus, P[DM|EDP] is the probability that the engineering Damage Measures exceed specified values given (i.e., conditional on knowing) that the Engineering Damage Parameters (e.g., the maximum inter-story drift, and/or the vector of cumulative hysteretic energies in all elements) are equal to particular values.

The final step in the PBEE-2 process is the calculation of Decision Variables (DVs) that serve to translate damage estimates into quantities that are useful to those tasked with making risk-related decisions. The DVs under development at this time at PEER relate to one or more of the three decision metrics identified in Figure 2-2, namely, direct dollar losses, downtime (or restoration time), and deaths (casualties). The products of this step are conditional probabilities, P[DV|DM], which are then integrated with P[DM] to calculate the occurrence frequency of DV, P[DV]. Thus, P[DV|DM] is the probability that the (vector of) decision variable(s) exceed specified values given (i.e., conditional on knowing) that the engineering Damage Measures are equal to particular values. The PBEE-2 process can be expressed in terms of a triple integral that is an application of the total probability theorem (ATC-58 2004):

$$\lambda(DV) = \iiint P[DV \mid DM]dP[DM \mid EDP]dP[EDP \mid IM]\,|\,d\lambda[IM]\,| \tag{2-1}$$

where DV, DM, EDP, and IM are decision variable, damage measure, Engineering Demand Parameters, and Intensity Measure, respectively. P[X|Y] is the probability density of X conditioned on knowledge of Y. $d\lambda[IM]$ is mean annual frequency of IM.

However, discussion of DVs and DMs are beyond the scope of this study. Probabilistic evaluation of EDPs in terms of Intensity Measures which, in PEER is referred to as Probabilistic Seismic Demand Analysis is a prerequisite for the computation of Equation 2-1 and the seismic reliability of structures. PSDA is built upon the more traditional PSHA and couples the probabilistic description of future ground motions from PSHA with their random dynamic effects on a structure. Results of PSDA provide the annual likelihood of different Performance Levels for a given hazard (e.g. by defining performance in terms of structural response). To include the effects of forward-directivity into PSDA, the principle of PSHA has to be extended. The next section is allocated to explain the conventional PSHA and its modification for forward-directivity ground motions.

2.2. Probabilistic Seismic Hazard Analysis

Probabilistic Seismic Hazard Analysis is routine for important projects in seismically active areas to estimate the ground motion intensity that should be considered when assessing a structure's performance. In this approach, uncertainties in the size, location, and rate of recurrence of earthquakes as well as uncertainties in the variation of ground motion characteristics with earthquake size and location are explicitly considered in the evaluation of seismic hazards.

Forward-directivity effects either have been ignored in PSHA or treated semi-deterministically. There has been the belief that the ground motion increase due to forward-directivity events would be negated by ground motion decrease due to backward directivity events when rupture directivity effects are considered probabilistically. Disagreeing with this argument, Travasarou et al. (2006) quantified the degree of conservatism associated with the

semi-deterministic approach relative to explicit integration of directivity effects in probabilistic seismic hazard calculations. In the semi-deterministic approach, a deterministically estimated scaling factor is multiplied by the probabilistically estimated ground motions without directivity effects. The deterministic scaling factors are based on a severe forward-directivity scenario. Travasarou's results showed that directivity effects are most significant for critical structures that are designed for long return periods, sites located close to faults (e.g., < 5 to 15 km), and for sites located close to segmentation points along major faults when the adjacent fault is relatively active. Conversely, directivity effects may not be important for less critical facilities designed for shorter return periods (i.e. on the order of 72 to 100 years) even for active faults, and for critical structures located next to less active faults. Therefore, treating directivity effects semi-deterministically can lead to a considerable over prediction of the ground motion hazard. The degree of conservatism associated with the deterministic approach increases with decreasing return period.

Therefore, either ignoring the effects of directivity in PSHA or including its effects semi-deterministically causes inaccuracy in estimation of the hazard. To accurately estimate the hazard at near-fault sites, directivity should be directly included in the hazard analysis. Researchers have proposed different methods to include the rupture directivity effects in the conventional PSHA. A case of special vector-valued PSHA computation was developed by Tothong et al. (2007) which extended the principles of PSHA to incorporate the possible occurrence of a velocity pulse in a near-fault ground motion in terms of elastic spectral acceleration. In their procedure, the PSHA is separated into two parts; the non-near-source contribution and the near-source contribution expressed as:

$$\lambda_{IM}(y) = \lambda_{IM,non-NS}(y) + \lambda_{IM,NS}(y) \quad (2\text{-}2)$$

The first term is simply a conventional PSHA while the second contribution is separated further into effects due to the event of experiencing a pulse-like motion and that when a pulse is not present.

Many of these methods are based on a scalar IM such as that explained in the next section.

2.3. Scalar Intensity Measures

Ground motion Intensity Measures are parameters that capture the important characteristic(s) of the ground motion that affect the response of the structure. In the past, researchers used Peak Ground Acceleration (PGA) as an Intensity Measure to estimate the response of structures to a ground motion time history. Further studies showed that PGA alone is not enough to capture the effects of a ground motion on a structure. Within a ground motion time history, the amount of energy that each frequency carries is different and changes from one earthquake to another. Therefore, ground motion records with the same value of PGA can cause different structural responses. In other words, one specific record may be highly damaging for some structures and less severe for others of different periods. That is why PGA was found to be a poor response indicator. Therefore, elastic spectral quantities such as spectral acceleration of the first mode of the structure, $S_a(T_1)$, took precedence. Compared to PGA, the spectral quantities enhance the estimation of structural response. However, $S_a(T_1)$ alone fails to accurately describe the seismic demands of a multi-degree-of-freedom (MDOF) structure when the contribution of higher modes is significant

and, therefore, it cannot completely capture the dynamic behavior of structures. Similar to PGA, ground motion records with the same value of $S_a(T_1)$ may cause a considerable variability in the level of structural response of a MDOF structure, particularly when they are subjected to pulse-like ground motions. In a non-linear MDOF structure, the effective period of its first mode is increased to a period longer than the fundamental period. In this case, $S_a(T_1)$ is no longer an effective IM even if response is dominated by the first mode. In spite of these shortcoming, $S_a(T_1)$ still is one of the most commonly used IMs for non-pulse-like ground motions due to its simplicity and relative accuracy.

Currently, all seismic guidelines and codes specify seismic demand using the response spectrum for both ordinary and pulse-like ground motions. The design values are defined based on spectral acceleration of the first-mode period of vibration, $S_a(T_1)$, obtained from the design response spectrum. The design response spectrum defined by IBC does not consider the effects of rupture directivity. In Chapter 3, it will be discussed that $S_a(T_1)$ cannot be an efficient and sufficient IM for near-fault ground motions when forward-directivity pulses are dominant. But, for cases in which forward-directivity pulses are not dominant, $S_a(T_1)$ may still be used to predict the structural response.

It is important to note that the response spectra for pulse-like ground motions are different from those associated with ordinary ground motions. These differences in response spectra have been observed and addressed by many authors (Somerville et al. 1997; Abrahamson 1998a; Abrahamson 1998b). The effects of forward-directivity in the response spectra can be considered by necessary modifications to an attenuation relation through two different approaches: broadband and narrow band models, as have been explained in the

following sections. Based on the broadband directivity model, the response spectra increase monotonically with magnitude at all periods. On the other hand, in a narrow band directivity model, the response spectrum for near-fault ground motion becomes richer for a larger magnitude earthquake because of the pulse period. This has been illustrated in Figure 2-3 and Figure 2-4.

2.4. Broadband Directivity Model

Somerville (1997) proposed a broadband model to include the amplitude and duration effects of rupture directivity to the ground motion attenuation relations proposed by Abrahamson and Silva (1997). Somerville's model comprises two period-dependent scaling factors that may be applied to the horizontal attenuation relationship. One of the factors accounts for the change in shaking intensity in the average horizontal component of motion due to near-fault rupture directivity effects (higher ground motions for rupture toward the site and lower ground motions for rupture away from the site). The second factor reflects the directional nature of the shaking intensity using two ratios: fault normal (FN) and fault parallel (FP) versus the average (FA) component ratios.

This model was later refined by Abrahamson (2000) to incorporate rupture directivity into probabilistic seismic hazard analysis. Initially, Somerville's directivity model was independent of distance and applicable to magnitudes greater than 6.5. Abrahamson applied a distance dependent taper function to the model that reduces the effect to zero for distances greater than 60 km. Also, a magnitude taper was applied that reduces the effect to zero for magnitudes less than 6.0 and interpolates linearly for magnitudes between 6 and 6.5. Based on an evaluation of empirical recordings and numerical simulations, the form of the

directivity function was modified to reach a maximum at $\xi\cos(\theta) = 0.4$, where ξ=S/L is defined as the fraction of the fault length that ruptures toward the site; S is the projected distance (along the rupture plane) from the epicenter toward the site; L is the fault rupture length; and θ is the Azimuth angle between the fault plane and the ray path to site. Due to adding the directivity term into the ground motion model, a period dependent reduction was applied to the standard deviation of the attenuation relation. The final broadband model results in a monotonic increase in the response spectra at all periods larger than 0.6 sec with an increase of magnitude. However, later studies showed that pulse-like ground motions cannot be adequately described by the monotonic broadband scaling and, therefore, a narrow band model was proposed.

2.5. Narrow Band Rupture Directivity Model

Somerville (2003b) proposed a narrow band directivity model where the response spectrum does not increase monotonically with magnitude at all periods, as is the case in conventional ground motion models. Instead, the response spectra for near-fault ground motions become richer in longer periods as a result of a magnitude increase which lengthens the pulse period. Earthquakes with higher magnitude result in pulses with longer periods. Consequently, longer period pulses increase the level of response spectra for longer periods. This shifts the peak response spectral acceleration of the strike-normal component to longer periods. Thus, the response spectrum values from smaller earthquakes may exceed those of larger earthquakes at shorter and intermediate periods.

The response spectrum is the elastic response of a single degree of freedom that is meant to represent the structural response in terms of displacement, velocity, or acceleration.

Structural response can be presented in different terms, as explained below. However, responsive Engineering Demand Parameters should be selected to improve the accuracy of the prediction of the structural response.

2.6. Engineering Demand Parameters

As previously explained, in PSDA, Intensity Measures are correlated to structural response parameters through a probabilistic means. Following the terminology convention of PEER, Engineering Demand Parameter is used here to refer to those structural response parameters. EDPs are structural response quantities that can be used to estimate damage to structural and nonstructural components and systems. Researchers have used different EDPs that are useful for engineering design decision-making. Primary EDPs are related to deformation that can be associated with structural and nonstructural damage, such as roof drift, story drifts, maximum inter-story drift ratio, ductility demands, and maximum peak story drift angle (Krawinkler and Alavi 1998; Luco and Cornell 2001; Krawinkler et al. 2003b; Baker and Cornell 2005). Different EDPs can be defined to correlate best with the various types of damage. Sensitive Engineering Demand Parameters enhance the accuracy of the prediction of structural response. For example, the average of the maximum story drift ratio is a good measure when damage is linearly related to drift. The maximum roof drift (roof displacement over height) is considered as a reference or global measure of damage. The inter-story drift ratio is relevant to collapse. Shear distortions in joints and rotations at plastic hinges are other indicators of structural damage. In Chapter 3, the selected Engineering Demand Parameter for this study and its advantages will be explained.

In general, the above mentioned Engineering Demand Parameters are obtained from the response of a structure subjected to ground motions that may or may not have been scaled. In the next section, this matter is considered.

2.7. Scaling Ground Motions

Lack of recorded data from a specific fault often necessitates scaling of ground motions to make them compatible with the site specific hazard. Also, when ensembles of scaled ground motions are used, variability of the structural response is minimized, thus requiring fewer records and dynamic analyses. For example, the response of a structure to the ground motions scaled to the spectral acceleration at the structure's fundamental period of vibration, $S_a(T_1)$, shows smaller dispersion compared to unscaled records. Therefore, relationships between EDPs and IMs are more stable for a lower number of analyses. However, when there are sufficient numbers of ground motion records, no scaling is required. Nevertheless, when scaling is required, near-fault ground motion records should be treated with much care.

Scaling of ground motions can be conducted using a time-domain and/or a frequency-domain approach. Time-domain scaling involves a linear scaling of the amplitude of the ground motions to match a target ground motion parameter, such as the PGA, the PGV, the Arias Intensity, or spectral acceleration at the first or other elastic modal periods. In the frequency-domain approach, the frequency content is changed to match a target spectral response. Even though the former approach maintains the frequency content of ground motions, there is a significant dispersion in response spectra of ground motions scaled by this method. The latter approach changes the physical characteristics of the ground motions. Therefore, forward-directivity pulses can be distorted in this process. However, both of these

methods result in significant dispersion in the estimation of the nonlinear response of a structure. This issue has become an attractive matter for researchers. Many studies have aimed to reduce the dispersion in estimates of structural response parameters in order to find the most appropriate method for scaling near-fault and ordinary ground motions.

For example, Krawinkler et al. (2003a) selected ensembles of records with about the same magnitude and distance and scaled them so that they have an identical spectral acceleration at the period of 0.5 sec. Figure 2-5 shows spectra of the 20 ordinary ground motions designated as Large Magnitude-Short Distance ($6.5 \leq M_w \leq 7.0$, 13 km $\leq R \leq$ 30 km) scaled to the same spectral acceleration at T = 0.5 sec (Krawinkler et al. 2003a). As shown in Figure 2-5, there is large dispersion in spectral accelerations at all other periods, even those very close to 0.5 sec. Even this dispersion gets much larger for the near-fault spectra than for ordinary ones. The dispersion results in a significant scatter in the elastic response of structures whose fundamental periods are not equal to 0.5 sec. The amount of this scatter depends on the importance of higher mode effects.

Similarly, Kurama and Farrow (2003) compared different methods of scaling. They investigated the effectiveness of seven ground motion scaling methods in reducing the dispersion in peak lateral displacement demand estimated from non-linear dynamic time-history analyses. The response of a series of linear and non-linear single-degree-of-freedom and multi-degree-of-freedom structures was considered for the following IMs:

1. Peak ground acceleration: each ground motion record is scaled to the arithmetic mean PGA of the ground motion ensemble.

2. Effective peak acceleration (EPA): each ground motion record is scaled to the arithmetic mean EPA of the ground motion ensemble. According to NEHRP 1994, EPA is calculated as the mean linear-elastic 5%-damped spectral acceleration for the period range of 0.1 to 0.5 sec divided by 2.5. The 2.5 coefficient relates back to the formulation of the design response spectra in ATC-3-06 (1978).

3. Arias intensity-based parameter (A95): each ground motion record is scaled to the arithmetic mean A95 of the ground motion ensemble. The term A95, is defined by Sarama and Yang (1987) as the acceleration for which its squared value contains 95% of the Arias Intensity.

4. Effective peak velocity (EPV): each ground motion is scaled to the arithmetic mean EPV of the ensemble. According to NEHRP, EPV is equal to the linear-elastic 5% damped spectral pseudo-velocity at period, T =1 sec.

5. Maximum incremental velocity (MIV): each ground motion is scaled to the arithmetic mean MIV of the ground motion ensemble. Incremental velocity, IV, is the area under the acceleration time-history of a ground motion between two consecutive zero acceleration crossings.

6. Spectral response acceleration at the structure fundamental period: each ground motion is scaled to the arithmetic mean linear-elastic 5% damped spectral acceleration of the ground motion ensemble at the linear-elastic fundamental period of the structure, $S_a(T_1)$.

7. Spectral acceleration over a range of structure periods ($S_a(T_1 \rightarrow T_\mu)$): each ground motion is scaled to the arithmetic mean linear-elastic 5% damped spectral acceleration of the ground motion ensemble over a range of structural periods (Martinez-Rueda 1998; Nassar and Krawinkler 1991; Shome and Cornell 1998). First, the mean spectral acceleration, $S_a(T_1 \rightarrow T_\mu)$, of the ensemble over the period range $T_1 \rightarrow T_\mu$ is calculated. Then, the records are scaled such that the mean spectral acceleration of each ground motion over the period range, $T_1 \rightarrow T_\mu$, is equal to $S_a(T_1 \rightarrow T_\mu)$.

Kurama and Farrow (2003) concluded that, for the near-field ground motion ensembles, the effectiveness of the $S_a(T_1)$ and $S_a(T_1 \rightarrow T_\mu)$ methods with respect to the PGA method is significantly decreased and in the long period range their effectiveness decreases as R (defined as the linear-elastic force demand under a ground motion divided by the yield strength of the structure) increases. In general, the dependency of the scatter in the peak displacement demand on R is large. For the PGA, EPA, and A95 scaling methods, the dependency of the scatter in the peak displacement demand on the period significantly decreases for the near-field ground motion ensemble. Basically, it is hard to select an effective scaling method for near-field ground motions that can reduce the scatter in peak lateral displacement demand for all ranges of site and structure characteristics. However, between all proposed scaling methods by Kurama and Farrow (2003), the MIV method is the most effective one, but the biggest disadvantage for the implementation of the MIV scaling method in current seismic design procedures is the lack of methods to estimate the mean annual frequency of exceedance of MIV.

Alternatively, one can utilize more Intensity Measure parameters to improve the accuracy of the structural response prediction statistical models rather than using a scalar IM. The following introduces combinations of different IMs proposed by many researchers.

2.8. Vector-Valued Intensity Measures

In this section, Vector-Valued Intensity Measures are discussed. Before going further, it is helpful to define two terminologies: efficiency and sufficiency (Luco and Cornell 2007). An efficient IM is defined (from the perspective of a structural engineer) as one that results in a relatively small variability of the structural demand measure given as an IM. A sufficient IM, on the other hand, is defined here as one that renders DM conditionally independent, given an IM of earthquake magnitude (M_w) and source-to-site distance (R_{rup}).

As previously mentioned, according to recent studies, for tall, long-period, or buildings subjected to pulse-like ground motions, the conventional intensity measure, $S_a(T_1)$, cannot be efficient and sufficient even for ordinary ground motions. Moreover, the spectral acceleration at the structure's fundamental period of vibration becomes less effective for near-fault ground motions when forward-directivity pulses are dominant. Therefore, $S_a(T_1)$ should be replaced or combined with more effective IMs to improve the accuracy of the estimation of the structural response. Due to the shortcomings of $S_a(T_1)$, many other IMs which are capable of being adequate demand predictors have been proposed. For instance, for multi-mode dominated structures, a combination of spectral quantities at different frequencies can be used to enhance accuracy of the response prediction (e.g., the spectral value of the third mode of elastic response in addition to the first and second modes). Bazzurro (1998), as well as Shoma and Cornell (1998), have considered Vector-Valued IMs comprised of $S_a(T_1)$ and

the ratio of $S_a(T_2)/ S_a(T_1)$, as well as a scalar IM that combines $S_a(T_1)$ and $S_a(T_2)$. Magnitude and distance, which influence the frequency content of ground motions, are other parameters of Vector-Valued IMs that can be considered as well as the predominant period of the ground motion. Others have proposed inelastic spectral quantities as efficient IMs for pulse-like ground motions (Luco 2002).

Baker and Cornell (2005) used the conventional intensity measure, $S_a(T_1)$, with other parameters such as magnitude, distance, and the epsilon (ε) associated with the ground motion (where ε is defined as the number of standard deviations by which an observed logarithmic spectral acceleration differs from the mean logarithmic spectral acceleration of a ground motion prediction equation). In other words, ε is computed by subtracting the mean predicted $\ln S_a(T_1)$ from the record's $\ln S_a(T_1)$, and dividing by the logarithmic standard deviation (as estimated by the prediction equation). ε is an indicator of the shape of the response spectrum. Since the shape of the spectrum does not change with scaling, ε, which is defined with respect to the unscaled record, will not change in value when the record is scaled. For a given ground motion record, ε is a function of T_1 (i.e. epsilon will have different values at different periods) and the ground motion prediction model used (because the mean and standard deviation of $\ln S_a(T_1)$ vary somewhat among models). Neglecting the effect of ε when computing the drift hazard curve leads to conservative estimates of the response of the structure.

(Luco and Cornell 2007) and Baker and Cornell (2008) investigated the efficiency and sufficiency of six alternative IMs defined in Table 2-1. In comparison with the conventional

intensity measure, $S_a(T_1)$, or equivalently IM_{1E}, the ground-motion intensity measure denoted by $IM_{1I\&2E}$, which takes into account the second-mode frequency content and inelasticity, is demonstrated to be relatively efficient and sufficient under both near-source and ordinary suites of earthquake records. The lone exception is for tall, long-period buildings subjected to near-source earthquake records. In that case, although $IM_{1I\&2E}$ is the most efficient of the intensity measures compared, it is not sufficient.

Table 2-1: Intensity measures defined by (Luco and Cornell 2007)

IM_{1E}	the first mode of elastic structural response
IM_{1I}	the first mode of inelastic structural response
$IM_{1E\&2E}$	the first two modes of elastic structural response combined by the square-root-of-sum-of-squares (SRSS) rule
$IM_{1I\&2E}$	the first mode of inelastic and the second mode of elastic structural response
IM_{1eq}	the first mode of spectral displacement of an "equivalent" elastic SDOF oscillator
IM_{1eff}	the elastic structural response of an effective period longer than the first mode

Still more research is needed to find efficient and sufficient Vector-Valued IMs for near-fault ground motions.

Although the proposed IMs for near-fault ground motions by researchers have been dissimilar, all reach a consensus that Vector-Valued IMs would be more efficient and sufficient for the case of forward-directivity. Some researchers have considered time-domain rather than frequency-domain characteristics of earthquake records as IMs. Time-domain

features of near-source records, such as the amplitude and the period of the velocity pulse, considerably affect the building response and can be part of Vector-Valued IMs (Iwan et al. 1998; MacRae and Roeder 1999; Alavi and Krawinkler 2001).

Krawinkler et al (2003a) included equivalent pulse parameters (pulse period and intensity) as parts of a vector of IMs for near-fault ground motions. They noticed that for forward-directivity ground motions, the effect of frequency content on the prediction of demands is dominated by the dispersion of spectral values rather than the median shape of the spectrum. Krawinkler et al. also concluded that magnitude and distance dependence of spectral shapes is a moot issue and does not have a dominating effect for forward-directivity ground motions.

Bazzuro et al. (2005) also considered "non-stationary" features of near-source, forward-directivity accelerograms in addition to $S_a(T_1)$ to improve structural response estimation. The non-stationary time-domain features considered as potential response predictors are the number of half-pulses, the pulse period, and the peak velocity. The record duration was another parameter considered in their study. Results showed that velocity pulse characteristics and record duration do not appreciably improve the accuracy of the response estimates beyond that achieved by using linear elastic spectral values alone. The fact that these four ground motion parameters in Bazzurro's study do not explicitly account for the period or strength of the structure seems to limit their predictive power. This is because Bazzurro et al. did not consider the characteristics of the structure. On the contrary, Krawinkler et al. (2003a) considered the characteristics of the structure in combination with the equivalent pulse parameters. That is why Krawinkler, as opposed to Bazzurro, found that

pulse parameters are adequate representations of near-fault ground motions. In a later study, Bazzurro, by studying the inelastic spectral displacement of an elastic-perfectly-plastic SDOF oscillator, noticed that record characteristics that do not account for fundamental period and strength of the structure are not likely to be good response predictors.

Time-domain characteristics of near-fault ground motion, such as the parameters of the forward-directivity pulse, seem to be more proper as IMs since near-fault ground motions are distinct from ordinary ground motions for their intensive velocity pulse. Moreover, these pulse parameters are predictable based on seismological data such as site and fault information. Consequently, many researchers have chosen to represent the characteristics of near-fault ground motions with means of the equivalent pulses explained in the next chapter.

Even though estimation of ground motion hazard for scalar IMs is well developed using PSHA, incorporation of Vector-Valued IMs is still a challenging task. This is because one can select different parameters as Vector-Valued IMs and, subsequently, each selection needs a different treatment. For example, Vector-Valued IMs comprised of spectral acceleration and ε (Baker and Cornell 2005) can be obtained from scalar hazard curves combined with standard deaggregation results. In other cases, such as Vector-Valued IMs consisting of spectral acceleration values at multiple periods (Bazzurro 1998; Shome and Cornell 1998), special Vector-Valued PSHA computations are needed.

2.9. Equivalent Pulse Models:

The predictive power of time-domain parameters of the near-fault ground motion records has led seismologists and engineers to develop techniques to numerically simulate

pulse-like ground motions. Forward-directivity pulses play an important role in the response of structures in near-fault zones due to the seismic energy that is carried by them at the beginning of the motion. The coincidence of the equivalent pulse period and the period corresponding to the peak pseudo-velocity response spectrum reinforces the idea that the velocity pulse carries the most energy of the ground motion. This energy is carried in a narrow period band centered about the period of the forward-directivity pulse. Therefore, simplified representations of pulse-like ground motions have been developed to describe near-fault ground motions and to predict the response of structures subjected to this type of motion. In the following sections, different equivalent pulses presented by researchers are introduced.

2.9.1. A, B, and C_n Pulses (Makris 1997; Makris and Chang 1998)

Makris and Chang (1997 and 1998) proposed an equivalent pulse model to approximate the near-fault ground motion by sine and cosine pulses. They classified the near-fault ground motion displacement pulses into three distinct tri-geometric functions, a type-A pulse, a type-B pulse or a type-C_n pulse. A Type-A, pulse which is a one-sine pulse, models the forward ground motion; a type-B pulse, which is a one-cosine pulse, models a forward and backward motion, and a type-C_n pulse approximates a recorded motion that exhibits *n* main pulses in its displacement time history. These pulses have been plotted in Figure 2-6. Parameters used to define these pulses are the amplitude and the circular frequency of the pulse. A Type-C_n pulse has an additional parameter which is the phase angle. The phase angle is determined by requiring that the ground motion displacement at the end of the pulse be zero. Later, they obtained closed form solutions for a SDOF subjected to each type of pulse. However, their

proposed models poorly match the velocity pulses of all of the recorded ground motions (Makris and Chang 2000).

2.9.2. Sine pulse (Somerville 1998)

Somerville (1998) developed a preliminary model that relates time-domain parameters of the near-fault ground motion pulse to the earthquake magnitude and distance. The pulse parameters of single pulse of his model are the period and peak amplitude of the largest cycle of motion of the velocity pulse. He postulated that the period of the pulse is directly related to the rise time, which is correlated to the faulting mechanism. He concluded that the period of the pulse is thus equal to about twice the rise time of slip on the fault, which is consistent with the fact that the rise time is a lower bound on the period of the pulse. He postulated that the number of half sine pulses in the velocity time history might be associated with the number of asperities in a fault. His model assumes a bilinear relationship between the logarithm of the PGV, magnitude, and the logarithm of distance, which may not be realistic at very close distances. To avoid unrealistic predictions of PGV at short distances, Somerville used a distance cut-off of 3 km. His proposed relation between magnitude and pulse period for rock and soil respectively are:

$$\log_{10} T_{Dir} = -31.7 + 0.5 M_w \tag{2-3}$$

$$\log_{10} T_{Dir} = -2.02 + 0.346 M_w \tag{2-4}$$

Near-fault ground motions containing forward rupture directivity are not always simple enough to be represented by a single pulse. Considering pulse-like records which have more

than two peaks or troughs, it is obvious that the single pulse proposed by Somerville does not fit these ground motion pulses well.

2.9.3. P1, P2, and P3 Pulses (Krawinkler and Alavi 1998)

Krawinkler and Alavi (1998) used Somerville's relationship between magnitude, distance, and PGV and defined P1, P2, and P3 pulses to classify near-fault ground motion pulses. P1, P2, and P3 are a half pulse, a full pulse, and multiple pulses, respectively (see Figure 2-7). These pulses are defined by their period and amplitude and are used to represent the ground motion velocity pulses. The pulse period of the model is determined from the peaks of the elastic velocity spectra. For single pulse motions, the period of the equivalent pulse almost coincides with the period corresponding to the peak of the pseudo-velocity spectrum, but for more complex records, they can differ significantly. In their procedure, the amplitude of the equivalent pulse is found by minimizing the differences between the maximum story ductility demand from the near-fault record and the corresponding demand obtained from an equivalent pulse representation for a certain range of ductility. Based on their study, the equivalent pulse velocity lies within 20% of the PGV of the record, for nearly all cases. The pulse type is judged based on an inspection of the time history trace and on a comparison between ground motion and pulse spectral shapes.

2.9.4. Decaying Sinusoidal Pulses (Agrawal and He 2002)

Agrawal and He (2002) proposed decaying (damped) sinusoidal pulses to represent dominant kinematic characteristics of the ground motion (see Figure 2-8). The pulse parameters of their model are the natural frequency, amplitude of the velocity pulse, and the damping factor of the decaying sinusoid which controls the shape and duration of the

velocity pulse. The values of the parameters are judged based on the time history of the ground motion. They found that while their proposed approximation captures the dominant kinematic characteristics of displacement and velocity of recorded ground motions in forward rupture directivity conditions, the resulting predictions of accelerations are poor because of the exclusion of the high frequency fluctuations that override long duration pulses in recorded ground motions. Their study showed that high frequency components which override the long-period components of the recorded acceleration time history can not contribute to the response of flexible structures. Therefore, the proposed approximation is not reliable for these kinds of structures subjected to near-fault earthquakes. Sometimes the second peak or trough of the forward rupture directivity pulses is larger than the first one in amplitude, which is not possible to represent with decaying (damped) sinusoidal pulses.

2.9.5. Wavelet Pulses (Mavroeidis and Papageorgiou 2003)

Mavroeidis and Papageorgiou (2003) used wavelet pulses to represent near-fault ground motion velocity pulses. Similar to Krawinkler and Alavi (1998), Mavroeidis and Papageorgiou determined a pulse period so that the pseudo-velocity response spectra of the synthetic and recorded near-fault ground motions exhibit their peak at approximately the same natural period. The amplitude of their synthetic velocity pulse is determined so that the amplitude of the synthetic velocity pulse and its peak pseudo spectral velocity agree well with the corresponding quantities of the actual record. The amplitude of their synthetic velocity pulse was found to agree closely with PGV. The number and phase of half cycles and the epoch of the envelope's peak are other parameters to define the waveform of their proposed equivalent pulse. The phase parameter defines symmetric and anti-symmetric

signals. Although their proposed model successfully simulates the entire set of available near-fault displacement, velocity, and (in many cases) acceleration time histories, as well as the corresponding deformation, velocity, and acceleration response spectra, the response of structures to these wavelet pulses was not studied.

2.9.6. Sine Pulse (Bray and Rodriguez-Marek 2004)

Bray and Rodriquez-Marek (2004) developed a simplified time-domain representation of pulse-like ground motion using half-sine pulses. Parameters of this representation are amplitude, pulse period, and the number of significant pulses in the velocity-time history (see Figure 2-9). A regression analysis was developed to correlate these pulse parameters with magnitude and distance. The regression analysis indicated a systematic difference between pulses recorded in rock and in soil. The predictive equations of the Bray and Rodriguez-Marek model are given by:

$$\ln(PGV_{ij}) = a + bM_w + c\ln(R^2 + d^2) + \eta_i + \varepsilon_{ij} \tag{2-5}$$

$$\ln(T_v)_{ij} = a + bM_w + \eta_i + \varepsilon_{ij} \tag{2-6}$$

where PGV_{ij} and $(T_v)_{ij}$ are the *PGV* and pulse period in units of cm/s of the j^{th} recording from the i^{th} event, respectively; M_w is moment magnitude of event *i*; *R* is rupture distance in km; η_i and ε_{ij} represent the inter- and intra-event variations, respectively, obtained using the random effects model; and *a*, *b*, *c*, and *d* are regression parameters (for more information about the above parameters, see Bray and Rodriguez-Marek, 2004). The proposed definition of pulse period uses either the zero crossing time or the time at which velocity is equal to 10% of the peak velocity for this pulse. The latter definition is necessary for pulses in which the pulse is

preceded by a small drift in the velocity–time history. Another alternative for defining the dominant pulse period is a weighted average period of all significant cycles of motion. The number of cycles of motion (referred to as the number of significant pulses) is defined as the number of half-cycle velocity pulses that have an amplitude of at least 50% of the PGV of the ground motion. Considering site-effects, they predict longer periods at soil sites than at rock sites for lower magnitude events. This difference diminishes as magnitude increases and disappears for large magnitudes.

The aforementioned models rely on user judgment to determine zero crossings in the presence of noise or to select reasonable starting points which can be very time-consuming and inaccuracies inevitably creep in. Recently, Baker proposed a computerized method which is independent of user judgment.

2.9.7. Daubechies Wavelet of Order 4 (Baker 2007a)

Baker (2007) proposed an automated screening and classification procedure to identify and extract the largest velocity pulse from a ground motion using wavelet-based signal processing (the Daubechies wavelet of order 4). The approach uses wavelet analysis to extract the largest velocity pulse from a given ground motion. The size of the extracted pulse relative to the original ground motion is used to develop a quantitative criterion for classifying a ground motion as "pulse-like." To identify the subset of these pulse-like records potentially caused by directivity effects, two additional criteria are applied: the pulse arrives early in the ground motion and the absolute amplitude of the velocity pulse is large. Baker used the period associated with the maximum Fourier amplitude of a wavelet to define a pseudo-period for extracted wavelet pulses. The amplitude of the wavelet pulses is obtained

from the wavelet transform computation. Baker also used a linear regression analysis and found a predictive relationship between pulse period and earthquake magnitude similar to other authors (Somerville 1998; Mavroeidis and Papageorgiou 2003; Bray and Rodriguez-Marek 2004) as:

$$Ln(T_p) = -5.78 + 1.02 M_w \qquad \text{with} \qquad \sigma = 0.55 \tag{2-7}$$

where T_p, M_w, and σ are defined as pulse period, moment magnitude, and standard deviation, respectively. Note that, the extracted pulses by the Baker procedure are referred to as extracted pulses in the following sections.

2.9.8. Comparison of the available equivalent pulse models

None of the aforementioned researchers has considered the response of MDOF structures to their proposed models (with the exception of Krawinkler and Alavi (1998)). In spite of conclusive study of Krawinkler and Alavi, it is not clear whether maximum ductility demand is due to the first part of the record, which contains the forward-directivity pulse, or the entire record. Krawinkler and Alavi pointed out that the influence of P-Δ effects varies from negligible to dominant based on their case study. Nevertheless, they decided not consider P-Δ effects in their study. Also, their data base was scaled in such a manner that the spectrum of each individual record matches the NEHRP soil type D spectrum (frequency-domain scaling method). However, as mentioned in section 2.7, this kind of scaling should be done with much care for pulse-like ground motions. In this scaling process, the frequency content of ground motions is changed and forward-directivity pulses can be distorted.

In the next chapter, an equivalent pulse model addressing the aforementioned ambiguities is introduced.

2.10. Methodologies to Correlate EDPs to IMs

The numerical evaluation of demand parameters makes it possible to develop statistically representative relationships between EDPs that were obtained on the basis of previously discussed ground motion IMs. Many such methods have been proposed by different authors, including correlations to scalar and vector IMs. Some of these methods are discussed here and one will be selected for our purpose. For example, Baker (2007) proposed a few different methods to estimate the probabilistic relationship between ground motion intensity and structural response from a statistical inference perspective. The field of statistical inference is concerned with estimating the properties of a random variable from a finite sample of data. Baker considered two classes of statistical inference approaches to determine EDPs from given IMs. These approaches are discussed below.

2.10.1. Parametric Approaches:

In this approach, it is assumed that the random variable EDP has some probability distribution (e.g. lognormal) that is defined by a few parameters. Then, these parameters are estimated to define the distribution (Lehmann and D'Abrera 1998). Two parametric estimation methods discussed are as follows:

2.10.1.1. Cloud Method

With this method, the nonlinear dynamic analysis of a structure is performed using a set of unscaled ground motion records (or records scaled by a constant factor). Regression can

be used with the records' IM values and associated EDP values obtained from nonlinear dynamic analysis to compute the conditional mean and standard deviation of the EDP given the IM. A log-linear relationship between the logarithms of the two variables often provides a reasonable estimate of the mean value of the EDP over a restricted range. Figure 2-10 shows a cloud of Ln EDP|IM data, the conditional mean value from linear regression, and a Gaussian CCDF fitted to the mean and standard deviation from the regression.

2.10.1.2. Strip Method

Rather than using regression analysis with ground motions having a range of IM levels, the motions can be scaled instead so that each motion has the IM level of interest, and then the distribution of EDP can be estimated directly from the resulting structural responses. This method is similar to that described in 2.10.1.1, except that here a regression analysis is used to define the moments of the statistical distribution of the EDP, while the method described in Section 2.10.1.1 uses an empirical cumulative distribution function. Figure 2-11 shows a strip of Ln EDP data and a Gaussian CCDF based on the sample mean and standard deviation.

2.10.1.3. Capacity Method

With this method, the probability distribution of EDP for a given IM is not estimated directly. Rather, the results from Incremental Dynamic Analysis (Dimitrios and Cornell 2002) are used to determine the probability that the IM level of a ground motion is less than IM, given that the ground motion caused a level of response EDP = y (Kennedy et al. 1984; Bazzurro and Cornell 1994a; Bazzurro and Cornell 1994b). Figure 2-12 shows incremental

dynamic analysis curves, and a Gaussian CDF of Ln IM_{Cap} obtained from the sample mean and standard deviation of the first exceedance of maximum inter-story drift ratio=0.01

2.10.2. Non-Parametric Approaches

A non-parametric approach does not require any assumptions about the distribution of the data (Lehmann and D'Abrera 1998) and has the advantage of being robust when the data do not fit a specified parametric distribution, but it generally requires more data for estimation in cases where the data do fit a parametric distribution. Two different non-parametric estimation methods reviewed by Baker are as follows:

2.10.2.1. Empirical Distribution for Response

Rather than using regression analysis with ground motions having a range of IM levels (as in the cloud method), the motions can be scaled instead such that each motion has the IM level of interest, and then the distribution of EDP can be estimated from an empirical complementary cumulative distribution function (Lehmann and D'Abrera 1998). With this approach, no assumptions are needed regarding distributions or functional relationships between EDP and IM. The eliminated assumptions have a cost, however, because more data are needed to characterize the conditional distributions. Empirical distributions can also have difficulties in estimating accurately the probability of exceeding extreme values, which are often of concern for reliability analysis. Figure 2-13 shows a strip of Ln EDP data and its empirical CCDF.

2.10.3. Comparison of Statistical Methods

The aforementioned methods can be developed for scalar or Vector-Valued IMs. Among these methods, some are preferable in the sense of accuracy and a reduced number of analyses required. The shortcomings of the cloud method could be addressed by requiring the relationship between EDPs and IMs to be linear, or by performing the regression over a more narrow range of IMs. This method does not severely restrict the functional form of the mean response versus IM relationship, while also not requiring excessive numbers of structural analyses to be performed. The level of confidence in the result depends on the nature of the data used in the regression analysis. More data makes the regression more stable. The strip method potentially requires more structural analyses than required for the cloud method. A drawback of the capacity method is that it will likely require more analyses than for a cloud analysis (although it will provide more accuracy than the cloud method if used over a large range of IMs). The empirical distribution method is potentially very accurate, but may require a prohibitive number of dynamic analyses, especially for IM vectors containing many parameters.

In the next chapter, a statistical model using the Cloud method is developed to correlate EDPs to IM. The cloud method requires a fewer number of analyses.

2.11. Figures

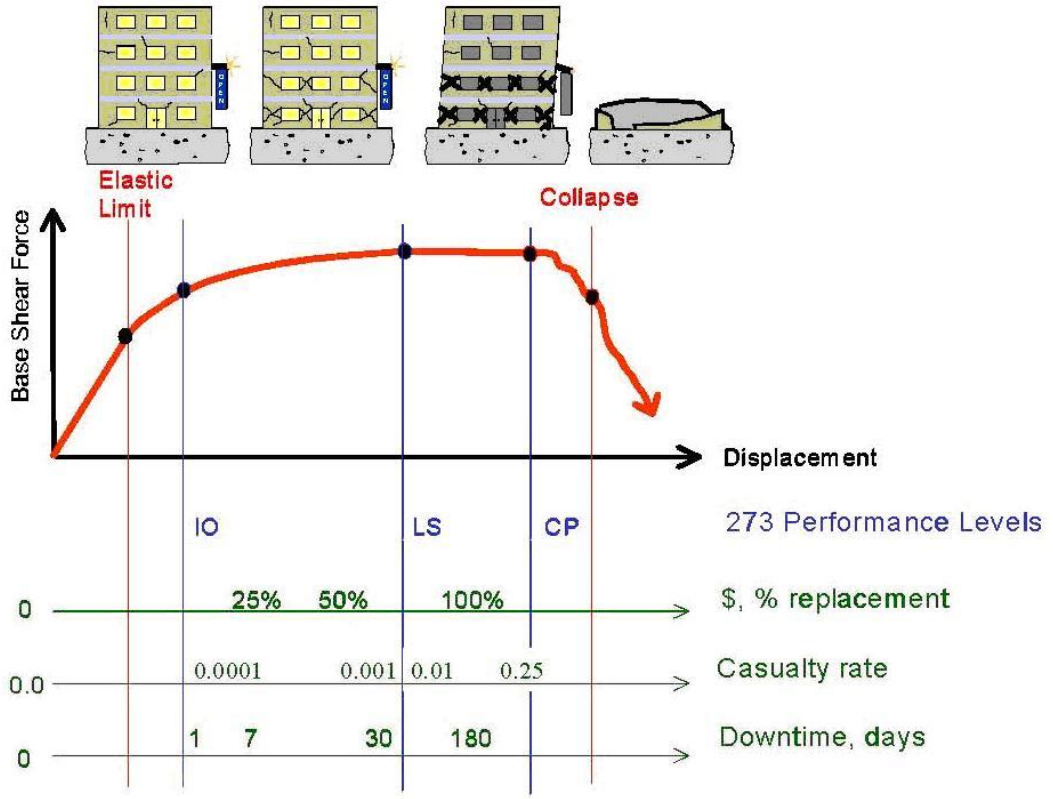

Figure 2-1: Illustration of performance-based earthquake engineering (ATC-58 2004)

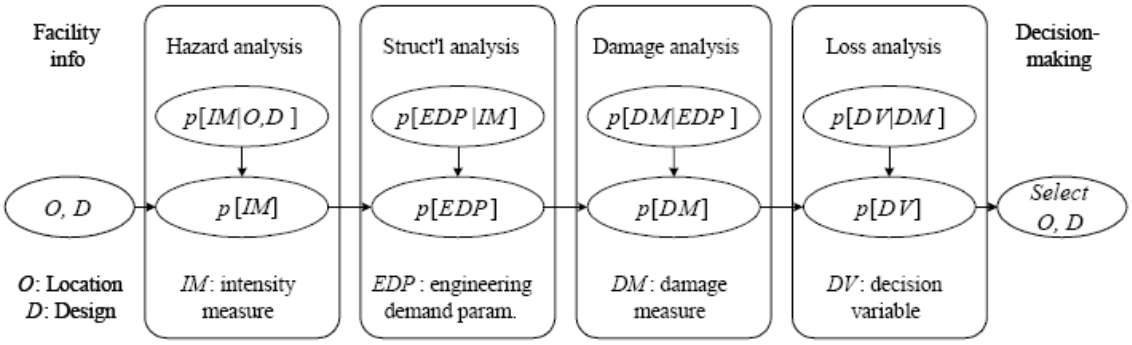

Figure 2-2: Steps in the PBEE-2 procedure (Moehle 2003)

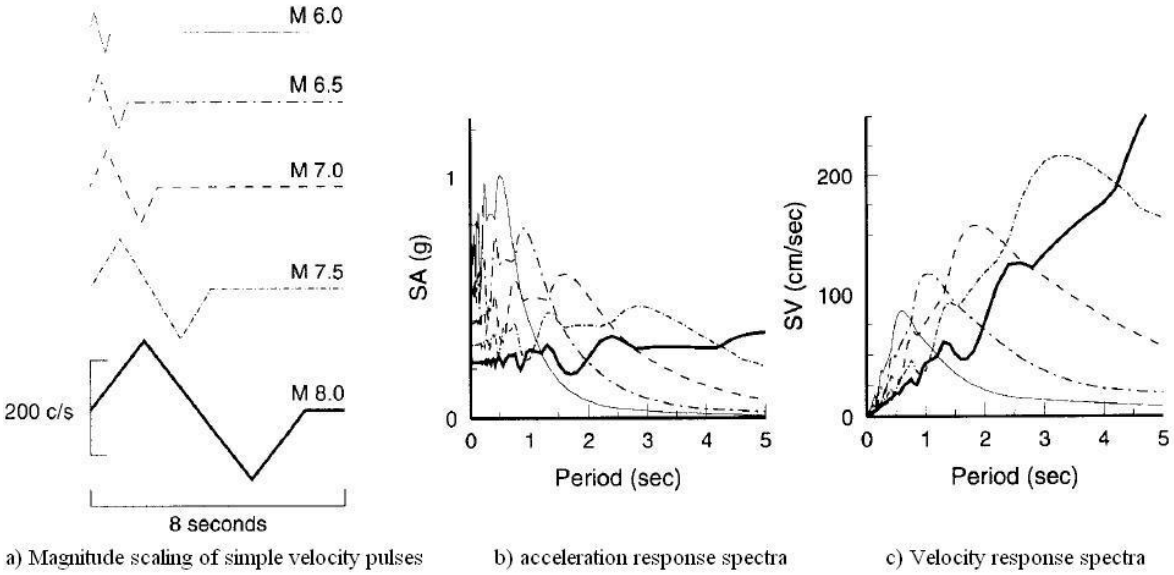

a) Magnitude scaling of simple velocity pulses b) acceleration response spectra c) Velocity response spectra

Figure 2-3: Simplified representation of forward-directivity pulses and their acceleration and velocity response spectra (Somerville et al. 2003)

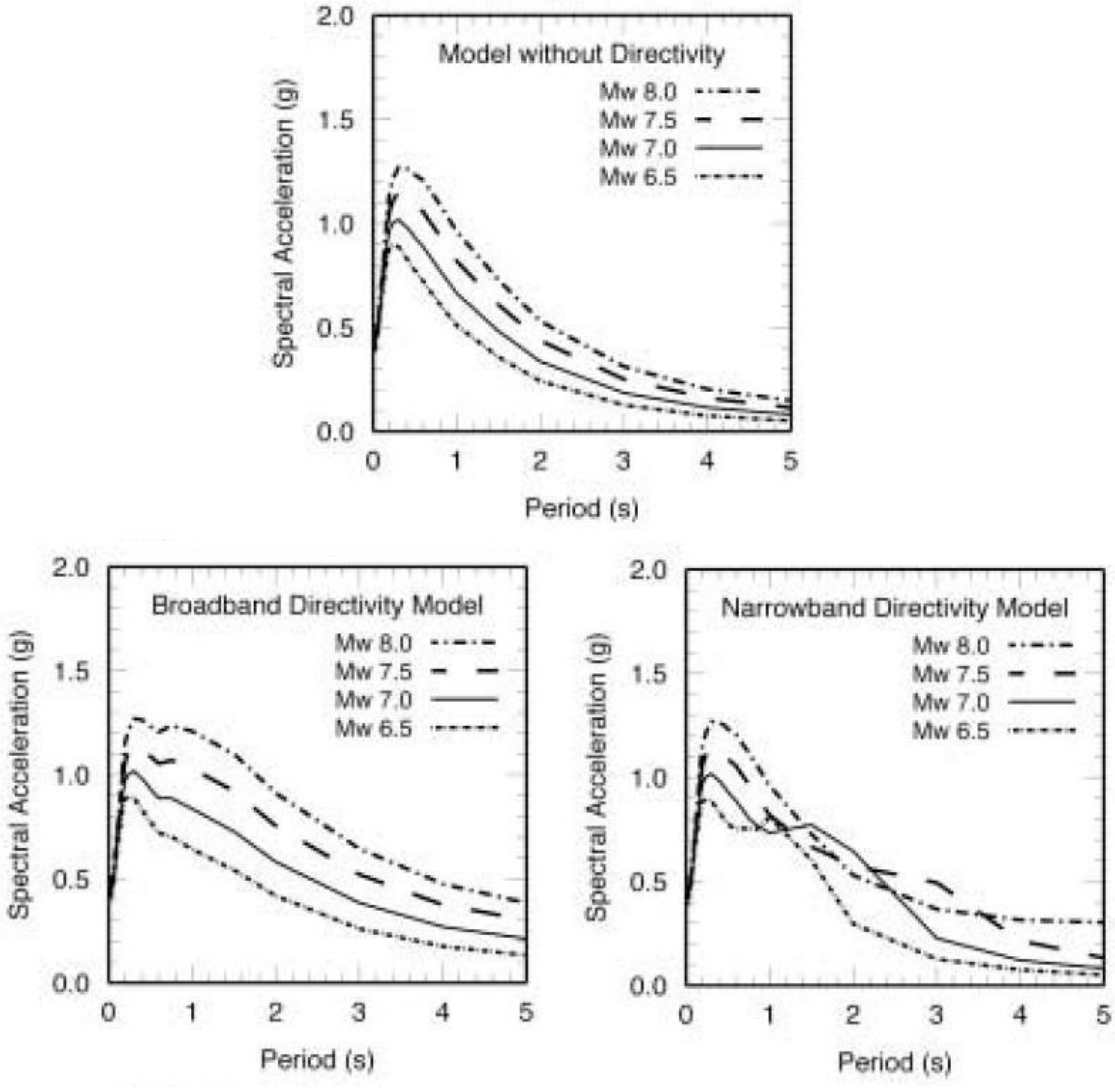

Figure 2-4: Near fault response spectral model, strike-slip, 5 km for soil sites.
Top: model without directivity (Abrahamson and Silva 1997). Bottom-left: Broadband directivity model (Somerville et al. 1997). Bottom-right: Narrow band directivity model (Somerville 2003)

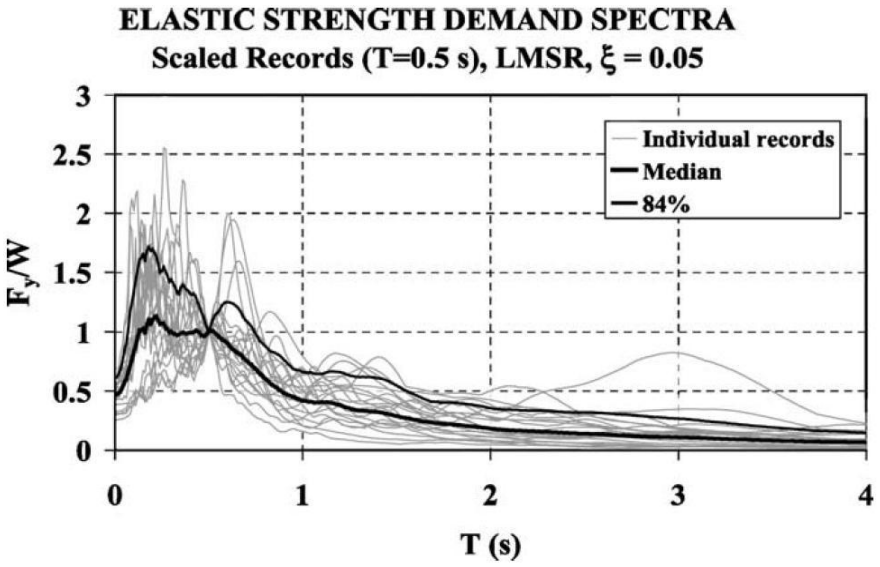

Figure 2-5: Spectra of the 20 ordinary ground motions scaled to the same spectral acceleration at T = 0.5 sec (Krawinkler et al. 2003a)

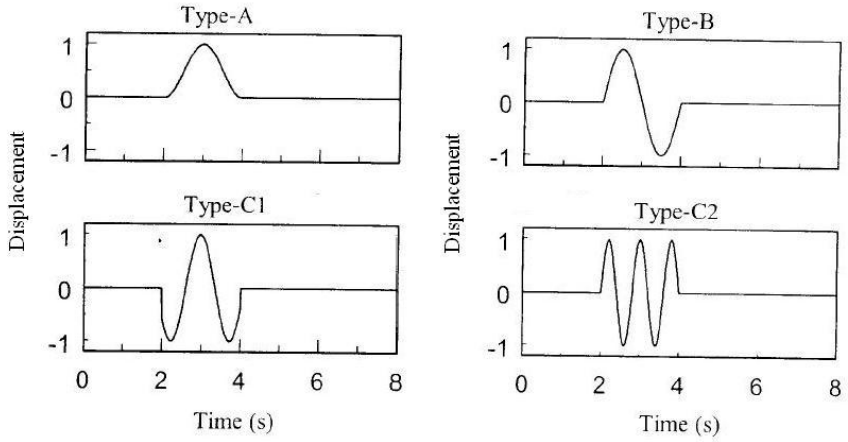

Figure 2-6: Type A, B, and C_n pulses (Makris 1997; Makris and Chang 1998)

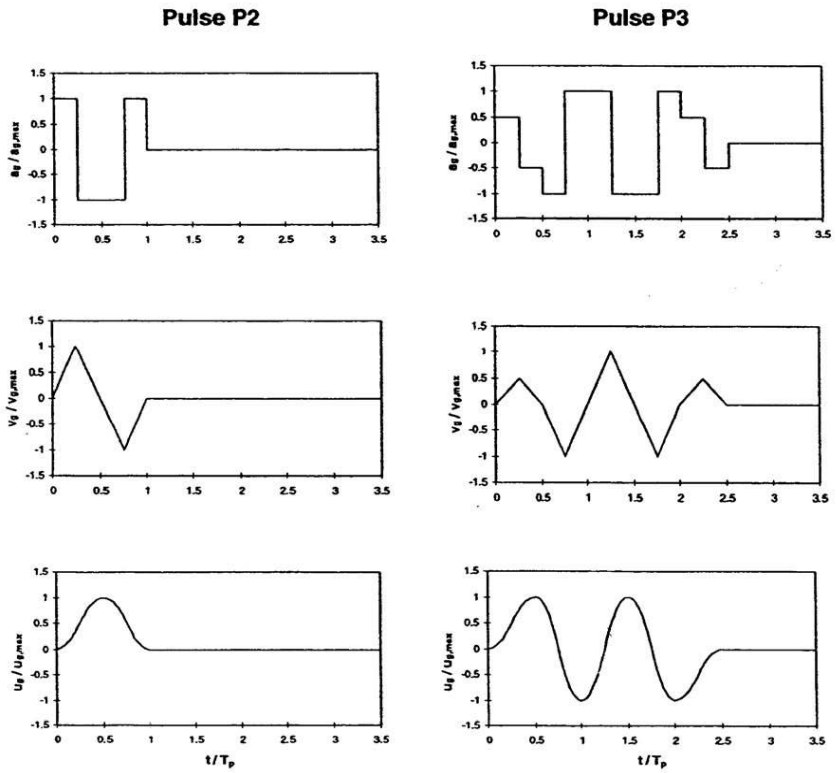

Figure 2-7: Acceleration, velocity, and displacement time histories of pulses P2 and P3 (Krawinkler and Alavi 1998)

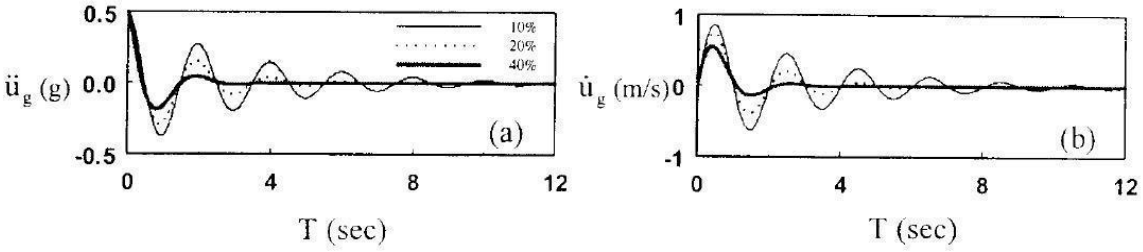

Figure 2-8: Acceleration and velocity time history of near-fault ground motion pulse with different decaying factors (Agrawal and He 2002)

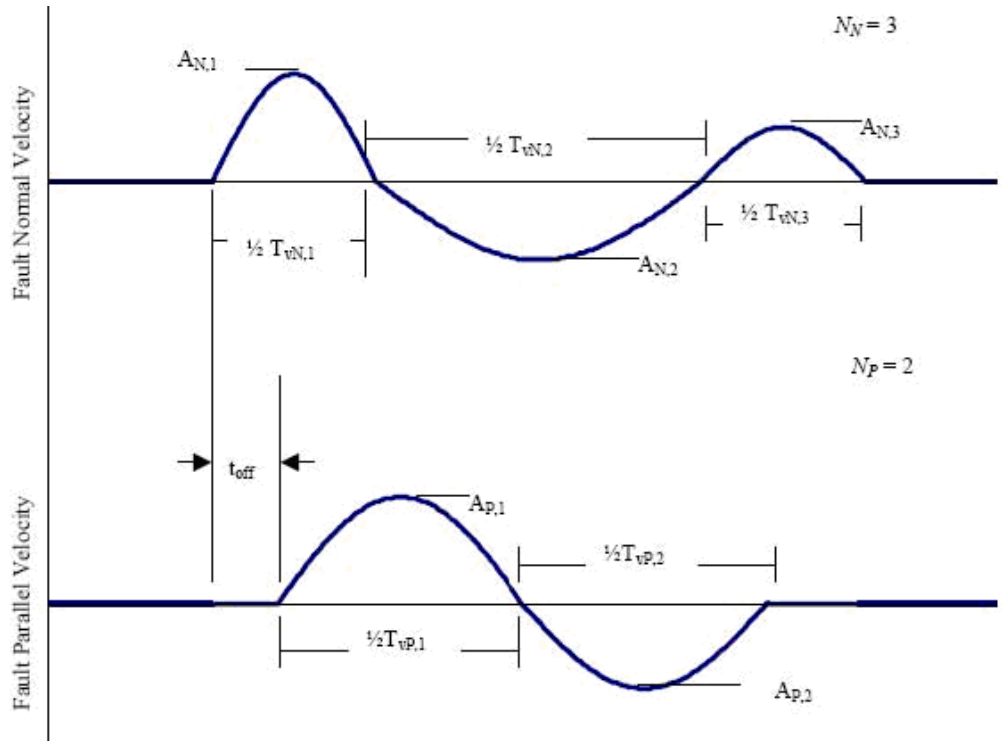

Figure 2-9: Simplified half-sine pulses (Bray and Rodriguez-Marek 2004)

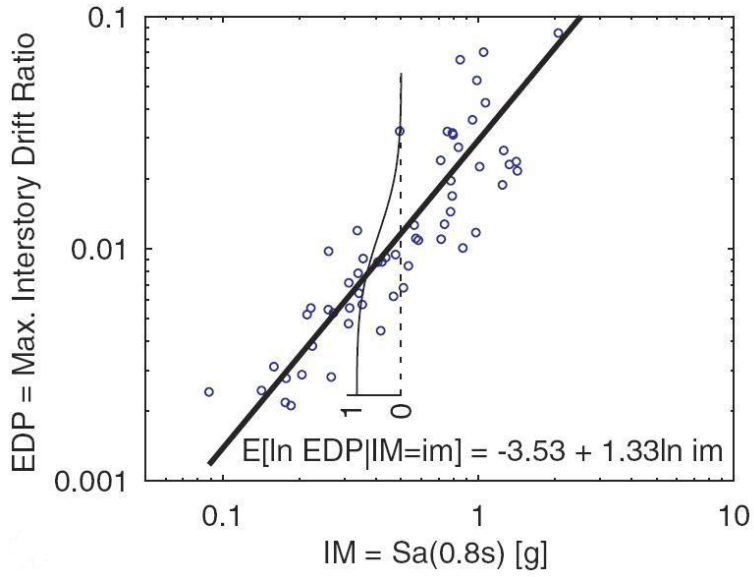

Figure 2-10: A cloud of Ln EDP|IM data

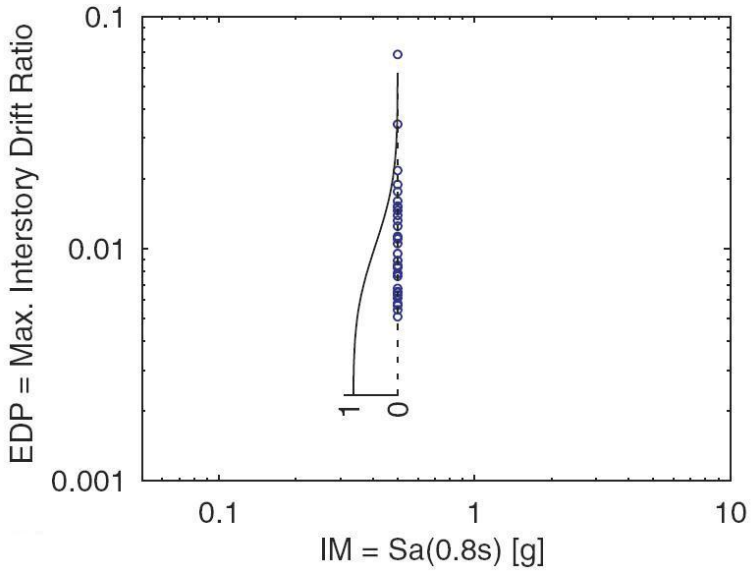

Figure 2-11: A strip of Ln EDP and its Gaussian CCDF

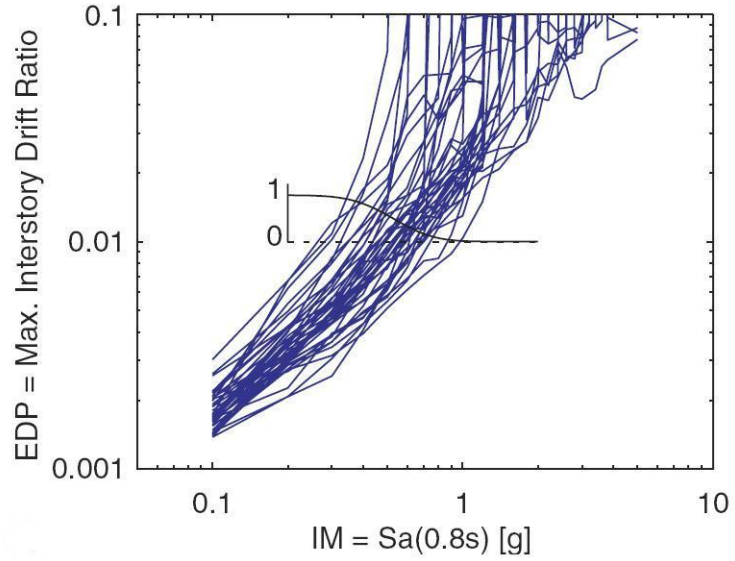

Figure 2-12: Incremental Dynamic Analysis curve and a Gaussian CCDF of Ln IM_{Cap}

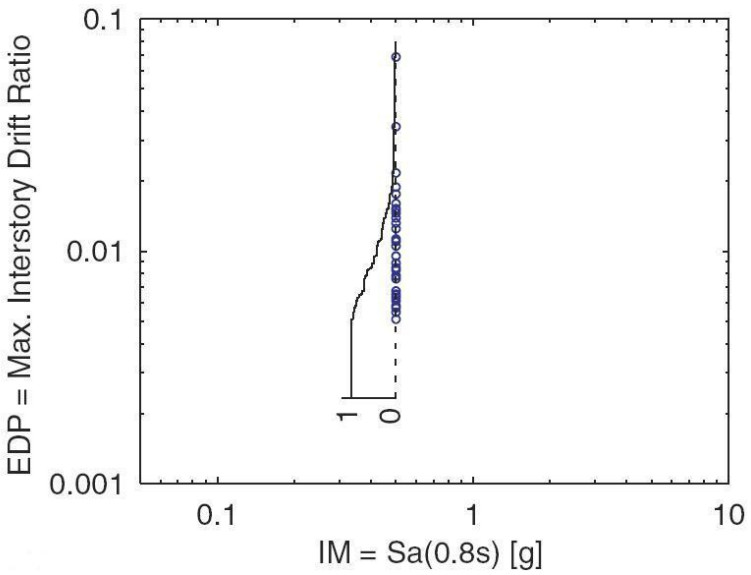

Figure 2-13: A strip of Ln EDP data and its empirical CCDF

CHAPTER THREE

RESPONSE OF MULTI-STORY STRUCTURES TO NEAR-FAULT GROUND MOTIONS

3.1. Introduction

Ground motions close to a fault affected by directivity effects are different from ordinary ground motions (e.g. see Chapter 1). They typically initiate with a high intensity velocity pulse at the beginning of time history records (e.g., see Figure 0-1). In the current state-of-the-practice, forward-directivity effects are introduced in seismic hazard analyses by modifying the ground motion elastic response spectra (Somerville et al. 1997; Abrahamson 2000) and using spectral-based intensity measures to capture structural response (Baker and Cornell 2008). Nevertheless, forward-directivity ground motions typically have large intensities and tend to drive structures into the nonlinear range. For these cases, a linear response spectrum, and in particular the spectral acceleration at the first-mode period of the structure, $S_a(T_1)$, no longer serves as an effective intensity measure (Baker and Cornell 2008). However, forward-directivity ground motions have relatively simple time-domain representations and can be characterized by the period and amplitude of the velocity pulse (Agrawal and He 2002; Mavroeidis and Papageorgiou 2003; Bray and Rodriguez-Marek 2004; Baker 2007a), and these parameters can be used as intensity measures. Moreover, the narrow band nature of the forward-directivity pulse implies that forward-directivity ground motions can be represented using equivalent pulse models (Agrawal and He 2002; Mavroeidis and Papageorgiou 2003). These models have been shown to be an acceptable proxy for pulse-like motions.

In this chapter, the seismic response of three multi-story structures to equivalent pulses is studied. An equivalent pulse model based on the modified Gabor wavelet pulse is selected (Gabor 1946; Mavroeidis and Papageorgiou 2003). The cases for which this equivalent pulse model can capture structural response to forward-directivity ground motions are identified, with particular care to consider separately the response of the structures to the forward-directivity pulse from their response to the high-frequency motion that follows or sometimes overrides the initial pulse. Fifty four forward-directivity and ordinary ground motions are used to obtain statistically significant results.

This chapter first presents a description of the ground motion database used in this study, along with the methodology employed to extract equivalent pulses from the recorded ground motions. The structural models are then described, and their responses to ordinary and forward-directivity ground motion are compared. The parameters of the simplified wavelet pulses are then calibrated such that the equivalent pulses render a similar structural response to that of the recorded forward-directivity records. These parameters are compared to parameters of forward-directivity pulses extracted directly from the recorded ground motions, and cases in which structural response can be predicted with the simplified pulses are identified. Finally, the response of the structures to pulse-type ground motions is summarized in terms of a response surface.

3.2. Ground Motion Records Used in this Study

Twenty-seven forward-directivity ground motions and twenty-seven ordinary ground motions from six earthquakes with moment magnitude (M_w) greater than 6.5 were compiled into a database (Table 3-1 to Table 3-3; Figure 3-1 and Figure 3-2). All records were taken

from stations within 20 km of the fault rupture. Records were selected from a database by Bray and Rodriguez-Marek (Bray and Rodriguez-Marek 2004) and were obtained from the Pacific Earthquake Engineering Research Center database (PEER 1999). Baker's procedure (2007) was used to obtain a pulse-period and amplitude for each of the motions in the forward-directivity database (Table 3-2). The mean value for the ratio of the amplitude of the extracted pulses over the peak ground velocity is 0.73 for the forward-directivity ensemble.

In this study, both the time-domain and frequency-domain scaling methods were examined. The frequency-domain scaling (e.g., scaling to a target spectral acceleration) was not chosen because it alters the characteristics of some of the pulse-like ground motions. In particular, spectral matching using the RSPMatch2005 program (Abrahamson 1993) changed the pulse-like characteristics of two of the pulse-like ground motion records. The time-domain scaling method elevated or plunged response spectra of the records unreasonably. Therefore, a large number of ground motions without any scaling were used to stabilize the statistical analyses.

3.3. Multi-Story Systems

To study the effects of forward-directivity pulses on buildings, three generic buildings were considered. The buildings are seven-story, fourteen-story, and twenty one-stories high. The buildings are devoid of any irregularities. They are designed to have fundamental periods of exactly 1, 2, and 3 seconds, for the seven, fourteen, and twenty one-story buildings, respectively. The structures were designed to have the same base shear coefficient (defined as the base shear that causes yielding in the structure divided by the total weight of the structure). The base shear coefficient was arbitrarily selected to be 0.07. The seismic

resisting system, in the weak direction, consists of four moment resisting steel frames. Each frame has three 20 foot long by 12.5 foot high spans. Details of the building in the strong direction are irrelevant in this study because the structures were only loaded in their weak directions. To reduce computational efforts, the structures were simplified as shear building models.

A MATLAB program (The MathWorks Inc.) was written for conducting 2D nonlinear dynamic analyses of the frames. The step-by-step integration method with the Wilson-Theta modification (Chopra 1995) was used for time integration and the Modified Newton-Raphson Method (Chopra 1995) was used to iterate within each time step. Steel material nonlinearity was modeled by an elastoplastic kinematic hardening relationship, having identical properties in tension and compression. The frames were assumed to have a viscous damping ratio equal to 5%. To enhance analysis accuracy, each story was modeled in SAP2000 and subjected to pushover analysis to get a force-displacement curve for that story. Plastic hinge properties of each member were modeled with a bilinear non-degrading moment-curvature model with a range of strain hardening from 2.5% to 3.5%. These models were obtained from the commercial Xtract software (Imbsen & Associates Inc.) and were assigned to the SAP model at the top and bottom of columns. The member hardening behavior in each story resulted in a story hardening stiffness range of 10% to 12% in the form of force-displacement curves. The force-displacement curves obtained from the SAP pushover analyses for each story were used by the MATLAB program for the dynamic analyses.

P-Δ effects, which can have a significant role in the response of near-fault structures with an excessive drift, were approximated by adding geometric stiffness to the first order stiffness matrix. The geometric stiffness was calculated assuming that axial forces remain constant for the entire duration of the ground motion. Geometric stiffness was calculated based on the shape functions of each column with the two ends fixed against rotation and found to be equal to 1.2P/L where P is axial load and L is length of column.

3.4. Analysis Results

Structural analyses were preformed for each of the three structures described in the previous paragraph using the input ground motions listed in Table 3-2 and Table 3-3 (forward-directivity and ordinary ground motions, respectively). Only the fault normal component of each record was applied to the structures and it was assumed that the weak axes of the structures are perpendicular to the fault. Engineering Demand Parameters such as drift ratio, ductility demand, and story shear forces were monitored. However, the maximum story displacement ductility demand (MSDD) was selected to describe the inelastic response of the structures. The MSDD becomes greater than 1.0 when the relative displacement in any story is larger than the story yield displacement. The maximum inter-story ductility demand (MIDD) was defined as the maximum value of the MSDD over all the stories.

3.5. MSDD for Forward-Directivity and Ordinary Ground Motions

The results of the structural analyses for the ordinary and the forward-directivity ground motion sets are shown in Figure 3-3. The maximum standard deviation of the MSDD for all stories (σ_{max}) is shown for each structure. Observe that the mean structural response is consistently higher for the forward-directivity ground motion set (Figure 3-3b). Even though

the ordinary and the forward-directivity ground motion sets have approximately the same mean PGA (0.49g and 0.48g, respectively), their PGVs are distinctly different due to the presence of the initial velocity pulse (the mean PGV of the forward-directivity set is 81.7 cm/s compared to 42.0 cm/s for the ordinary ground motion set). The initial pulse leads to larger nonlinearities in the system, and thus to a larger structural demand. Moreover, since the structural response appears to be controlled by the initial pulse, and this pulse varies widely from one ground motion to another, the dispersion in the structural response is larger for the forward-directivity set, as evidenced by the larger values of the maximum standard deviation (σ_{max}) of MSDD when the structure is subject to forward-directivity ground motions (Figure 3-3b) as opposed to ordinary ground motions (Figure 3-3a).

The observations made in Figure 3-3 are reinforced when a comparison is made of the inelastic response of the 7-story structure to forward-directivity and ordinary records from selected earthquakes (Figure 3-4). The structural response is different for ordinary and forward-directivity ground motion ensembles within the same earthquake; the mean value of response for each earthquake shows that forward-directivity ground motions impose higher demand to the structure compared to ordinary ground motions. Results for the other two buildings are qualitatively similar.

The force-displacement curves of the seven-story structure subjected to ordinary and pulse-like records are shown in Figure 3-5. As shown in the figure, the lateral displacement and shear forces under forward-directivity ground motions are much higher than those under ordinary ground motions with the same PGA but different PGV. It is worth noting that the peak displacement and the corresponding forces are generated at the beginning of the record

due to the forward-directivity pulse. This pulse imposes severe demands to the structure. The arrival of the velocity pulse causes the structure to dissipate considerable input energy in relatively few plastic cycles.

Different damping values ranging from 5 to 15% were considered in order to investigate the effects of damping on the response of the structures subjected to pulse-like ground motions and ordinary ground motions. It was found that damping does not play a larger role in the response of the structures subjected to pulse-like ground motions than it does in structures subjected to ordinary ground motions, as would be expected given that viscous damping is proportional to velocity. Moreover, damping forces are slightly less effective when the structures are subjected to pulse-like ground motions compared to ordinary ground motions. This is because damping forces do not have enough time to dissipate significant energy in forward-directivity ground motions because of the short duration of the large-amplitude cycle. The same result was obtained by Naeim (1996). For this reason, variations in structural response with respect to damping are ignored in the reminder of this chapter and results are presented only for a viscous damping value of 5%.

3.6. Predictive Power of different IMs

The response of the three structures in terms of MIDD as a function of three different intensity measures (PGA, $S_a(T_1)$, and PGV) are presented in Figure 3-6. The best-fit curve for the data is also shown separately for the forward-directivity and ordinary ground motion sets. A power-law model was used to correlate MIDD with each intensity measure. This model is constrained to increase monotonically and to produce values of MIDD ≥ 1. The best-fit parameters were obtained using Maximum Likelihood estimation and are given in

Table 3-4. No effort was made to use functional forms that can be extrapolated; hence the curves shown are valid only within the range of the data shown. Observe that when the IM is either PGA or the spectral acceleration at the first mode period, the MIDD for the forward-directivity ground motions is higher than the MIDD for the ordinary ground motions; hence, different correlations should be used for forward-directivity and ordinary ground motions, in particular for higher IM. When the IM is PGV, the MIDD values for both the forward-directivity and the ordinary ground motion sets are similar over the range of the data. These observations suggest that PGV is a more stable IM for near-fault ground motions.

The standard deviation of the residuals (e.g. the MIDD for each ground motion minus the best fit curve) is a measure of how well an IM can predict the MIDD. However, the standard deviations of the residuals for the plots shown in Figure 3-6 increase with IM. Hence, a direct comparison of standard deviations of the forward-directivity and the ordinary ground motion sets cannot be made because the forward-directivity ground motion data set has, in general, higher values of the IM. The use of the coefficient of variation (e.g. the standard deviation normalized by the mean) is also misleading because of the wide range of MIDD values within each data set. Hence, an alternate normalization procedure is proposed with the objective of obtaining a single measure that can serve to quantify the quality of the fit for the relationships shown in Table 3-4. First, the standard deviation was allowed to vary linearly within the Maximum Likelihood model. A new parameter, σ_{10}, was then defined as the standard deviation when MIDD is equal to 10. This parameter permits a comparison of the standard deviations at a single value of MIDD and hence can be used on data sets with widely different values of MIDD. A large σ_{10} implies a poor correlation between MIDD and the IM, while a small σ_{10} implies that the IM is a good predictor of MIDD. The σ_{10} values

computed separately for forward-directivity and ordinary ground motions are shown in Figure 3-6 and listed in Table 3-5. For completeness, other measures of dispersion (e.g. standard deviation and coefficient of variation) are also listed in Table 3-5.

The poor correlation between MIDD and PGA (Figure 3-6a; also see the high values of σ_{10} in Table 3-5 for PGA compared to those for other IM) indicates that PGA is a poor predictor of structural response for both ordinary and forward-directivity ground motions. Also observe that $S_a(T_1)$ is a better predictor of MIDD for ordinary ground motions than for forward-directivity ground motions (Figure 3-6b; also see in Table 3-5 that σ_{10} is significantly lower for non-forward-directivity ground motions than for forward-directivity ground motions). This variability in standard deviations can be important when using traditional hazard analyses for forward-directivity ground motions. PGV is a better predictor of MIDD than $S_a(T_1)$ for all the cases studied except for the 21-story building subject to the ordinary ground motion data set (Figure 3-6c, Table 3-5). This suggests that PGV is a better predictor of structural response both for ordinary and forward-directivity ground motions recorded in the near-fault region, and hence it should be used as an IM instead of spectral accelerations at the first mode period. The above results highlight the need to search for alternative ways to determine structural demand for structures subjected to forward-directivity ground motions. In the next sections, an alternative approach using simplified pulse representations of forward-directivity motions is explored.

3.7. Equivalent Gabor Pulse Model

Wavelets are basis functions that can be used to divide a given function or continuous-time signal into different frequency components. One such wavelet was proposed by Gabor

(1946). Later, Mavroeidis et al. (2003) replaced the Gaussian envelope of the Gabor wavelet with another symmetric bell-shaped function that possesses a simpler analytical expression. The velocity time history of the resulting wavelet is expressed as:

$$V(t) = \begin{cases} A\frac{1}{2}[1+\cos(\frac{2\pi f_p}{\gamma}(t-t_0))]\cos[2\pi f_p(t-t_0)+\nu], & t_0 - \frac{\gamma}{2f_p} \le t \le t_0 + \frac{\gamma}{2f_p} \quad \textit{with} \quad \gamma > 1 \\ 0, \textit{ otherwise} \end{cases} \tag{3-1}$$

where, A controls the amplitude of the wavelet, f_p is the frequency of the amplitude-modulated harmonic (or the prevailing frequency of the signal), ν is the phase of the amplitude-modulated harmonic (i.e., $\nu = 0$ and $\nu = \pm\pi/2$ define symmetric and antisymmetric signals, respectively), γ is a parameter that defines the oscillatory character (i.e., zero crossings) of the signal, and t_o specifies the location in time of the envelope's peak. An illustrative example of this pulse is shown in Figure 3-7. In this study, only $\nu = 0$ was considered in order to achieve an equivalent pulse with a lower number of parameters. Hence, the parameters needed to define the Gabor wavelet pulse are A, f_p, and γ.

A methodology was developed to constrain the parameters of the Gabor pulse such that the structural response to the pulses is similar to the structural response to recorded forward-directivity ground motions. The parameter γ was selected based on the number of peaks and troughs of the forward-directivity pulse extracted using Baker's procedure. Parameters A and f_p were obtained by minimizing the differences between the MSDD due to the recorded forward-directivity ground motions and the MSDD values due to the Gabor wavelet pulses. The minimization criterion was defined as

$$factor_{Minimization} = \frac{\sum_{i=1}^{\#story} \frac{\left|(MSDD_{pulse-like})_i - (MSDD_{Gabor})_i\right|}{(MSDD_{pulse-like})_i}}{\#story} \quad (3\text{-}2)$$

where, $(MSDD_{pulse\text{-}like})_i$ is the maximum story ductility demand due to the pulse-like ground motion in each story and $(MSDD_{Gabor})_i$ is the maximum story ductility demand due to the Gabor wavelet pulse in each story. The parameters of the Gabor wavelet pulse after minimization are tabulated in Table 3-6. Structural response was not very sensitive to the value of the parameter γ, hence only two parameters (A_p and f_p) control structural response. The MSDD due to the Gabor pulses were compared to the MSDD due to the pulse-like ground motions for cases in which the period of the forward-directivity pulses are roughly equal to the period of the structures (Figure 3-8b) and cases in which the periods are significantly different (Figure 3-8a and c). Observe that there is a close agreement between the displacement ductility demand due to the simplified pulses and the recorded forward-directivity ground motions.

Different damping values were considered to investigate the effects of damping on the response of the structure subjected to pulse-like ground motions versus ordinary ground motions. The structural responses of the buildings with 5%, 10%, and 15% damping ratios subjected to pulse-like and ordinary ground motions were compared using a simple criterion defined as the following:

$$(contributi\ on_{damping})_{FD} = \frac{1}{\#records} \cdot \sum_{i=1}^{\#records} \frac{[(MIDD_{5\%})_{FD}]_i - [(MIDD_{10\%or15\%})_{FD}]_i}{[(MIDD_{5\%})_{FD}]_i} \quad (3\text{-}3)$$

$$(contributi\ on_{damping})_{NonFD} = \frac{1}{\#records} \cdot \sum_{i=1}^{\#records} \frac{[(MIDD_{5\%})_{NonFD}]_i - [(MIDD_{10\%or15\%})_{NonFD}]_i}{[(MIDD_{5\%})_{NonFD}]_i} \quad (3\text{-}4)$$

where $(MIDD_{\zeta})_{FD}$ and $(MIDD_{\zeta})_{NonFD}$ are the maximum inter-story ductility demands of the structure with damping ratio ζ for pulse-like and ordinary ground motions, respectively. $(contribution_{damping})_{FD}$ and $(contribution_{damping})_{NonFD}$ are additional damping forces due to the increase of damping of the structure subjected to pulse-like and ordinary ground motions, respectively.

As an example, results for a 7-story building are tabulated in Table 3-7. It was found that the damping value does not play a more significant role in structures subjected to pulse-like ground motions than structures subjected to ordinary ground motions. Moreover, damping forces are less effective when the structures are subjected pulse-like ground motion compared to ordinary ground motions. As explained by Naeim (1996), this is due to

> "… the maximum response to an impulse load will generally be attained on the first cycle. For this reason, the damping forces do not have time to absorb much energy from the structure. Therefore, damping has a limited effect in controlling the maximum response and is usually neglected when considering the maximum response to impulse type loads" (Naeim, 1996).

3.8. Discussion

The parameters of the Gabor pulses (pulse period and pulse amplitude) were obtained by matching the structural response of the multi-story structures such that the response to the

Gabor pulse was similar to the response of recorded forward-directivity pulses. When the pulse parameters match those obtained directly from the velocity time histories of recorded ground motions (using Baker's procedure (2007)), it implies that structural response is controlled by the forward-directivity pulses. This is the case when the ratio of pulse period to the fundamental period of the structure falls in a range between 0.5 and 2.5 (Figure 3-9). In this range of pulse periods, 85% of the Gabor pulse periods are within 20% of the pulse period of the extracted forward-directivity pulses. Therefore, in this range of periods the response is controlled by the forward-directivity pulse and the Gabor wavelet pulses are capable of both reproducing structural response to forward-directivity ground motions and accurately resembling the recorded motions. Outside of this range, additional analyses indicated that structural response is controlled by the higher frequency content of the ground motions that either overrides or follows after the forward-directivity pulse. The higher frequency content elicits contribution of higher structural modes. In these cases, the pulse parameters are not adequate IM. Note that the Gabor pulses are still able to mimic structural response to recorded ground motions, but in these cases those pulses have no resemblance to the recorded ground motions and have no predictive value. The amplitude of the Gabor pulses obtained using the minimization procedure in Equation 3-2 is on average 73% of the PGV (with standard deviation of 0.22). Hence, attenuation relationships for PGV can be used to predict the amplitude of the pulses.

To better understand why structural response is controlled by the forward-directivity pulse only when $0.5 \leq T_{pulse}/T_{structure} \leq 2.5$, it is helpful to look at the response spectra of the ground motions, the forward-directivity pulse alone, and the Gabor pulse used to match structural response. Figure 3-10 shows the velocity response spectra of recorded forward-

directivity pulses, the extracted pulses using Baker's procedure, and the Gabor pulses with parameters selected to match the MIDD of the structure. Fundamental periods of the structures have been marked on the horizontal axes. Note that when $0.5 \leq T_{pulse}/T_{structure} \leq 2.5$, the recorded ground motions, the extracted pulses, and the Gabor pulses have peaks at approximately the same spectral period and, importantly, this period coincides with the fundamental structural period (Figure 3-10b). On the other hand, when the period of the forward-directivity pulse is much shorter or longer than the fundamental period of the structure ($T_{pulse}/T_{structure}<0.5$ or $T_{pulse}/T_{structure} > 2.5$), the velocity response spectrum of the Gabor pulses does not closely match the velocity response of the extracted pulses and ground motion records. However, there is another peak in the velocity response spectrum of the ground motion records in the vicinity of the fundamental period of the structure that controls the behavior of the structure (Figure 3-10a and c). In Figure 3-10a, these peaks are related to shorter periods (higher frequencies) in the recorded ground motions that are filtered out when simplified pulses are used to represent the ground motions. In Figure 3-10c, the periods of forward-directivity pulses are too long to excite the structure. Therefore the response of the structure is governed by other frequencies, close to those of the structure.

The distribution of the MSDD changes depending on the value of the pulse parameters. The critical story shifts from the base of the structure to higher stories with a decrease of the period of the pulse. However, the value of the ductility demand decreases as the period of the pulse decreases. In general, the distribution of the MSDD may be classified into three groups (Figure 3-11). For example, if we consider the 14-story structure, for pulses with long periods ($T_p > 0.7$ sec), the critical story is at the base. For pulses in the intermediate period range ($0.4 < T_p \leq 0.7$ sec), the critical story moves to higher stories. For pulses with shorter

periods ($T_p \leq 0.4$ sec), the distribution of the MSDD tends toward a uniform shape over the height of the structure. These period ranges change from structure to structure. This distribution of the MSDD cannot be captured by an elastic or spectral analysis which is based on $S_a(T_1)$.

Given that Gabor wavelet pulses can reasonably represent near-fault ground motions when their pulse period is in the neighborhood of the fundamental period of the structure ($0.5 \leq T_{pulse}/T_{structure} \leq 2.5$ for the structures studied herein), multiple runs can be used to predict the inelastic response of the structure for pulses with all possible amplitudes and periods in this range. Thus, the inelastic response of structures can be predicted for a range of forward-directivity pulses with realistic amplitudes and frequencies (Figure 3-12). The short period region of the response surface in Figure 3-12 is less smooth than the response at other period ranges, indicating that there are no clearly defined trends in the response of the structure in this region. This likely happens because the contribution of higher modes becomes predominant. A response surface such as that shown in Figure 3-12 can be coupled with Probabilistic Seismic Hazard Analyses to predict structural response (see Chapter 4). When $T_{pulse}/T_{structure}$ is outside of the defined range, the forward-directivity pulse may not control response and other IMs must be selected for predicting structural response.

In the International Building Code (IBC 2006), vertical distribution of seismic forces in buildings that comply with the limitations for the use of the *Simplified Analysis* and *Equivalent Lateral Force Procedures* is based on first mode domination. This implies that maximum demand occurs at the base of the building. By contrast, for forward-directivity

input motions, the critical story (the story which has maximum MSDD) is not always at the base of the structure.

Analyses were repeated without consideration of P-Δ effects. The mean values of MSDD for each ensemble with and without consideration of P-Δ effects are shown in Figure 3-13. It was found that the P-Δ effect decreases the stiffness of the system, elongates the fundamental period of the structure, and imposes more demand to the base of the structure. P-Δ effects are more significant for records that cause more drift to the structure. Figure 3-13 shows that P-Δ effects are more significant for forward-directivity records and especially for taller structures. For example, when P-Δ effects are considered, the mean value of MSDD computed at the base of the 7, 14, and 21-story structures increased by 6%, 16%, and 22%, respectively, for the forward-directivity ground motion data set. For all the cases when the critical story occurs at the base, P-Δ effects increased MIDD and the critical story remained at the base. On the other hand, no consistent trend was observed when the critical story was one of the middle stories. On 75% of these cases, P-Δ effects increased the value of MIDD and the critical story either stayed in the same floor, moved to the base, or shifted to other stories. In the remaining 25% of the cases, the critical story location either remained or shifted to other floors, but the value of MIDD decreased.

Response of the structures with different damping ratios (5%, 10%, and 15%) to pulse-like and ordinary ground motions was studied. Since the maximum response of the structures to pulse-like ground motions is attained on the first cycles, the damping forces do not have time to absorb much energy from the structures and they are not as effective as when the structures are excited with ordinary ground motions.

3.9. Conclusions

In this chapter, the inelastic dynamic response of three different typical steel structures has been investigated to study the effects of forward-directivity. In addition, the idea of simplifying near-fault ground motions with equivalent pulses to predict the behavior of structures in the near-fault region was investigated. It was shown that, in general, the spectral acceleration at the first-mode period of vibration is not the ideal IM to capture structural response to pulse-like ground motions. On the other hand, dynamic analyses using an equivalent pulse model renders similar structural response to that computed for forward-directivity pulses when $0.5 \leq T_{pulse}/T_{structure} \leq 2.5$. In this period range, the response of structures is controlled by forward-directivity pulses and equivalent pulses can be used to predict structural response. Outside of this range, the response of the structures is not controlled by the forward-directivity pulse.

The shape of the MSDD distribution and location of the critical story are influenced heavily by the period and amplitude of the forward-directivity pulse. The MSDD is higher at the base when ground motions contain forward-directivity pulses with longer periods (e.g., for larger magnitude earthquakes). The critical story shifts up when the pulse period is shorter. This distribution of the MSDD has not been considered in building codes such as the IBC which assume that the maximum demand occurs at the base. Therefore, revisions for the codes to consider this issue are recommended.

P-Δ effects can be significant for structures subject to forward-directivity ground motions and should be accounted for in design. On the other hand, damping forces are less important in structures that are subjected to pulse-like ground motion compared to ordinary

ground motions. This study was based on the response of three generic buildings, hence care must be exercised when generalizing the results presented herein. Moreover, only the response of the buildings to the fault-normal component of all ground motions was considered.

3.10. Figures

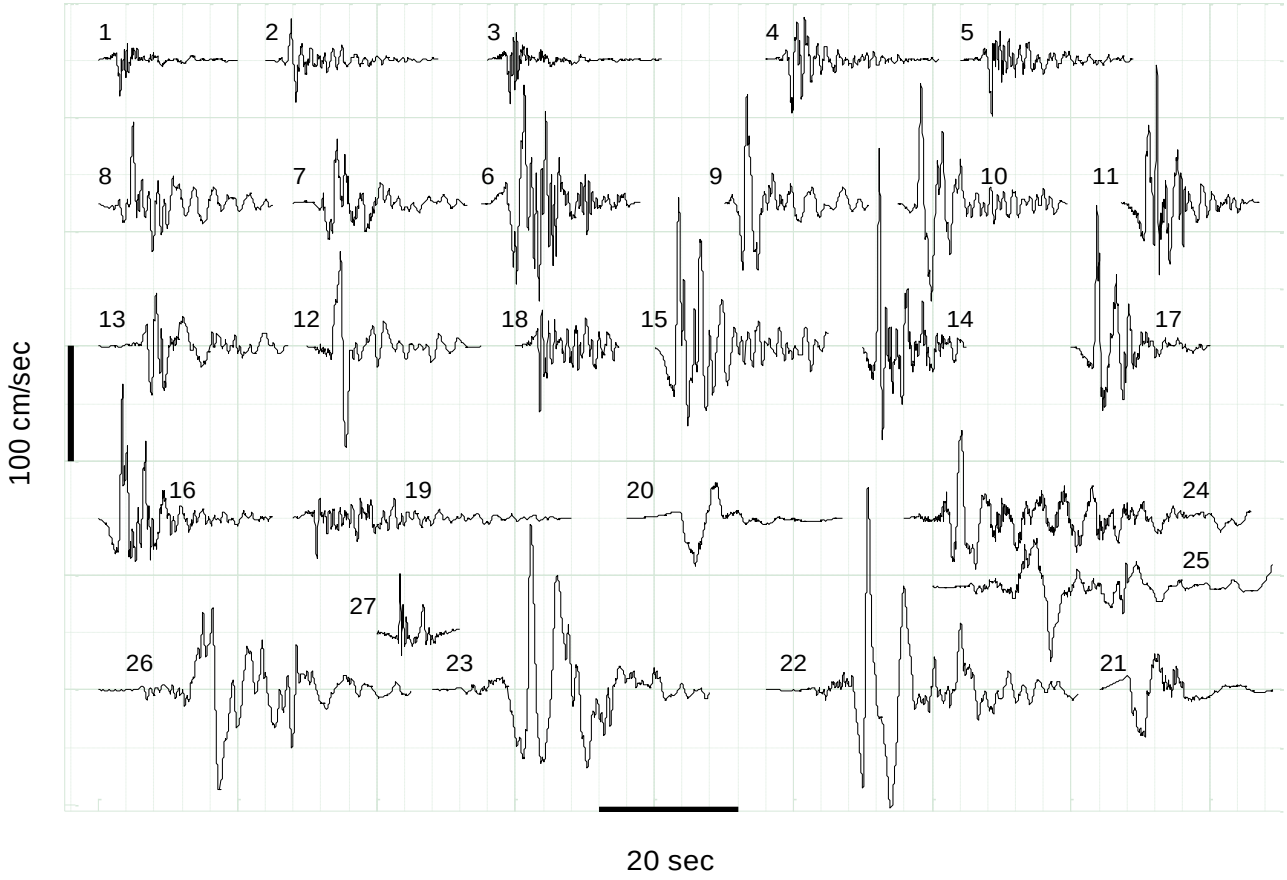

Figure 3-1: Velocity time histories of the forward-directivity ground motions used in this study.
For ground motion information see Table 3-2

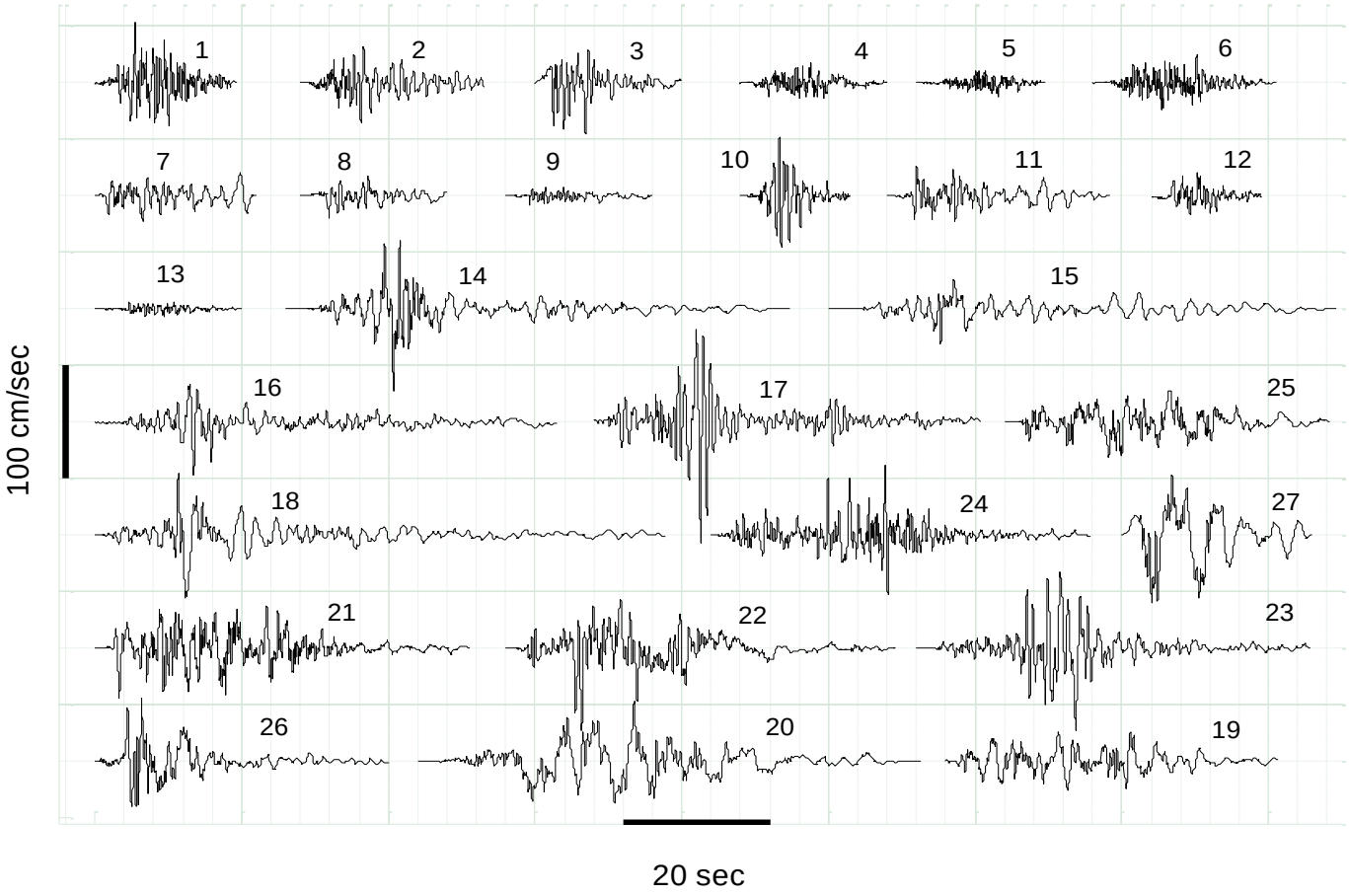

Figure 3-2: Velocity time history of the near-fault ordinary ground motions used in this study.
For ground motion information see Table 3-3

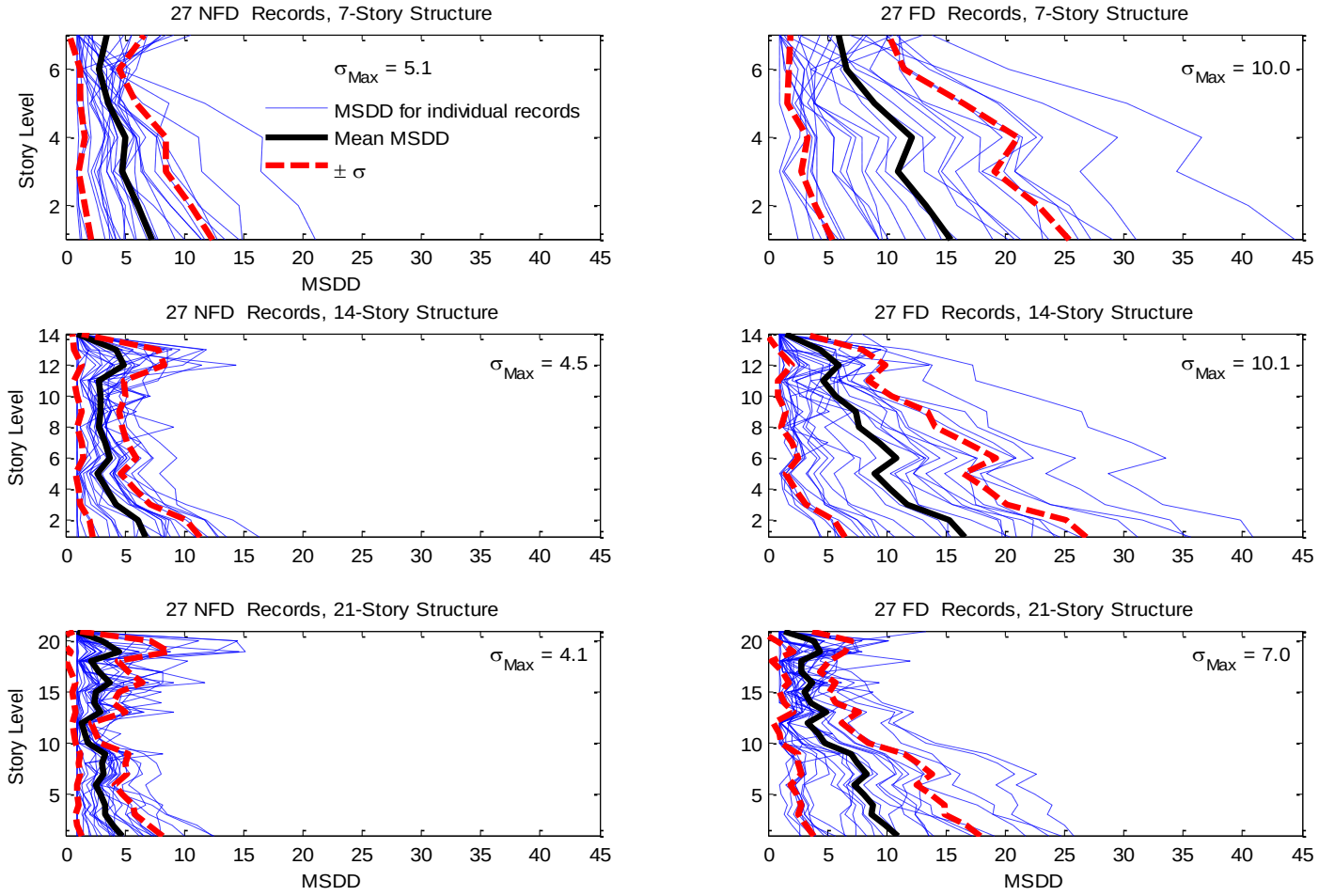

Figure 3-3: Maximum story ductility demand for (a) 27 non forward-directivity (NFD) records and (b) 27 forward-directivity (FD) records

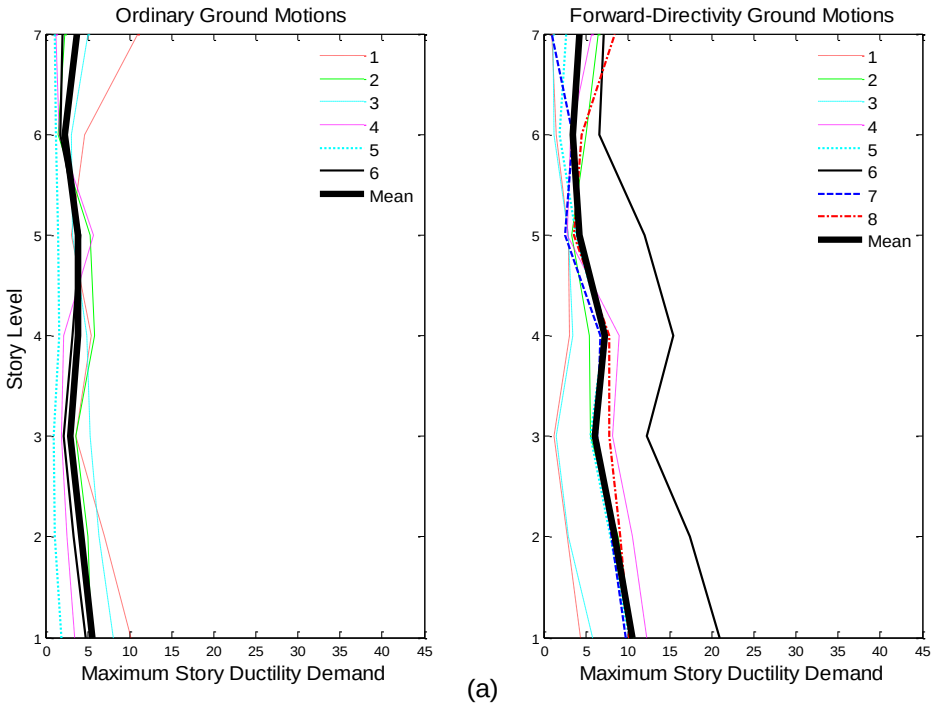
Ordinary Ground Motions
Forward-Directivity Ground Motions
Story Level
Maximum Story Ductility Demand
1
2
3
4
5
6
7
8
Mean

(a)

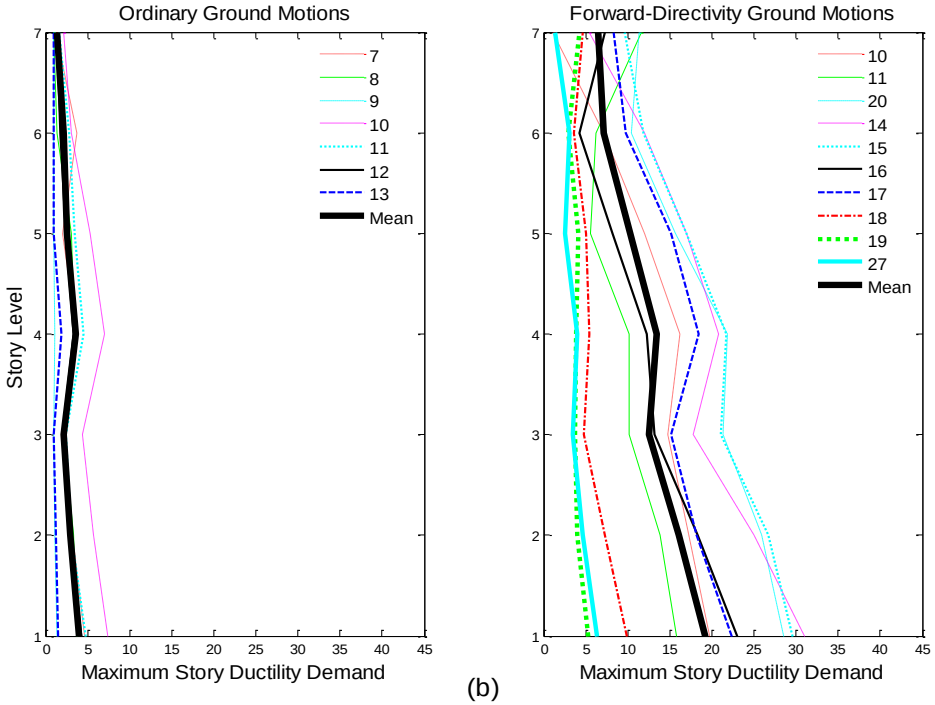
Ordinary Ground Motions
Forward-Directivity Ground Motions
Story Level
Maximum Story Ductility Demand
7
8
9
10
11
12
13
Mean
20
14
15
16
17
18
19
27

(b)

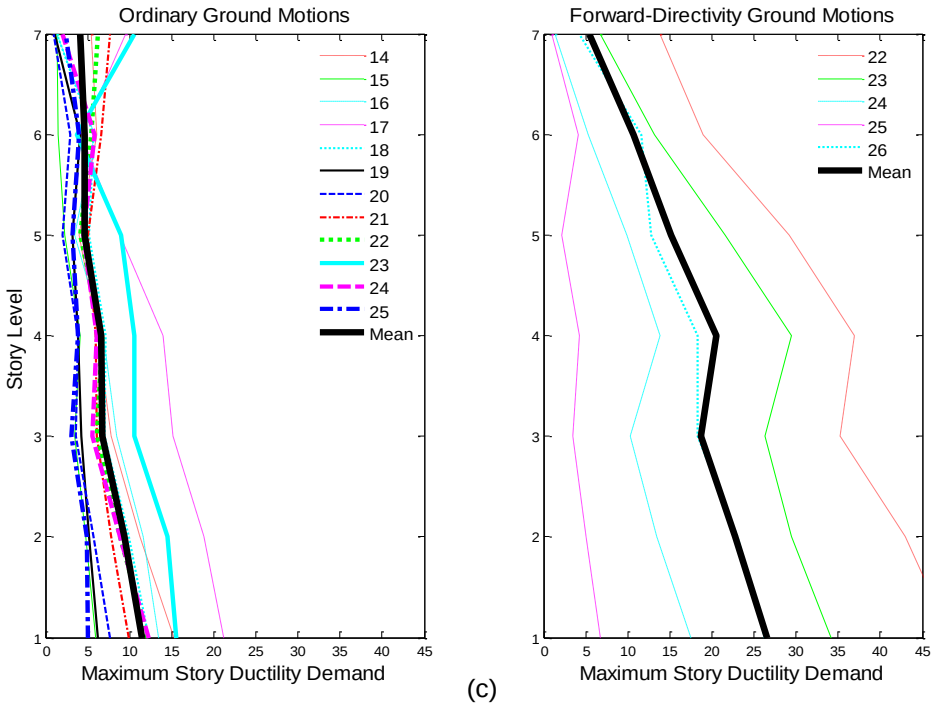

Figure 3-4: Maximum story ductility demand of the 7-story structure subjected to ordinary and forward-directivity ground motions from the (a) Loma Prieta, (b) Northridge, and (c) Chi-Chi earthquakes. For ground motion see Table 3-2 and Table 3-3.

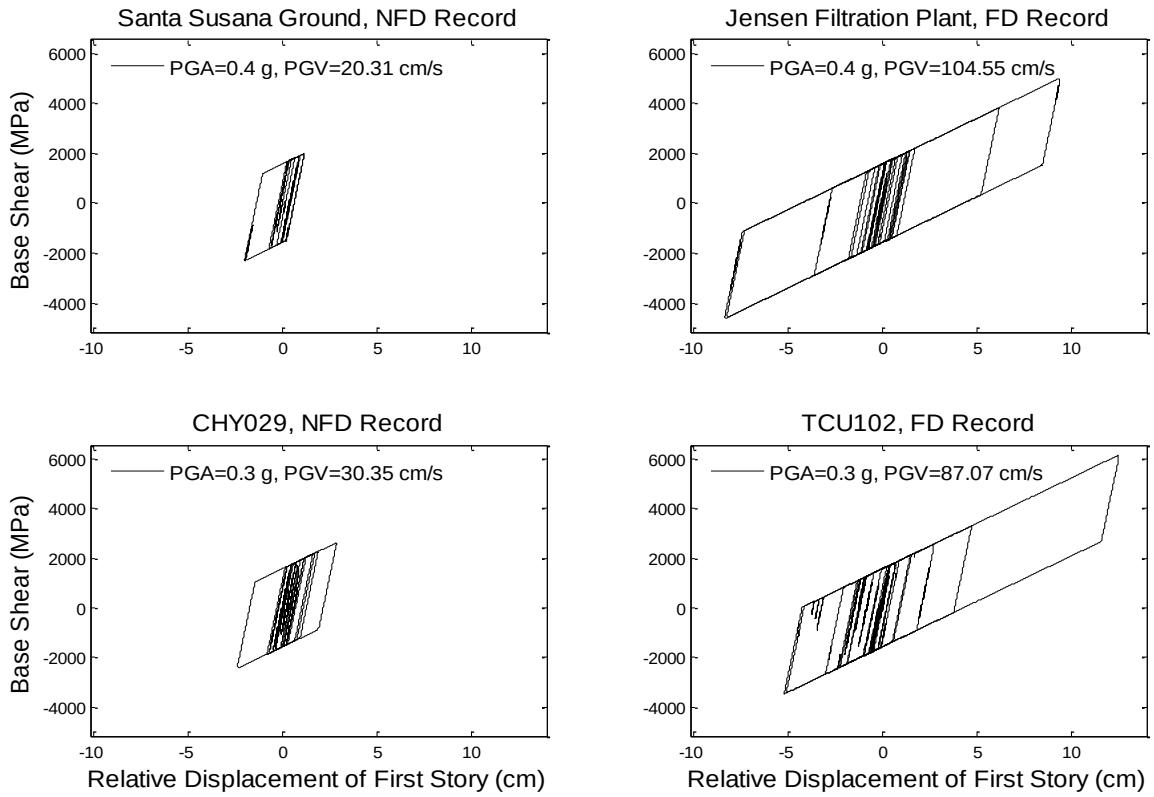

Figure 3-5: Story shear vs. relative displacement of the 7-story structure at its base, for (a) ordinary ground motion (e.g. Non-Forward-Directivity, NFD) and (b) pulse-like ground motions (e.g. Forward-Directivity, FD)

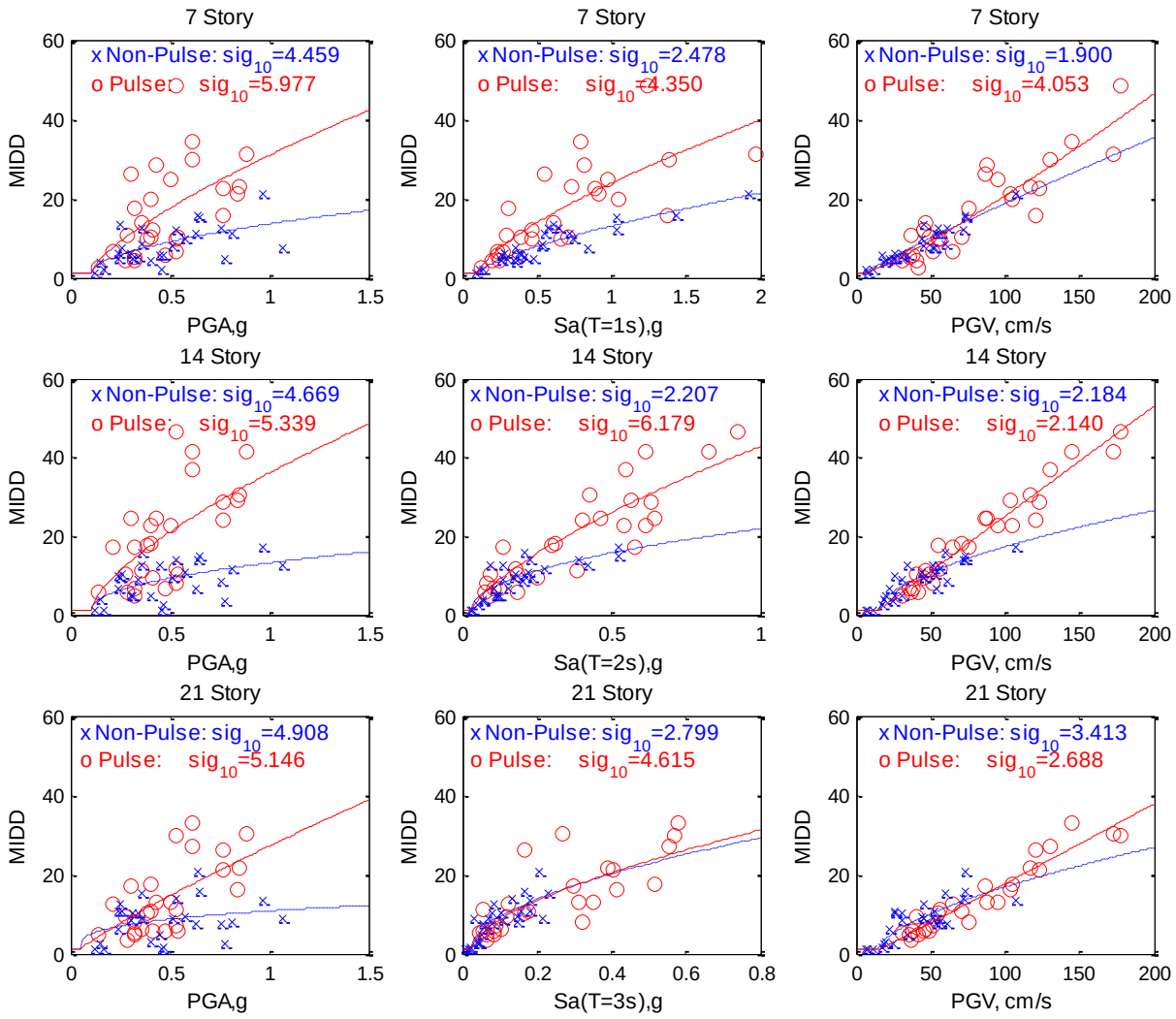

Figure 3-6: Maximum inter-story ductility demand for the 7, 14, and 21 story structures subjected to pulse and non-pulse ground motion ensembles plotted versus different Intensity Measures. Continuous and dashed lines represent the median response for the Pulse and Non-Pulse ground motion ensembles, respectively.

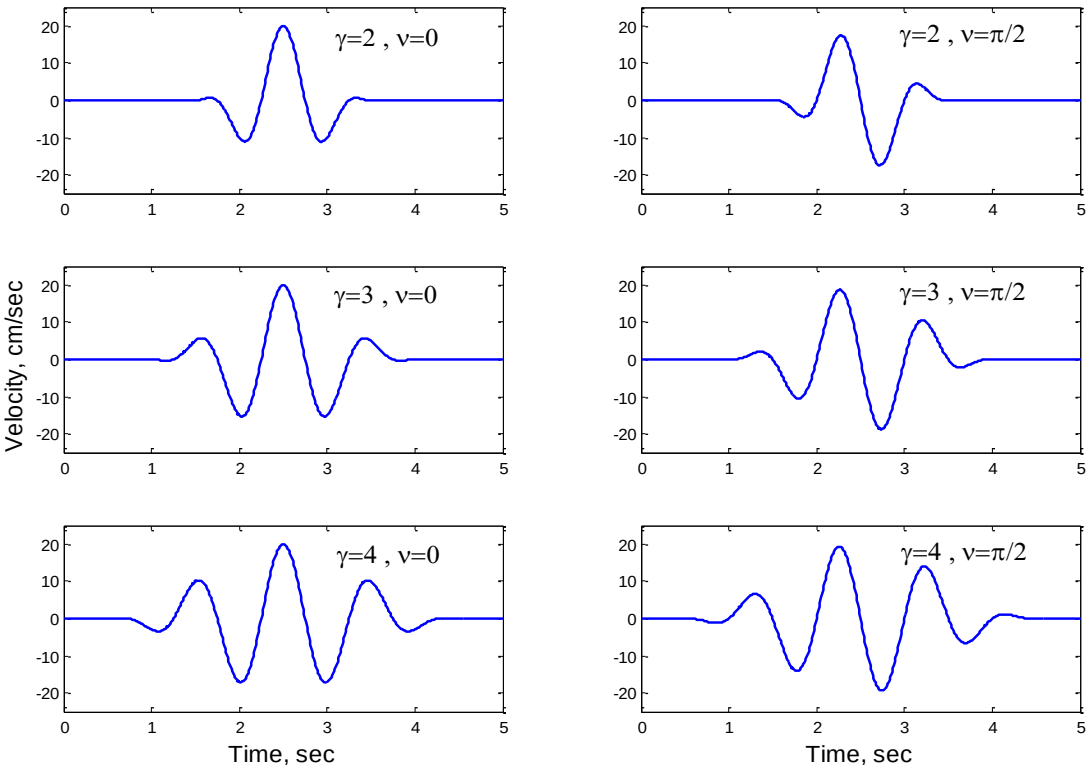

Figure 3-7: Gabor wavelet pulses with parameters A = 20 cm/sec, f_p = 1 Hz, and t_o = 2.5 sec.

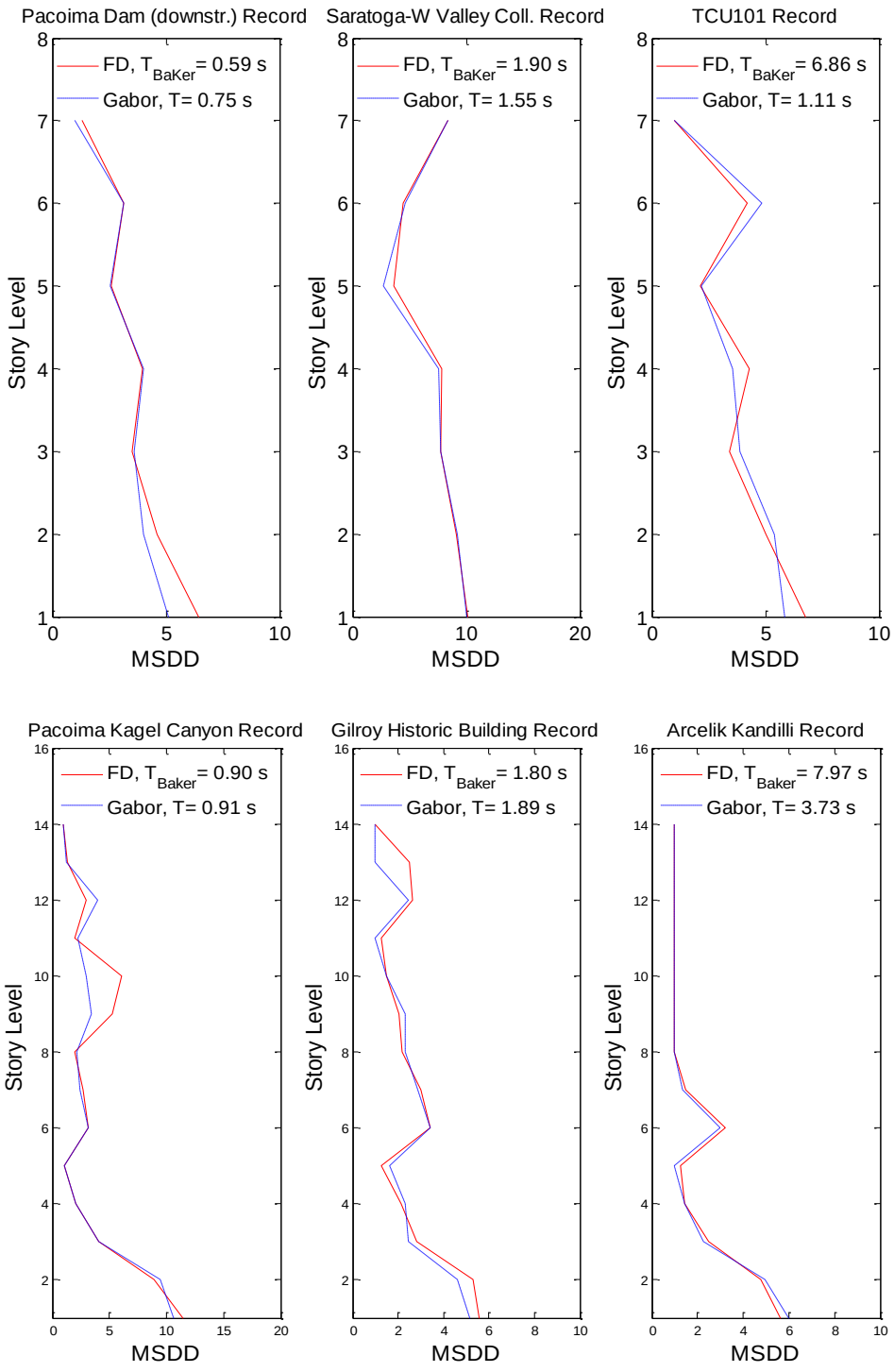
Pacoima Dam (downstr.) Record
FD, T_BaKer= 0.59 s
Gabor, T= 0.75 s
Saratoga-W Valley Coll. Record
FD, T_BaKer= 1.90 s
Gabor, T= 1.55 s
TCU101 Record
FD, T_BaKer= 6.86 s
Gabor, T= 1.11 s
Pacoima Kagel Canyon Record
FD, T_Baker= 0.90 s
Gabor, T= 0.91 s
Gilroy Historic Building Record
FD, T_Baker= 1.80 s
Gabor, T= 1.89 s
Arcelik Kandilli Record
FD, T_Baker= 7.97 s
Gabor, T= 3.73 s
Story Level
MSDD

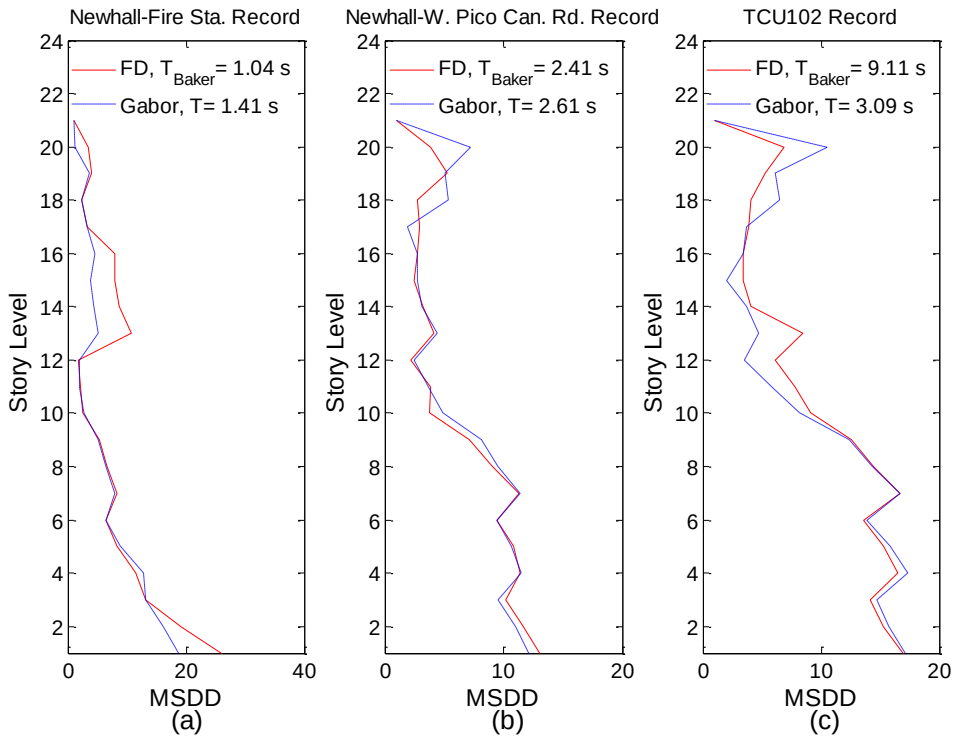

Figure 3-8: Maximum story ductility demand for pulse-like ground motion and Gabor wavelet pulses.
(a) when pulse period is significantly shorter than structural period (b) when pulse period approximately matches structural period (c) when pulse period is significantly longer than structural period. The first, second, and third rows correspond to the 7, 14, and 21 story structures, respectively.

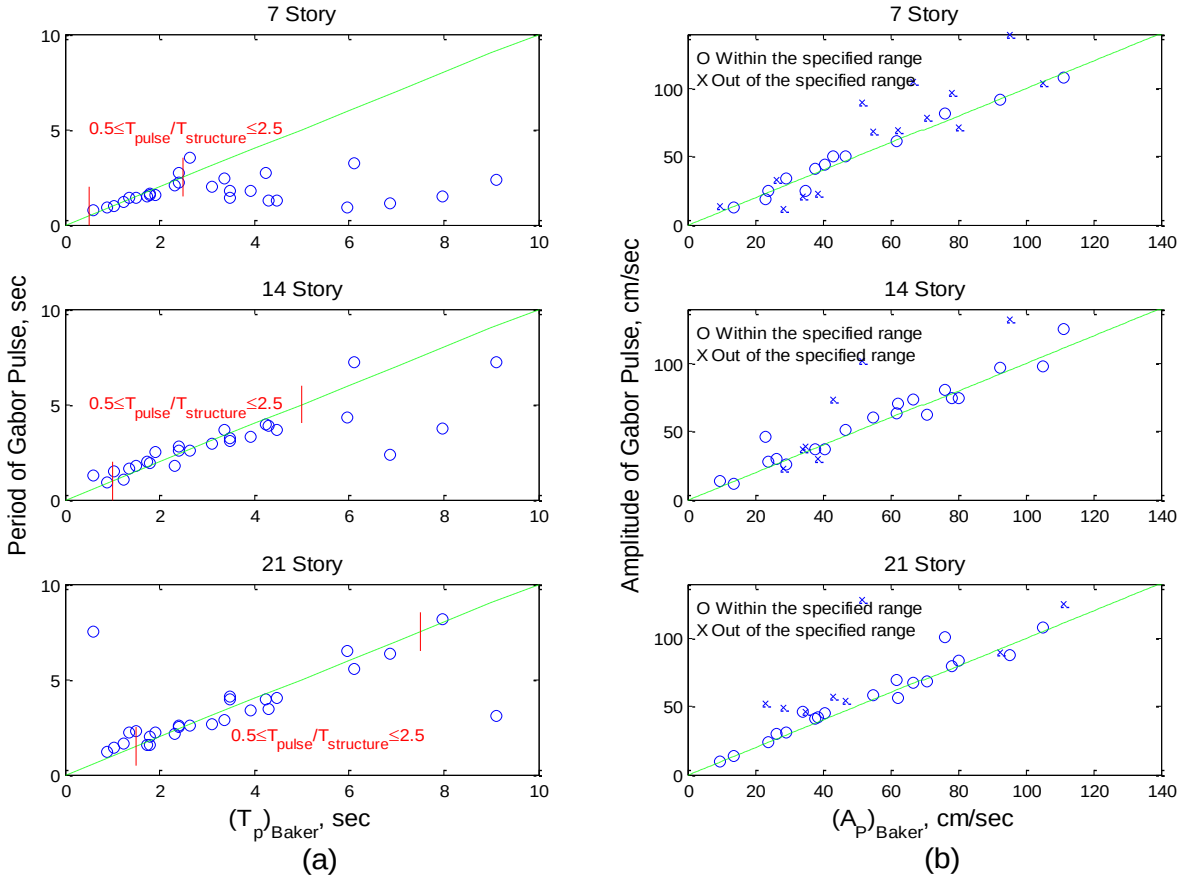

Figure 3-9: Comparison of (a) the periods and (b) the amplitudes of the Gabor pulses and the parameters of the forward-directivity pulses.

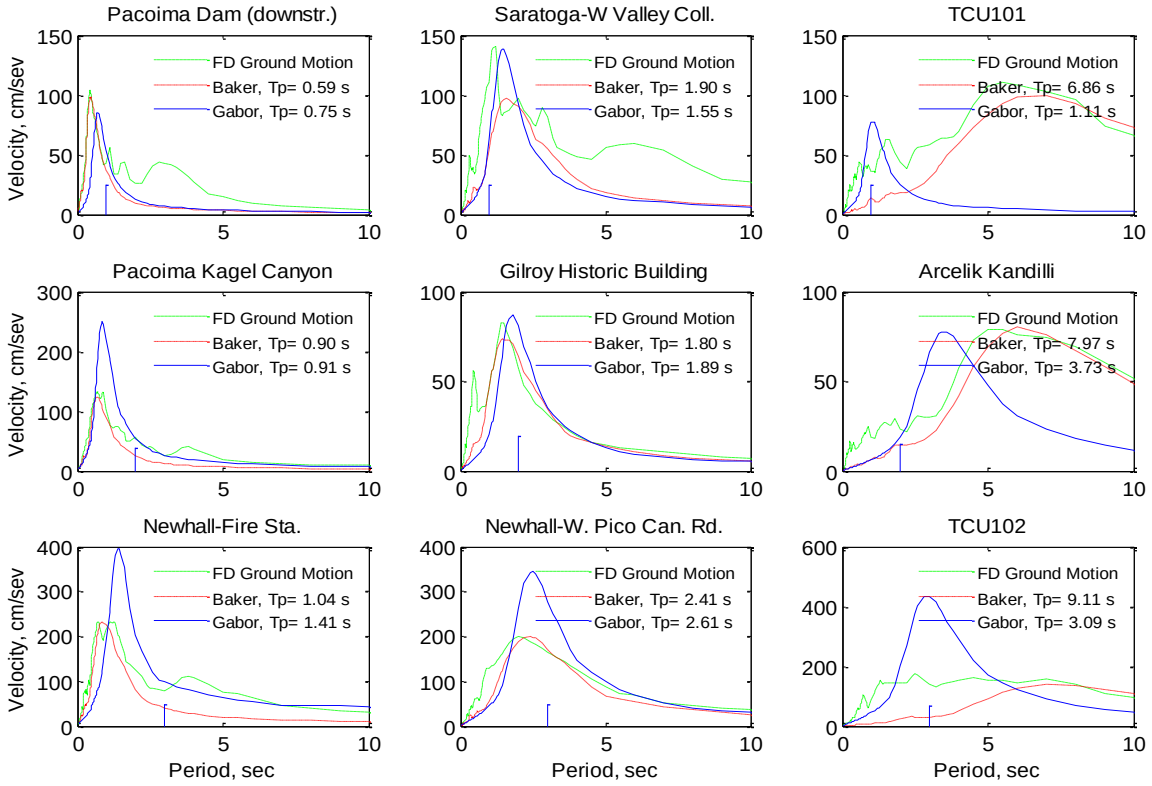

Figure 3-10: Velocity response spectra for the recorded pulse-like ground motion
The extracted wavelet pulse, and the Gabor wavelet pulse for selected forward-directivity ground motions (a) when $0.5 > T_{pulse}/T_{structure}$, (b) when $0.5 \leq T_{pulse}/T_{structure} \leq 2.5$, (c) when $T_{pulse}/T_{structure} > 2.5$. The first, second, and third rows correspond to the 7, 14, and 21 story structures, respectively. (These spectra correspond to the input ground motions used in the analyses shown in Figure 3-8).

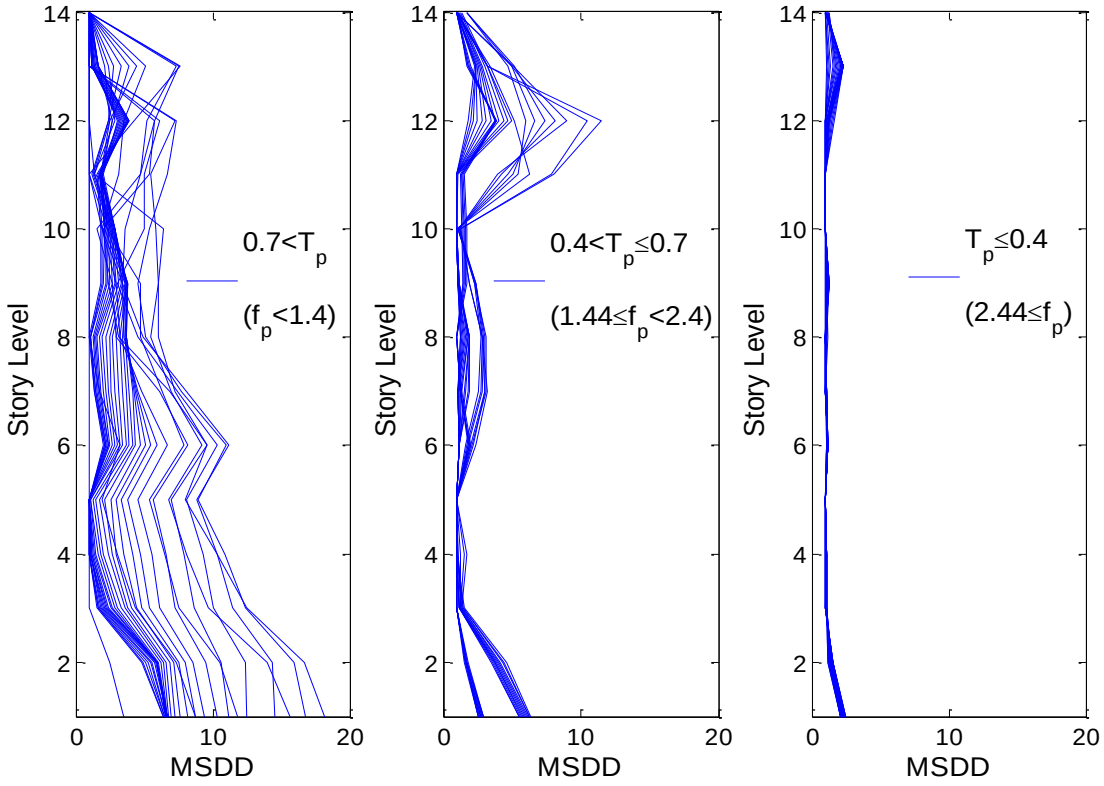

Figure 3-11: Distribution of maximum story ductility demand of the 14-story building for Gabor wavelet pulses with long ($T_p > 0.7$ sec), intermediate ($0.4 < T_p \leq 0.7$ sec), and short periods ($T_p \leq 0.4$ sec) A=40 cm/sec. Results for other buildings are qualitatively similar.

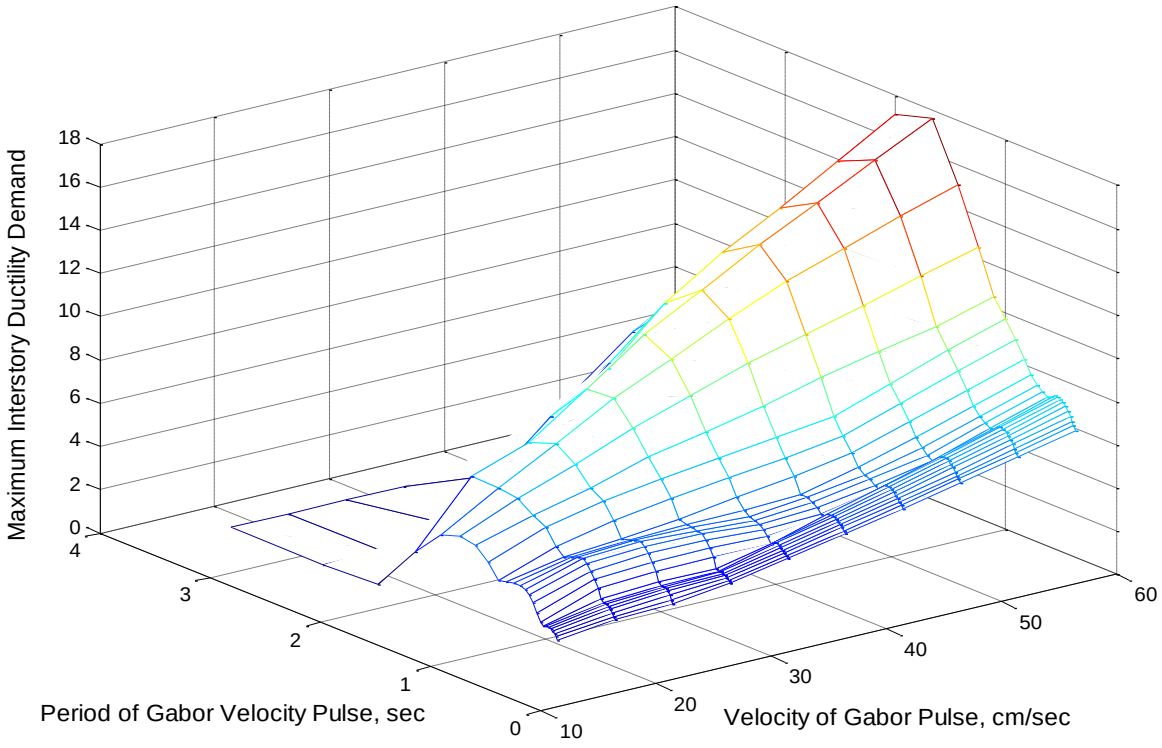

Figure 3-12: Maximum inter-story ductility demand of the 7-story structure for Gabor pulses with parameters $\gamma = 3$, $15 < A < 60$ cm/s, and $0.37 < T_p < 3.33$ s.

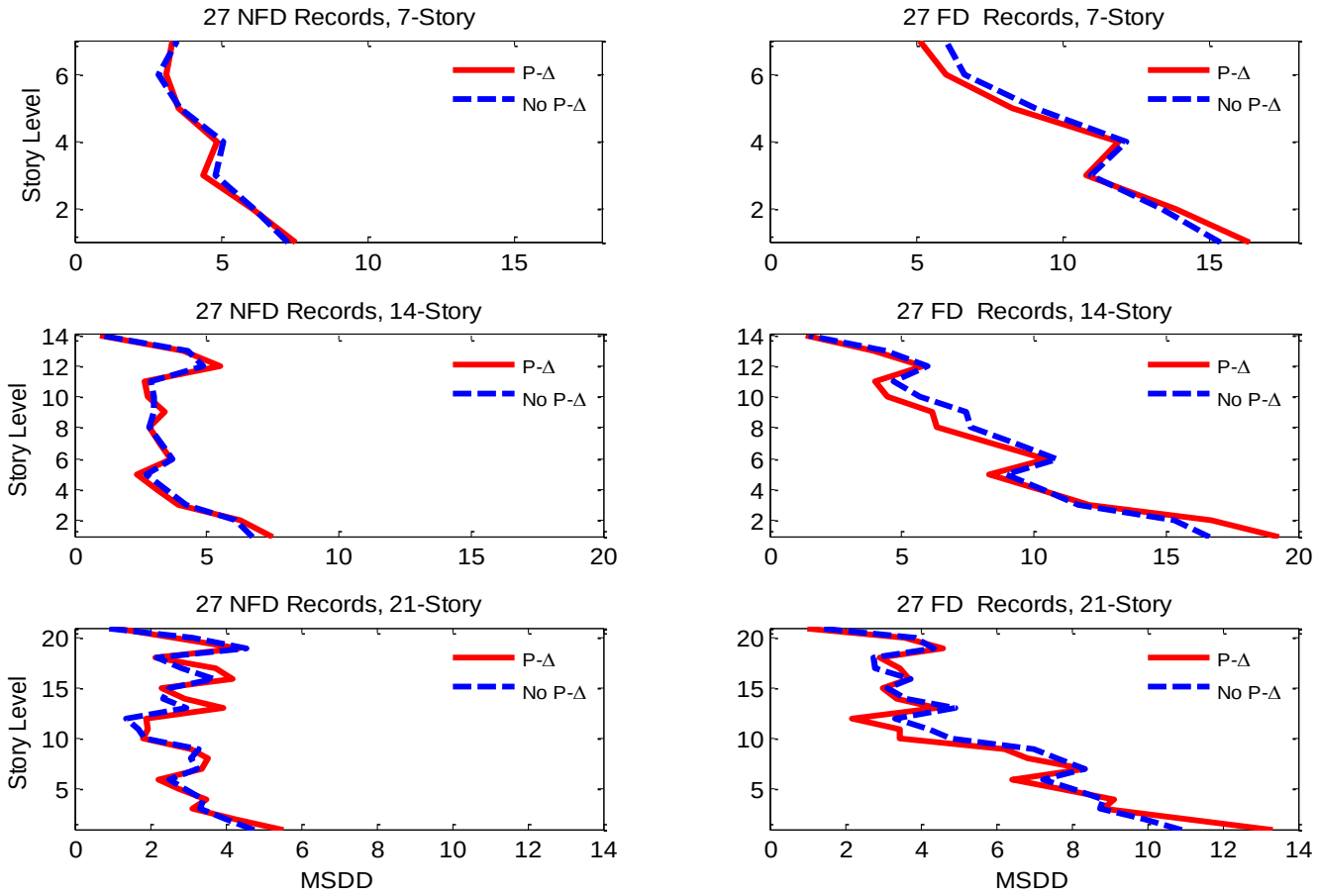

Figure 3-13: Mean value of MSDD with and without P-Δ effects for (a) ordinary and (b) forward-directivity ground motions.

3.11. Tables

Table 3-1: Earthquakes that recorded the ground motions used in this study.

Earthquake	**Date**	**Moment magnitude**
Parkfield (PF)	6/27/66	6.1
San Fernando (SF)	2/9/71	6.6
Imperial valley (IV)	10/15/79	6.5
Morgan Hill (MH)	4/24/84	6.2
Superstition Hills (SH)	11/24/87	6.6
Loma Prieta (LP)	10/17/89	7
Erzincan, Turkey (EZ)	3/13/92	6.7
Landers (L)	6/28/92	7.3
Northridge (N)	1/17/94	6.7
Kobe (KB)	1/17/95	6.9
Kocaeli (K)	8/17/99	7.4
Chi-Chi (CH)	9/21/99	7.6
Duzce (D)	11/12/99	7.1
Palm Springs (PS)	7/8/86	6.0
Denali(DE)	11/3/02	7.9
San Simeon (SS)	12/23/03	6.5
Bam (B)	12/26/03	6.5

Table 3-2: Ground motions with forward-directivity effects (selected from Bray and Rodriguez-Marek (2004)).

#	Station	Agency	Station #	Event[a]	R[b] (km)	Site[c]	PGA (g)	PGV (cm/s)	$T_{v\text{-}p}$ [e](s)	$(T_p)_{Baker}$ [f] (s)	$(A_p)_{Baker}$ [g] (cm/s)
1	Gilroy-Gavilan Coll.	CDMG	47006	LP	11.6	r	0.32	30.81	0.38	1.80	13.8
2	Gilroy-Historic Bldg.	CDMG	57476	LP	12.7	s	0.29	36.82	1.47	1.80	29.2
3	Gilroy Array#1	CDMG	47379	LP	11.2	r	0.48	38.61	0.4	4.31	9.4
4	Gilroy Array#2	CDMG	47380	LP	12.7	s	0.41	45.67	1.46	1.72	40.4
5	Gilroy Array#3	CDMG	47381	LP	14.4	s	0.54	49.34	0.48	2.32	23.8
6	LGPC	UCSC	16	LP	6.1	r	0.84	103.18	0.79	3.92	62.1
7	Saratoga-Aloha Ave.	CDMG	58065	LP	13.0	s	0.39	55.58	1.55	4.47	26.5
8	Saratoga-W Valley Coll.	CDMG	58235	LP	13.7	s	0.40	71.33	1.14	1.90	37.7
9	Erzincan		95	EZ	2.0	s	0.50	95.56	2.23	2.65	66.6
10	Jensen Filtration Plant	USGS	655	N	6.2	s	0.40	104.55	2.86	3.36	80.3
11	Newhall-Fire Sta.	CDMG	24279	N	7.1	s	0.77	120.27	0.71	1.04	92.6
12	Newhall-W. Pico Can. Rd	USC	90056	N	7.1	s	0.43	87.75	2.03	2.41	76.0
27	Pacoima Dam (downstr.)	CDMG	24207	N	8.0	r	0.53	51.24	0.44	0.59	35.0
14	Rinaldi Receiving Sta.	DWP	77	N	7.1	s	0.89	173.07	1.06	1.50	111.3
15	Sylmar-Converter Sta.	DWP	74	N	6.2	s	0.61	130.27	1.1	3.48	78.4

Table 3-2 (Cont.)

#	Station	Agency	Station #	Event[a]	R[b] (km)	Site[c]	PGA (g)	PGV (cm/s)	$T_{v\text{-}p}$ [e] (s)	$(T_p)_{Baker}$ [f] (s)	$(A_p)_{Baker}$ [g] (cm/s)
16	Sylmar-Converter Sta. E.	DWP	75	N	6.1	s	0.85	116.56	2.92	3.49	55.0
17	Sylmar-Olive View FF	CDMG	24514	N	6.4	s	0.77	122.72	2.42	3.11	71.0
18	Pacoima Kagel Canyon	CDMG	24088	N	7.3	r	0.53	56.00	0.88	0.90	43.0
19	Arleta-Nordhoff Fire Sta.	CDMG	24087	N	8.7	s	0.32	35.50	1.49	1.23	23.0
13	Duzce	ERD	–	K	12.7	s	0.36	46.41	1.37	1.36	46.7
20	Arcelik Kandilli		–	K	17.0	r	0.14	42.35	5.24	7.97	28.4
21	Gebze	ERD	–	K	17.0	r	0.28	40.69	4.62	5.97	34.0
22	TCU052[h, i]	CWB	–	CH	0.2	s	0.53	177.27	4.48	6.12	95.2
23	TCU068[h]	CWB	–	CH	1.1	s	0.61	145.13	4.06	4.25	104.9
24	TCU075[i]	CWB	–	CH	1.5	s	0.32	76.14	2.03	2.41	61.8
25	TCU101[i]	CWB	–	CH	2.9	s	0.21	65.19	8.62	6.86	38.4
26	TCU102[i]	CWB	–	CH	1.8	s	0.30	87.07	2.52	9.11	51.7

[a] See Table 3-1.
[b] Closest distance to the fault plane.
[c] Soil (s) or rock (r).
[e] Period corresponding to the peak in the velocity response spectrum.
[f] Pulse period determined with the procedure of Baker (2007).
[g] Pulse amplitude determined with the procedure of Baker (2007).
[h] The fault normal direction for these records was assumed to be the direction oriented with the largest velocity pulse (N122º for TCU052 and N199º for TCU068).
[i] The fling step was removed using the procedure described in Bray and Rodriquez-Marek (2004).

Table 3-3: Near-fault ground motions included in the non-FD database (e.g. those that do not have pulse-like characteristics).

#	Station	Agency	Station #	Event[a]	R [b] (km)	Site[c]	PGA (g)	PGV (cm/sec)	T_{v-p} [d]
1	BRAN	UCSC	13	LP	10.7	r	0.63	53.34	0.49
2	Capitola	CDMG	47125	LP	15.2	s	0.45	34.56	0.64
3	Corralitos	CDMG	57007	LP	3.9	r	0.51	45.48	0.75
4	UCSC Lick Observatory	CDMG	15	LP	18.4	r	0.47	17.69	0.36
5	UCSC	UCSC	58135	LP	18.5	r	0.46	11.61	0.16
6	WAHO	UCSC	14	LP	17.5	r	0.78	25.42	0.23
7	N Hollywood – Coldwater Can.	USC	90009	N	12.5	r	0.24	22.89	1.2
8	Sunland – Mt Gleason Ave.	USC	90058	N	13.4	r	0.15	19.25	1.04
9	Burbank – Howard Rd.		90059	N	16.9	r	0.12	8.14	0.64
10	Simi Valley – Katherine Rd.	USC	90055	N	13.4	r	1.07	51.4	0.62
11	Sun Valley – Roscoe Blvd.	USC	90006	N	10.1	s	0.31	25.86	1.01
12	Santa Susana Ground	USGS	5108	N	16.7	r	0.4	20.31	0.69
13	Big Tujunga, Angeles Nat F	USC	90061	N	19.7	r	0.17	6.67	0.64
14	CHY028	CWB	-	CH	3.1	s	0.65	72.86	0.62
15	CHY029	CWB	-	CH	11.0	s	0.3	30.35	0.67
16	CHY035	CWB	-	CH	12.7	s	0.25	45.61	1.28
17	CHY080	CWB	-	CH	2.7	s	0.97	107.61	0.88
18	CHY006	CWB	-	CH	9.8	s	0.36	55.44	1.81
19	TCU055	CWB	-	CH	6.4	s	0.24	26.23	2.15
20	TCU070	CWB	-	CH	19.0	s	0.26	52.16	5.1
21	TCU071	CWB	-	CH	5.3	s	0.58	44.52	0.56
22	TCU072	CWB	-	CH	7.0	s	0.53	71.8	0.88
23	TCU074	CWB	-	CH	13.5	s	0.64	73.4	1.47
24	TCU079	CWB	-	CH	11.0	s	0.76	61.24	0.6
25	TCU089	CWB	-	CH	8.9	s	0.34	30.93	5.42

#	Station	Agency	Station #	Event[a]	R [b] (km)	Site[c]	PGA (g)	PGV (cm/sec)	T_{v-p} [d]
26	Bolu	ERD	-	D	17.6	s	0.81	56.51	0.79
27	Duzce	ERD	-	D	8.2	s	0.36	59.99	5.50

[a] See Table 3-1.
[b] Closest distance to the fault plane.
[c] Soil (s) or rock (r).
[d] Period corresponding to the peak in the velocity response spectrum.

Table 3-4: Parameters for the power-law model* used to correlate MIDD with different intensity measures

Structure	GM set	IM = PGA			IM = Sa(T_1)			IM = PGV		
		a	***b***	x_o	***a***	***b***	x_o	***a***	***b***	x_o
7 story	FD	32.3	0.73	0.1	24.6	0.71	0.1	0.095	1.17	5
	NFD	13.3	0.55	0.1	13	0.70	0.1	0.266	0.92	5
14 story	FD	37.6	0.69	0.1	42.8	0.71	0.03	0.286	1.00	15
	NFD	12.8	0.47	0.1	21.2	0.48	0.03	1.227	0.58	15
21 story	FD	27.3	0.87	0.05	35.1	0.61	0.02	0.174	1.03	15
	NFD	9.9	0.32	0.05	32.3	0.54	0.02	0.949	0.63	15

* $MIDD = \max\left[1 + a\left(IM - x_o\right)^b, 1\right]$

Table 3-5: Measures of fit for the correlations between MIDD and different intensity measures

Structure	GM set	IM = PGA			IM = Sa(T_1)			IM = PGV		
		σ_{10} [a]	σ_{res} [b]	ρ_{res} [c]	σ_{10} [a]	σ_{res} [b]	ρ_{res} [c]	σ_{10} [a]	σ_{res} [b]	ρ_{res} [c]
7 story	FD	5.98	9.41	0.57	4.35	7.11	0.43	4.05	4.85	0.29
	NFD	4.46	3.81	0.47	2.48	1.87	0.23	1.9	1.55	0.19
14 story	FD	5.34	9.28	0.48	6.18	5.52	0.28	2.14	2.73	0.14
	NFD	4.67	4.05	0.48	2.21	2.36	0.28	2.18	2.02	0.24
21 story	FD	5.15	6.57	0.48	4.62	5.36	0.39	2.69	2.57	0.19
	NFD	4.91	4.71	0.58	2.80	2.69	0.33	3.41	2.84	0.35

[a] σ_{10} = standard deviation of residuals when MIDD = 10.

[b] σ_{res} = standard deviation of residuals (assuming a constant standard deviation).

[c] ρ_{res} = coefficient of variation of residuals given by σ_{res} divided by the mean MIDD.

Table 3-6: Parameters of Gabor Wavelet pulses (Equation 3-1) obtained through minimization.

Station	**7-Story (T_1 = 1sec)**			**14-Story (T_1 = 2sec)**			**21-Story (T_1 = 3sec)**		
	T_p (sec)	**γ**	**A (cm/sec)**	**T_p (sec)**	**γ**	**A (cm/sec)**	**T_p (sec)**	**γ**	**A (cm/sec)**
Gilroy - Gavilan Coll.	1.60	3.0	13.0	1.89	3.0	11.7	1.99	3.0	13.6
Gilroy - Historic Bldg.	1.59	3.0	34.2	1.89	3.0	25.6	1.56	3.0	30.9
Gilroy Array#1	1.24	2.0	13.3	3.91	2.0	13.2	3.45	2.0	10.1
Gilroy Array#2	1.49	2.5	44.0	1.96	2.5	37.4	1.53	2.5	45.4
Gilroy Array#3	2.10	3.0	25.3	1.78	3.0	27.7	2.15	3.0	23.7
LGPC	1.75	3.0	70.0	3.26	3.0	70.0	3.37	3.0	56.5
Saratoga - Aloha Ave.	1.30	3.0	33.3	3.63	3.0	29.5	4.04	3.0	30.1
Saratoga - W Valley Coll.	1.55	3.0	41.0	2.49	3.0	37.0	2.24	3.0	41.2
Erzincan	3.53	3.0	105.1	2.57	3.0	73.1	2.57	3.0	67.6
JensenFiltration Plant	2.39	3.0	71.3	3.67	3.0	74.6	2.84	3.0	83.6
Newhall - Fire Sta.	1.01	4.0	92.0	1.49	4.0	96.4	1.41	4.0	89.9
Newhall - W. Pico Can. Rd	2.69	2.0	82.1	2.57	2.0	81.0	2.61	2.0	101.3
Pacoima Dam (downstr.)	0.75	3.0	25.2	1.29	3.0	38.6	7.51	3.0	45.9
Rinaldi Receiving Sta.	1.40	2.5	108.2	1.78	2.5	125.0	2.26	2.5	124.9
Sylmar - Converter Sta.	1.77	2.5	97.2	3.25	2.5	74.6	3.95	2.5	80.1
Sylmar - Converter Sta. E.	1.45	2.5	68.3	3.08	2.5	60.7	4.10	2.5	58.8
Sylmar - Olive View FF	1.96	2.5	78.2	2.90	2.5	62.1	2.62	2.5	68.5
Pacoima Kagel Canyon	0.90	3.0	49.9	0.91	3.0	73.4	1.23	3.0	57.7
Arleta – Nordhoff Fire Sta.	1.17	2.5	19.1	1.06	2.5	46.5	1.66	2.5	52.1
Duzce	1.41	2.5	50.2	1.67	2.5	51.6	2.19	2.5	54.0
Arcelik Kandilli	1.47	3.0	11.5	3.73	3.0	22.9	8.12	3.0	49.5
Gebze	0.87	3.0	20.6	4.34	3.0	37.5	6.50	3.0	46.6
TCU052	3.20	3.0	139.6	7.24	3.0	131.9	5.54	3.0	87.3
TCU068	2.75	3.0	103.9	3.98	3.0	98.3	3.95	3.0	107.9
TCU075	2.19	3.0	61.4	2.79	3.0	63.3	2.54	3.0	69.8
TCU101	1.11	2.0	23.0	2.38	2.0	30.1	6.33	2.0	42.0
TCU102	2.34	2.5	89.9	7.21	2.5	101.5	3.09	2.5	128.6

Table 3-7: Normalized differences in response of 7-story structure due to increase of damping.

Mean of differences in the maximum interstory ductility demand of 7-story subjected to:			
Pulse-like records when ζ was increased from		Ordinary records when ζ was increased from	
5% to 10%	5% to 15%	5% to 10%	5% to 15%
0.137	0.242	0.150	0.267

CHAPTER FOUR

PROBABILISTIC SEISMIC DEMAND ANALYSIS FOR THE NEAR-FAULT ZONE

4.1. Introduction

In the current state-of-the-practice, forward-directivity effects are introduced in seismic hazard analyses by modifying the ground motion elastic response spectra. Nevertheless, forward-directivity ground motions typically have large intensities and tend to drive structures into the nonlinear range. For these cases, the spectral acceleration at the first-mode period of the structure, denoted as $S_a(T_1)$, no longer serves as an effective Intensity Measure (Luco and Cornell 2007; Baker and Cornell 2008).

Alternatively, Vector-Valued IMs can be used to improve the accuracy of the estimation of the structural response (Baker and Cornell 2005; Luco and Cornell 2007; Baker and Cornell 2008). As discussed in previous chapters, forward-directivity ground motions have relatively simple time-domain representations and can be characterized by the period and amplitude of the velocity pulse. These parameters can be used as alternative Intensity Measures. Moreover, the narrow band nature of the forward-directivity pulse implies that forward-directivity ground motions can be represented using equivalent pulse models such as the Gabor pulse model presented in Chapter 3. This model was shown to be an acceptable proxy for pulse-like motions (see Chapter 3). Hence, the Gabor pulse can be used to compute structural response for pulse-like motion using time-domain analyses.

A prerequisite of Performance-Based Earthquake Engineering is Probabilistic Seismic Demand Analysis in which hazard curves are obtained for an arbitrary Engineering Demand

Parameter (EDP). PSDA is built upon PSHA and couples the probabilistic description of future ground motions from PSHA with a probabilistic description of their effects on a structure. In traditional PSHA, forward-directivity effects are either ignored, treated semi-deterministically, or considered through a broadband directivity model that captures the average effect of forward-directivity on response spectra (e.g., Somerville et al.'s broadband-directivity model (1997) as modified by Abrahamson (2000), or Spudich and Chiou (2008) model based on Isochrone theory). Travasarou et al. (2006) quantified the degree of conservatism associated with the semi-deterministic approach relative to explicit integration of directivity effects in probabilistic seismic hazard calculations using Somerville et al.'s model. Results of the study showed that directivity effects are most significant for critical structures that are designed for long return periods, sites located close to faults (e.g., < 5 to 15 km), and for sites located close to segmentation points along major faults when the adjacent fault is relatively active. Travasarou et al. (2006) concluded that treating directivity effects semi-deterministically can lead to considerable over prediction of ground motion hazard. On the other hand, traditional PSHA is based on elastic-pseudo acceleration of the fundamental period of the structure. While the effects of forward-directivity can be included in response spectral predictions using a broad band directivity model to modify response spectra, this approach does not account for the particularities of structural response to pulse-type ground motions. In fact, Luco and Cornell (2007) proved that the elastic response spectrum at the fundamental period of the structure is neither a sufficient nor efficient IM for pulse-like ground motions. Therefore, both ignoring the effects of directivity on PSHA and including these effects semi-deterministically or through a broadband-directivity model, can lead to an inaccurate estimation of the seismic hazard. In order to accurately estimate the

hazard at near-fault sites, an appropriate quantification of the hazard due to pulse-like motions must be considered.

In traditional PSDA analyses, a statistical correlation between IMs and EDP (usually referred to as fragility curves) is used to predict structural response. The use of IMs to characterize earthquake ground motions is necessary because of the impossibility of predicting full time histories for ordinary earthquake scenarios. Moreover, the statistical treatment of structural response is necessary because IMs (even when considering a vector of IMs) are not full descriptors of a ground motion time history, and as a result the relationship between structural response and the IM is not unique and must be described statistically even for idealized structures that have a deterministic response. However, as previously discussed, the most widely used IM (the spectral acceleration at the structure's fundamental period of vibration) is not an adequate IM for near-fault ground motions (see Section 2.3). In particular, when the period of forward-directivity pulses are roughly equivalent to the fundamental period of the structure, structural response is controlled by forward-directivity pulses. In these cases, it is tempting to use pulse parameters as additional IM within a Vector-Valued PSDA approach. An alternative approach is to use predictive relationships for pulse period and pulse amplitude and develop an equivalent pulse model to fully characterize the ground motion time histories and then use time-domain structural analysis methodologies to predict structural response.

In this study, forward-directivity effects are considered using time-domain analyses. In the time-domain approach, the amplitude and period of the pulse are used to generate equivalent pulse representations of the forward-directivity ground motion and these

representations are used in structural response analyses to predict the response of the structure when response is controlled by the pulse. Pulse parameters are predicted based on magnitude, site location with respect to the fault, and fault rupture geometry and orientation. In addition, the probability of pulse occurrence is included in the probabilistic analysis. For cases in which no directivity pulse is predicted, the PSDA is conducted using a more traditional approach. The results are hazard curves for PSDA that are more consistent with the behavior of the structure.

The methodology to couple the traditional PSDA analyses for non-pulse ground motions with the proposed time-domain methodology is presented in this chapter. In addition, PSDA analyses using fragility curves developed specifically for near-fault ground motions are also conducted for comparison. An example is presented in order to illustrate the procedure and to show the applicability and limitations of the proposed methodology.

4.2. Probabilistic Seismic Demand Analysis

The second generation of Performance-Based Earthquake Engineering assessment and design procedures (PBEE-2) which were postulated based on probability-based performance assessment tools (Cornell et al. 2002) was introduced in Section 2.2. PBEE-2 was expressed in terms of a triple integral which, is an application of the total probability theorem and is rewritten here for convenience:

$$\lambda(DV) = \iiint P[DV \mid DM]dP[DM \mid EDP]dP[EDP \mid IM]\,|\,d\lambda[IM]\,| \qquad (4\text{-}1)$$

where DV, DM, EDP, and IM are Decision Variables, Damage Measures, Engineering Demand Parameters, and Intensity Measures, respectively; P[X|Y] is the probability density of X conditioned on knowledge of Y; and $d\lambda[IM]$ is mean annual frequency of occurrence of the IM.

PSDA is the intermediate step in PBEE where the mean annual rate of exceedance of an engineering demand parameter is computed, PSDA is embodied in the following equation (ATC-58 2004):

$$\lambda_{EDP}(x) = \int P[EDP \geq x \mid IM = y] \mid d\lambda_{IM}(y) \mid \tag{4-2}$$

where $\lambda_{EDP}(x)$ is the mean annual frequency of EDP exceeding the value *x*, $P[EDP \geq x \mid IM = y]$ is the probability of EDP exceeding *x* given that IM equals y, $d\lambda_{IM}(y)$ is the mean annual frequency of occurrence of IM equal to *y*, and $\lambda_{IM}(y)$ is mean annual frequency of IM exceeding *y* (ground motion hazard) which is obtained from conventional PSHA. Note that Equation 4-2 is a subset of Equation 4-1.

In this study, a new PSDA model (referred here as the New-PSDA model) is proposed for the analysis of sites located near a fault. The hazard is divided among the contribution of various scenarios (e.g. near-source, non-near-source) following the approach proposed by Tothong et al. (2007) for response spectra hazard curves that include the effect of forward-directivity. In the proposed method, the EDP for near-source events with dominant forward-directivity pulses are predicted using simplified pulses rather than using elastic-pseudo

acceleration response spectra. This provides an accurate prediction of structural response when forward-directivity pulses govern the structural behavior.

In addition to the proposed PSDA approach, three other PSDA analyses were conducted to serve as a basis for comparison with the proposed PSDA model:

1. A *traditional PSDA model without inclusion of forward-directivity effects*. In this model, elastic-pseudo acceleration of the fundamental period of a structure is used as the IM. The IM is obtained from an attenuation relationships (for simplicity, only one attenuation relationship was considered, the NGA attenuation relationships of Abrahamson and Silva (2007); more formally, an entire set of attenuation relationships should be considered to account for epistemic uncertainty). Directivity effects were ignored. EDPs were predicted through a statistical model which is developed based on results obtained from dynamic nonlinear time-history analyses of a structure subjected to ordinary and near-fault ground motions without forward-directivity effects. In this chapter, this model and the PSHA associated with it are referred to as Traditional-PSDA and Traditional-PSHA models, respectively.

2. A *Broadband PSDA model*. In this model the elastic-pseudo acceleration of the fundamental period of a structure was used as the IM. The IM predicted by the ground motion model of Abrahamson and Silva (2007) is modified by Somerville's broadband-directivity model (Somerville et al. 1997, Abrahamson 2000) to account for forward-directivity effects. Forward directivity is included in the PSHA analysis by randomizing the location of the hypocenter and the direction of rupture

(Abrahamson 2000). EDPs were predicted through the same statistical model used in the Traditional-PSDA. In this chapter, this model and the PSHA associated with it are referred to as Broadband-PSDA and Broadband-PSHA models, respectively.

3. An *Enhanced Broadband PSDA model*. To enhance the Broadband-PSDA model, Iervolino and Cornell's model (2008) to predict the occurrence of forward-directivity pulses was used to discriminate between the hazard resulting from pulse-like motions and the hazard from non-pulse-like motions. Forward-directivity is included as for the Broadband-PSDA model; however, for scenarios in which pulse-like motions are predicted, the EDPs are predicted by a statistical model based on dynamic nonlinear time-history analysis of a structure subjected to near-fault ground motions with pulses (see Section 4.10.1). In this chapter, this model is referred to as Enhanced-Broadband-PSDA. Note that PSHA associated with this model is as same as the Broadband-PSHA model.

In the following sections, the methodology of the proposed approach is elaborated, but first empirical correlations needed for developing the new PSDA model are presented.

4.3. Empirical Correlations Needed for Incorporating Forward-Directivity

The proposed PSDA model uses empirical correlations to predict the amplitude of the forward-directivity pulse (A_p) and its period (T_p) based on magnitude and distance. In addition, a predictive model for the occurrence of velocity pulses is also needed. These correlations are discussed in the following sections.

4.3.1. Predictive model for pulse period (T_p)

Pulse period was found to be a function of magnitude alone (Somerville 2003; Bray and Rodriguez-Marek 2004; Baker 2007a). The model by Baker (2007b) is used in this work, as discussed in Section 2.9.7 and repeated here for convenience:

$$Ln(\bar{T}_p) = -5.78 + 1.02M_w \qquad \text{with} \qquad \sigma_{\ln T_p} = 0.55 \tag{4-3}$$

where $\bar{T}_p$ is the median predicted value of pulse period in seconds as a function of magnitude, M_w; and $\sigma_{\ln T_p}$ is the standard deviation in natural log units of the pulse period. This equation implicitly assumes that the pulse period has a log normal distribution.

4.3.2. Predictive model for pulse amplitude (A_p)

The amplitude of forward-directivity pulses extracted using the procedure proposed by Baker (2007a) was found to be 73% of the PGV (Section 3.8). Hence, the pulse amplitude can be calculated using predictive relationships for PGV. The model of Bray and Rodriguez-Marek (2004) is used to estimate PGV at distances shorter than 20 km (the limit of applicability of that model):

$$Ln(\overline{PGV}) = 4.51 + 0.34M_w - 0.57Ln(r_{rup}{}^2 + 7^2) \quad \text{with} \quad \sigma_{PGV} = 0.49 \tag{4-4}$$

where $\overline{PGV}$ is in units of cm/sec, r_{rup} is the closest distance to the site in km, and σ_{PGV} is the standard deviation of PGV in log units. At distances larger than 60 km, the PGV is estimated using the Abrahamson & Silva NGA relationship (2007). For intermediate distances (e.g. between 20 km and 60 km), a cosine taper function is used to transit smoothly from the near-

source PGV correlation (Bray and Rodriguez-Marek 2004) to the NGA PGV correlation (Abrahamson and Silva 2007):

$$Ln(\overline{PGV}) = \phi.Ln(\overline{PGV}_{Rodriguez-Marek}) + (1-\phi).Ln(\overline{PGV}_{NGA}) \quad (4\text{-}5)$$

where $\phi = \frac{1}{2} + \frac{1}{2}\cos(\pi(\frac{r_{rup}}{40} - \frac{1}{2}))$. Figure 4-1 shows an example of the resulting PGV function. The standard deviation of PGV is similarly defined.

4.3.3. Correlation between pulse amplitude and pulse period

Bray and Rodriguez-Mark (2004) proposed empirical relationships for pulse amplitude and pulse period. However, that study fails to provide a cross-correlation between the two ground motion parameters. Therefore, sixty-six forward-directivity ground motions (listed in Table 3-2 and Table 4-1) were considered in order to determine the cross-correlation between pulse period and pulse amplitude. Baker's procedure (2007a) was used to extract forward-directivity pulses from the aforementioned records. Pulse parameters of ground motions (listed in Table 3-2 and Table 4-1) were used to define a correlation between pulse period and amplitude. The correlation is denoted as ρ and defined by Equation 4-6:

$$\rho = \frac{\sum (A_{p_i} - \bar{\bar{A}}_p)(T_{p_i} - \bar{\bar{T}}_p)}{\sqrt{\sum (A_{p_i} - \bar{\bar{A}}_p)^2}\sqrt{\sum (T_{p_i} - \bar{\bar{T}}_p)^2}} \quad (4\text{-}6)$$

where $\bar{\bar{A}}_p$ and $\bar{\bar{T}}_p$ define the mean amplitude and mean pulse period for each ground motion *i* as defined in Sections 4.3.1 and 4.3.2 for the corresponding magnitude and distance of that

recording. It was observed that no correlation exists between pulse period and amplitude for the data used (ρ = 0.08).

4.3.4. Occurrence of Pulse

Iervolino and Cornell (2008) developed an empirical model to predict the probability of a pulse occurring at the site determined by the following expression:

$$P(pulse \mid r_{rup}, S, \theta) = \frac{e^{\alpha + \beta_1 . r_{rup} + \beta_2 . S + \beta_3 . \theta}}{1 + e^{\alpha + \beta_1 . r_{rup} + \beta_2 . S + \beta_3 . \theta}} \quad (4\text{-}7)$$

where r_{rup} is the closest distance to the fault; S is the projected distance along the rupture plane from the epicenter to the site; θ is the azimuth between the fault plane and ray path to the site; α and β_i are parameters with values given by α = 0.85925, β_1= -0.11137, β_2 = 0.018704, β_3 = -0.04441. The parameters S and θ were originally defined by Somerville et al. (1997) to parameterize forward-directivity effects.

4.4. Proposed PSDA methodology using time-domain analyses

Similar to the procedure set forth by Tothong et al. (2007) (see Section 2.2), the proposed methodology separates the mean annual frequency of exceedance (MAF) of an Engineering Demand Parameter for a given Intensity Measure, $\lambda_{EDP}(x)$, into the contribution of near-source (NS) and non-near-source (non-NS) scenarios. This is expressed as:

$$\lambda_{EDP}(x) = \lambda_{EDP,non-NS}(x) + \lambda_{EDP,NS}(x) \quad (4\text{-}8)$$

The MAF of the EDP for the near-source case ($\lambda_{EDP,NS}$) includes hazard resulting from pulse- and non-pulse-like ground motions and can be separated into two parts: the near-source hazard from pulse-like ground motion events, $\lambda_{EDP,NS\&pulse}$, and the near-source hazard due to non–pulse-like records, $\lambda_{EDP,NS\&no-pulse}$:

$$\lambda_{EDP,NS}(x) = \lambda_{EDP,NS\&pulse}(x) + \lambda_{EDP,NS\&no-pulse}(x) \tag{4-9}$$

For near-source ground motion with forward-directivity pulses, two different cases are considered:

1. When forward-directivity pulses are not dominant: in this case, forward-directivity pulses do not control response of the structure, hence, $S_a(T_1)$ is used as an Intensity Measure. These cases are treated similarly to near-source events without pulse.

2. When forward-directivity pulses are dominant: in this case, forward-directivity pulses control structural response and simplified pulses are used to predict the EDP using time-domain analyses.

In Chapter 3 it was found that, for the MDOF structures analyzed therein, when the ratio of the pulse period and structural period are within 0.5 and 2.5 (i.e., $0.5 \leq T_{pulse}/T_{structure} \leq 2.5$), forward-directivity pulses are dominant and control the behavior of the structures. For these cases an Incremental Dynamic Analyses using the Gabor equivalent pulse model was performed to predict the EDP for possible forward-directivity pulses at the analysis site. Given that Gabor wavelet pulses can reasonably represent near-fault ground motions when forward-directivity pulses are dominant, multiple analyses can be

used to predict inelastic response of a structure for all possible pulse amplitudes and all pulse periods in this range. Hence, the inelastic response of a structure for a possible range of forward-directivity pulses with realistic amplitudes and frequencies can be predicted as illustrated in Figure 3-12. Note that the bounds for which the pulse controls (T_{lower} = 0.5 T_p and T_{upper} = 2.5 T_p for the MDOFs studied in Chapter 3) may be structure dependent. Nonetheless, the concept that the response of the structure is controlled by the pulse when the pulse period is in the neighborhood of the structural period is assumed to be generally applicable to all structures.

In summary, the EDP hazard at a site can be divided into

$$\lambda_{EDP}(x) = \lambda_{EDP,non-NS}(x) + \lambda_{EDP,NS\&no-pulse}(x) + \lambda_{EDP,NS\&pulse,\text{pulse is dominant}}(x) + \lambda_{EDP,NS\&pulse,\text{pulse is not dominant}}(x) \quad (4\text{-}10)$$

For non-NS ($\lambda_{EDP,non\text{-}NS}$), and near source cases with no pulse or in which the pulse is not dominant ($\lambda_{EDP,\ NS\&no\text{-}pulse}$ and $\lambda_{EDP,NS\&pulse,\ pulse\ is\ not\ dominant}$), the hazard ($\lambda_{EDP}$) is computed using Equation 4-2 and the EDP is estimated from statistical correlations with spectral acceleration. In these cases, the intensity measure hazard (λ_{Sa}) has to be deaggregated into the same four scenarios considered for λ_{EDP}, hence:

$$\lambda_{S_a}(x) = \lambda_{S_a,non-NS}(x) + \lambda_{S_a,NS\&no-pulse}(x) + \lambda_{S_a,NS\&pulse,\text{pulse is dominant}}(x) + \lambda_{S_a,NS\&pulse,\text{pulse is not dominant}}(x) \quad (4\text{-}11)$$

Each of these hazard components is discussed in Sections 4-5 to 4-8.

4.5. Hazard for non-near source scenarios [$\lambda_{EDP,non\text{-}NS}(x)$]

Whenever the closest distance to the ruptured fault for a given scenario is greater than 60 km, that scenario is considered to be a non-near source scenario. The 60 km threshold distance is based on Abrahamson's (2000) model. For these cases, the mean annual frequency of the Engineering Demand Parameter exceeding *x* for non-near-source events, $\lambda_{EDP,Non-NS}(x)$, is given by:

$$\lambda_{EDP,Non-NS}(x) = \int P[(EDP \geq x) \mid S_a = y] \mid d\lambda_{S_a,Non-NS}(y) \mid \tag{4-12}$$

where $P[(EDP \geq x) \mid S_a = y]$ is the conditional probability of EDP exceeding *x* given that $S_a(T_1) = y$, and is defined by the statistical model presented in Section 4.10.1; and $d\lambda_{S_a,Non-NS}(y)$ is the mean annual frequency of occurrence of $S_a(T_1) = y$ for non-near-source scenarios and is equal to $\lambda_{S_a}(y - \Delta/2) - \lambda_{S_a}(y + \Delta/2)$, where Δ is a selected Intensity Measure interval and $\lambda_{S_a,Non-NS}(y)$ is the mean annual frequency of elastic-pseudo spectral acceleration exceeding *y* and is obtained through conventional PSHA considering only non near-source scenarios, hence, $\lambda_{S_a,Non-NS}(y)$ is given by:

$$\begin{aligned}\lambda_{Sa,Non-NS}(y) = \sum_{i=1}^{\#\,faults} \nu_i \iint_{m_w, r_{rup}} \left[1 - I_{NS}\left(r_{rup}^i\right)\right] G_{Sa|M_w^i, R_{rup}^i}\left(y \mid m_w, r_{rup}\right) \\ . f_{M_w^i, R_{rup}^i}\left(m_w, r_{rup}\right) . dm_w . dr_{rup}\end{aligned} \tag{4-13}$$

where ν_i is the mean annual rate of occurrence of earthquakes on fault *i* above a minimum threshold magnitude, M_w is the moment magnitude, and R_{rup} is the closest distance from the

site to the rupture plane. The function $I_{NS}(r_{rup})$ is a flag that is set to one when r_{rup} < 60 km, and set to 0 when r_{rup} > 60 km. The term $f_{M^i,R^i_{rup}}(m_w, r_{rup})$ is the joint probability density function (PDF) of M_w and R_{rup} on fault *i*. The term, $G_{Sa|M^i_w,R^i_{rup}}(y \mid m_w, r_{rup})$, represents the Complementary Cumulative Gaussian probability density function (CCDF) of the log normally distributed random variable S_a, which is defined as:

$$G_{Sa|M^i_w,R^i_{rup}}(y \mid m_w, r_{rup}) = 1 - \Phi\left(\frac{\ln y - \mu_{\ln S_a|m_w,r_{rup}}}{\sigma_{\ln S_a|m_w,r_{rup}}}\right) \quad (4\text{-}14)$$

where $\Phi(...)$ is the standard Gaussian CDF, and $\mu_{\ln S_a|m_w,r_{rup}}$ and $\sigma_{\ln S_a|m_w,r_{rup}}$ are the conditional mean and standard deviation of the natural logarithm of S_a, respectively, as obtained from a ground motion prediction model (Abrahamson and Silva 2007), and *y* is a test value for S_a . Note that in Equations 4-13 and 4-14, random variables are denoted by uppercase characters while lowercase characters represent realizations of those random variables. This definition holds true for all equations presented herein. Equation 4-13 sums the hazard over all faults affecting a site. Without loss of generality, the presentation from here on assumes that a single fault contributes to hazard and the subscript *i* is ignored.

A note on the implementation of Equation 4-13 is in order here. The definition of the joint probability density function $f_{M,R_{rup}}(m_w, r_{rup})$ requires the definition of the probability density function for closest distance to the fault (R_{rup}) which in turn is a function of magnitude through the dependence of rupture length on magnitude. An alternative approach

is to iterate through all possible scenarios for magnitude and rupture length in which case Equation 4-13 becomes (for a single fault):

$$\lambda_{Sa,Non-NS}(y) = \upsilon \int_{m_w} \int_{rl} \int_{\chi} \left[1 - I_{NS}(r_{rup})\right] G_{Sa|M_w,R_{rup}}(y \mid m_w, r_{rup}) \cdot f_{M_w}(m_w) f_{RL}(m_w) f_X(m_w, rl).dm_w.drl.d\chi \quad (4\text{-}15)$$

where *RL* is the rupture length and *X* is the location of the ruptured segment within the given fault. Note that r_{rup} is a function of χ and *rl*, but the functionality is omitted from the notation of Eq. 4-15 for simplicity. The probability density function for magnitude, $f_{Mw}(m_w)$ can be obtained by geological or seismological studies (McGuire 2004). The probability density function for rupture length, $f_{RL}(m_w)$ is given by empirical relationships such as Wells and Coppersmith (1984). The probability density function for the location of rupture (f_X) is assumed to be uniform, implying equal probability of occurrence of rupture within the fault. This is a simplification that may not apply for faults with strong segmentation. Equation 4-15 is easier to implement numerically than Equation 4-13 and lends itself to implementation of forward-directivity as discussed in subsequent sections.

The implementation of Equation 4-15 is carried through the discretization of its integrals. The predictor variables for magnitude (M_w), rupture length (*RL*) and location of the rupture length (*X*) are first discretized into bins and then Equation 4-15 can be rewritten as:

$$\lambda_{Sa,Non-NS}(y) = \upsilon \sum_{m_{w_j}} \sum_{rl_k} \sum_{\chi_m} \left[1 - I_{NS}(r_{rup})\right] G_{Sa\ |M_w,R_{rup}}(y \mid m_{w_j}, r_{rup}) P_M(m_{w_j}) P_{RL}(rl_k) P_X(\chi_m) \quad (4\text{-}16)$$

where m_j, rl_k, and χ_m are the center point of the M_w, RL, and X bins, respectively; j, k, and m are summation indices; $P_M(m_j)$ denotes the probability that the magnitude falls within the j^{th} magnitude bin; $P_{RL}(rl_k)$ denotes the probability that the rupture length falls within the k^{th} rupture length bin; and $P_X(\chi_m)$ denotes the probability that the location of the rupture falls within the m^{th} bin for location of rupture. These discrete probabilities are obtained from the corresponding probability density functions in Equation 4-15.

4.6. Near source scenarios when no pulses are present [$\lambda_{EDP,NS\&No\text{-}Pulse}(x)$]

The approach for near-source ground motions without pulses is identical to that for non-near source ground motions, except that only the appropriate scenarios (near-source scenarios with no pulses) are considered when computing the intensity motion hazard (λ_{Sa}). Whenever the closest distance to the fault was less than 60 km, that scenario was considered as a near source scenario. The mean annual frequency of Engineering Demand Parameter exceeding x for near-source no-pulse-like events, $\lambda_{EDP,NS\&No\text{-}Pulse}$, is given by Equation 4-2 but using $S_{a,NS\&No\text{-}Pulse}$ as the intensity measure:

$$\lambda_{EDP,NS\&No-Pulse}(x) = \int P[(EDP \geq x) \mid S_a = y] \mid d\lambda_{S_a,NS\&No-Pulse}(y) \mid \qquad (4\text{-}17)$$

In Equation 4-17, $d\lambda_{S_{a,NS\&No-Pulse}}(y)$ is defined as the mean annual frequency of occurrence of S_a for the near-source hazard due to non–pulse-like records, which is obtained from the corresponding hazard curve for $\lambda_{S_{a,NS\&No-Pulse}}(y)$ and is given by:

$$\lambda_{Sa,NS\&No-Pulse}(y) = \nu \int_{m_w} \int_{rl} \int_{x} \int_{h} I_{NS}(r_{rup}) G_{Sa\,|M_w,R_{rup},No-Pulse}(y \mid m_w, r_{rup}, Z)$$
$$.(1 - P(pulse \mid r_{rup}, S, \theta)).f_{M_w}(m_w).f_{RL}(m_w).f_X(m_w, rl).f_H(h).dm_w.drl.dx.dh \quad (4\text{-}18)$$

where H is the location of the hypocenter defined between the interval [0,1] where h=0 and h=1 imply either end of the ruptured fault, and the variables Z, S, and θ are parameterizations used to characterize forward-directivity ground motions (Somerville et al. 1997). S, and θ were previously defined, and Z is defined as $\xi cos(\theta)$, where ξ is the fraction of the fault rupturing towards a site ($\xi = S/RL$). All other variables were previously defined. The probability of pulse occurrence *P(pulse)* is given by Iervolino and Cornel (2008) and is defined in Equation 4-7. The location of the hypocenter was assumed to be randomly located along the fault with a uniform distribution. Rupture was assumed to progress from the hypocenter towards each end of the ruptured fault. In Equation 4-18, r_{rup} is a function of rupture length (rl) and the location of the ruptured segment (χ). The variables S and θ are a function of the location of the hypocenter (h), the location of the fault segment (χ) and the rupture length. The term $G_{S_a|M_w,R_{rup},No-Pulse}$ is defined by Equation 4-14 and represents the Complementary Cumulative Gaussian distribution function of S_a conditioned on M_w, R_{rup} when no pulse-like ground motions are considered. Such an attenuation relationship could be derived by excluding pulse-like ground motion from the database. Although no such relationship has been derived to date, it could be approximated by considering the Somerville et al. (1997) model for backward directivity or simply by using a model that does not include directivity. Equation 4-18 is solved through a discretization similar to that described by Equation 4-16. Such discretization is omitted herein for brevity.

4.7. Near source scenarios when Forward-Directivity pulses are not Dominant [$\lambda_{EDP,NS\&Pulse,\ pulse\ not\ dominant}(x)$]

Chapter 3 discusses cases in which structures subjected to pulse-like forward-directivity ground motions are controlled by the forward-directivity pulse. In general, it was observed that whenever the forward-directivity pulse is within a certain interval that contains the predominant period of the structure, then the structural response is controlled by the forward-directivity pulse. Assuming a log-normal distribution for the period of the velocity pulse, the probability that the forward-directivity pulse is within a certain range of the structural period is given by:

$$P_{within}(T_1 | T_p, \sigma_{Tp}) = \Phi(ln(T_{upper}) \mid ln(T_p), \sigma_{Tp}) - \Phi(ln(T_{lower}) \mid ln(T_p), \sigma_{Tp}) \quad (4\text{-}19)$$

where T_1 is the predominant period of the structure, T_p and σ_{Tp} are the mean value and standard deviation of the pulse period which in turn are function of earthquake magnitude (Equation 4-3). T_{upper} and T_{lower} define the upper and lower period bounds where the structural response is controlled by the forward-directivity pulse. In Chapter 3, such ranges were deemed to be equal to $T_{upper} = 2.5\ T_1$ and $T_{lower} = 0.5\ T_1$ for the MDOF structures analyzed in that chapter.

The method of determining the mean annual frequency of exceedance of an EDP when forward-directivity pulses are not dominant is similar to Equation 4-2. The sole modification is that λ_{Sa} is defined as:

$$\lambda_{Sa,NS\&Pulse,not\ dominant}(y) = \nu \int_{m_w} \int_{rl} \int_{x} \int_{h} I_{NS}(r_{rup}) G_{Sa|M_w,R_{rup},Pulse}(y \mid m_w, r_{rup}, Z)$$
$$.(1 - P(pulse \mid r_{rup}, S, \theta)).(1 - P_{within}(T_1, M_w)).f_{M_w}(m_w).f_{RL}(m_w).f_X(m_w, rl) \quad (4\text{-}20)$$
$$.f_H(h).dm_w.drl.dx.dh$$

Note that in this section the Complementary Cumulative Gaussian distribution function of S_a ($G_{Sa|M,Rrup,Pulse}$) should be computed from an attenuation relationships that considers pulse-like ground motions, such as the broadband-directivity model of Somerville et al. (1997). Equation 4-20 is solved through a discretization similar to that described by Equation 4-16. Such discretization is omitted herein for brevity.

4.8. Near source scenarios when Forward-Directivity pulses are Dominant [$\lambda_{EDP,NS\&Pulse,pulse\ dominant}(x)$]

The treatment of near source scenarios (e.g. r_{rup} < 60 km) when the directivity pulses are dominant (e.g. $T_{lower} < T_p < T_{upper}$) differs from the treatment of other sources in hazard described in Sections 4.5 to 4.7. For other cases, Equation 4-2 was used to define the hazard for the EDP. On the other hand, when forward-directivity pulses control the ground motion hazard, each possible scenario is considered along with the probability of occurrence of that scenario and a numerically defined function that relates the EDP to the pulse period and pulse amplitude through IDA analyses of equivalent pulses.

For simplicity, $\lambda_{EDP,NS\&Pulse,\ pulse\ dominant}(x)$ is defined through a discrete form of the hazard integral rather than its integral form. In schematic form, it is given as:

$$\lambda_{EDP,NS\&Pulse,\ dominant}(y) = \nu \sum_{all\ scenarios} P_{scenario} \cdot I_{within}(T_p) \cdot I_{NS}(r_{rup}) \cdot P_{pulse} \cdot H(EDP_{scenario}(T_p, A_p) - x) \quad (4\text{-}21)$$

Where $I_{within}(.)$ is a flag that is equal to one when T_p falls within the interval [T_{lower}, T_{upper}] and zero otherwise, $I_{NS}(.)$ is a flag that is equal to 1 when $r_{rup} < 60$ km and zero otherwise, H is the Heaviside step function ($H(x) = 0$ for $x < 0$, and $H(x) = 1$ for $x \geq 0$), and P_{pulse} is discussed in Section 4.3.4. The functions $I_{within}(.)$, and $I_{NS}(.)$ are included in the summation to eliminate all scenarios that do not qualify as near-source scenarios with pulse period in the range where the pulse period is dominant. Each scenario is weighted by the probability of that scenario taking place (discussed below), and the probability of that scenario having a pulse, $P(pulse \mid r_{rup}, S, \theta)$. Finally, the function $H(.)$ ensures that only the scenarios that contribute to the hazard (e.g. where $EDP > x$) are considered for $\lambda_{EDP,NS\&Pulse,pulse\ dominant}(x)$. $EDP_{scenario}(T_p, A_p)$ is the EDP computed from time-domain analyses for a given pulse period and pulse amplitude using the Gabor pulse as the equivalent pulse representations (Chapter 3, Figure 3-12)

The summation over all possible scenarios implies a multiple summation over all possible realizations of the predictive variables, namely magnitude (M_w), rupture length (RL), rupture location (X), hypocenter location (H), pulse period (T_p), and pulse amplitude (A_p). Each of these variables is discretized into bins. The probability of an individual scenario is given by:

$$P_{scenario} = P_M(m_w)\, P_{RL}(rl|m_w)\, P_X(\chi|rl)\, P_H(h)\, P_{Tp}(t_p|m_w)\, P_{Ap}(a_p|m_w, r_{rup}) \quad (4\text{-}22)$$

where the lower case variables represent the center point of each corresponding bin (the summation indices are omitted for clarity). The discrete probabilities *P* are computed using the continuous definitions given earlier. Note that pulse period and pulse amplitude are assumed to be independent, log normally distributed random variables (Section 4.3.1and 4.3.2). Their mutual independence (Section 4.3.3) is crucial for the validity of Equation 4-22. As discussed earlier, the rupture length is assumed to be uniformly distributed along the fault and the location of the hypocenter is assumed to be uniformly distributed along the ruptured fault.

4.9. Numerical Implementation of the proposed PSDA analysis

Figure 4-2 and Figure 4-3 illustrate the flow chart of the numerical implementation of the proposed PSDA analysis. The implementation is described for a single fault. For multiple faults, hazard is computed for each fault individually and then it is added to compute the overall hazard. The implementation consists of four general modules, a Main Module where all the input parameters and the bin sizes for all the descriptive variables are defined, and each of the other modules is called (Figure 4-2), a PSHA module where the hazard curves for the intensity measure are computed (Figure 4-3), a traditional PSDA module where Equation 4-2 is implemented for all scenarios (Figure 4-4) except the near-source scenario with dominant pulses, and finally the time-domain PSDA module for the computation of Equation 4-21 (Figure 4-5). All the probability distributions used in the implementation are bounded at ±3 standard deviations. The probability density functions are renormalized such that they satisfy all necessary conditions.

Equation 4-2 requires the definition of $d\lambda_{Sa}$. $d\lambda_{Sa}$ can be approximated by discretizing *Sa* into bins and taking $d\lambda_{Sa} = \lambda_{Sa,i} - \lambda_{Sa,i-1}$ where *i* is a summation counter for a discrete version of Equation 4-2. This approach, however, is not practical because it forces the use of identical bin sizes in the PSHA analysis and the PSDA analyses. Alternatively, each of the resulting hazard curves for S_a can be interpolated using a piece-wise polynomial (e.g. a cubic spline interpolation) and the derivatives can be found analytically. Hence, Equation 4-2 can then be expressed as:

$$\lambda_{EDP}(x) = \sum_i P[EDP \geq x \mid Sa_i] \mid \lambda'_{Sa}(Sa = Sa_i)\Delta Sa_i \mid \quad (4\text{-}23)$$

Where $\lambda'_{Sa}(S_a=S_{ai})$ is the derivative of λ_{Sa} obtained analytically from the piece-wise polynomial interpolation at $S_a=S_{ai}$, and ΔS_{ai} is the bin size for S_a.

The heaviest computational cost of the proposed method lies in the definition of the response surface $EDP\ (T_p, A_p)$ (Section 3.8). Note that because of the short duration of the equivalent pulses, the computational cost for defining the response surface is not nearly as significant as it would be for recorded ground motions. Moreover, uncertainties in structural response or properties could be considered through structural reliability methods to define the response surface in probabilistic terms (e.g. $P(EDP>x|T_p, A_p)$, in which case variations due to structural response (in addition to those due to input motion variability which are considered in this study) can be also included in the analyses.

4.10. Example Application

To illustrate the methodology presented in this work, a PSDA analysis is conducted for the 7-story structure described in Chapter 3 located at various distances from an arbitrary fault. The structure is assumed to be on rock. In this example, only the fault normal component is considered, and it is assumed that the weak axis of the building is oriented in the fault normal direction. The Maximum Inter-story Ductility Demand (MIDD) is selected as the EDP for the analysis based on considerations presented in Chapter 3.

4.10.1. Statistical Models to Correlate EDPs to IMs

The 7-story building was subjected to ground motions recorded within 20 km from a fault (see Chapter 3). The near-fault ground motions were divided into two groups, one group consisting of ground motions with pulses as identified by the procedure of Baker (2007), and the other group for ground motions without pulses. MIDD was assumed to be normally distributed with mean *MIDD* and standard deviation σ. A power-law relationship between the mean MIDD and $S_a(T_1)$ was assumed. The parameters of the relationship were obtained using a Maximum Likelihood regression assuming a normal distribution for MIDD. For near-fault motions without pulses the resulting relationship is given by:

$$MIDD = \begin{cases} 1 + 13(S_a(T_1) - 0.1)^{0.7} & \text{for } Sa > 0.1 \\ 1 \quad \text{for } Sa \le 0.1 \end{cases} \tag{4-24a}$$

with σ given by

$$\sigma = \begin{cases} \sigma_{\min} \text{ for } S_a \le x_o \\ (\sigma_{\max} - \sigma_{\min}) \dfrac{S_a - x_o}{x_1 - x_o} + \sigma_{\min} \quad \text{for } x_1 > S_a > x_o \\ \sigma_{\max} \text{ for } S_a \ge x_1 \end{cases} \tag{4-24b}$$

where x_o = 0.1, x_1 = 0.57, $\sigma_{\max}$ = 1.98, and σ_{min} = 0.34. The range of applicability of equation 4-24 is $0 < S_a(T_1) \le 1.9$g. As indicated, it was assume that *MIDD* has a normal distribution, however, the normal distribution is truncated to prevent physically unrealizable MIDD values (e.g. MIDD<1). Similarly, another power relationship between $S_a(T_1)$ and *MIDD* from near-fault ground motion with forward-directivity effects was computed:

$$MIDD = 1 + 24.6(S_a(T_1) - 0.1)^{0.71} \tag{4-25}$$

with σ given by Equation 4-24b with x_o = 0.1, x_1 = 1.24, $\sigma_{\max}$ = 8.54, and σ_{min} = 2.11. The applicability range for Equation 4-25 is $0 < S_a(T_1) \le 1.9$g. Figure 4-6 compares predicted EDPs from Equation 4-24 and 4-25 with measured EDPs due to the associated ground motions. Note that the minimum value of MIDD is 1.0.

4.10.2. Fault and Site Information

A 240 km vertical strike-slip fault was considered as the single seismic source (Figure 4-7). An arbitrary coordinate system as shown in the figure was assigned. A truncated exponential model was used to define the probability density function for magnitude. A seismicity rate of 1 was used for simplicity and a minimum magnitude of M_w = 5.0 was considered, assuming that lower magnitude earthquake do not contribute to hazard. Rupture

lengths corresponding to each magnitude were estimated based on Equation 4-26, as presented by Wells and Coppersmith (1994):

$$\log(RLD) = -2.57 + 0.62M_w \qquad \text{with} \qquad \sigma = 0.15 \tag{4-26}$$

Where *RLD* is the mean value of the rupture length and σ is the standard deviation in log units for the rupture length. The rupture length is assumed to follow a log normal distribution.

The range of magnitudes (M_w), probability of each magnitude, rupture length (R_L) associated to each magnitude, and the probability of each rupture length are presented in Table 4-2 for a given choice of magnitude bins. The fault was assumed to be a linear source and its depth was neglected which assumes that the fault has a uniform probability of rupture along its depth and length. Shear velocity of the rock (V_s) was assumed as 760 m/sec. Depth to V_S=1.0 km/s at the site (defined as Z_1 in Abrahamson & Silva NGA) was taken as 23.5 m.

Locations with various distances from the fault were considered in order to study the effect of forward-directivity based on source-site distance. Hazard for each location was calculated using four methodologies previously discussed: the New-PSDA Model proposed in this work, the Traditional-PSDA, the Broadband-PSDA, and the Enhanced-Broadband-PSDA models (see Section 4.2).

4.10.3. Results

A grid of points of 10 km along strike and 5 km perpendicular to the fault was established and seismic hazard curves [$\lambda_{EDP}(x)$] were obtained using the four aforementioned

PSDA models at each node of the grid. As an example, results are illustrated in Figure 4-8 for four nodes located along an axis at the center of the fault and at fault distances of 6 km, 11 km, 16 km, and 21 km from the fault. As expected, the Traditional-PSHA which does not account for forward-directivity effects, underestimates the hazard in near-fault zone compared to the other PSDA models which include forward-directivity effects. The maximum difference between hazards predicted from the aforementioned methods occurs for sites close to the fault and reduces as the distance from the fault increases or as the hazard level decreases (shorter return period). Results from the Traditional-PSDA model converge to those from the Broadband-PSDA model and results from the Enhanced-Broadband-PSDA converge to those from the New-PSDA at a distance about 16 km. However, results from all models converge to the same level of hazard at a distance about 25 km. Recall that both the Enhanced-Broadband-PSDA and the New-PSDA models consider the special response of the structure to pulse-like motions, the Enhanced-Broadband-PSDA does it through separate relationships between EDP and $S_a(T_1)$ for pulse- and non-pulse-like ground motions (Equations 4-24 and 4-25), while the New-PSDA does it through time-domain analyses.

In Figure 4-8, the contributions to hazard to the Enhanced-Broadband-PSDA model are divided into the hazard due to pulse-like motions (BB-Pulse) and hazard due to non-pulse-like motions (BB-No Pulse). Observe how at low return periods, the hazard is controlled by non-pulse motions while the reverse is true for long return periods. This occurs because the likelihood of occurrence of pulse-scenarios is very low hence at low return periods there is a minimal contribution to hazard by these scenarios. On the other hand, at long return periods,

non-pulse scenarios cannot contribute significantly to hazard because of the low probability that such scenarios can generate large MIDDs.

Similarly, the hazard predicted by the New-PSDA model is summation of near-source scenarios with dominant pulses (NS-P-in), near-source scenarios with pulses but where the pulse does not control the response of the structure (NS-P-out), near-source scenarios without pulses (NS-NP) and non near-source scenarios (Non-NS). As expected, the Non-NS scenario does not contribute to hazard for any of the distances considered. Similarly near-source pulse scenarios that are outside the range where the pulse is dominant contribute little to hazard. This is because these scenarios have a very low probability of occurring (for example, for a site at 11 km from the fault, the probability of a near-source scenario with pulses is only 0.4%, and of those only 0.21% are scenarios with pulses outside of the range where the pulse is dominant). At low return periods, most of the hazard results from non-pulse scenarios (which contribute nearly 99.5% of all possible scenarios), and the pulse scenarios that are in the range where pulses are dominant. Those scenarios, while constituting only (on average) 0.2% of all possible scenarios, contribute significantly to hazard because time-domain analyses do predict large EDPs for these scenarios.

Figure 4-9 shows the magnitude-distance deaggregation of hazard for some of the cases considered in Figure 6. Several interesting observations with significant relevance to hazard analysis can be inferred from the deaggregation plots. For close distances to the fault (Figure 4-9a), the proposed model predicts an increase in the contribution to hazard from small magnitude earthquakes with respect to the predictions using other PSDA models. This difference is due to the ability of the time-domain analyses to capture the large EDPs that

result from resonance when the pulse period matches the structural period. When forward-directivity is included through a broadband model the effect of the pulse-type motions on the response spectra is smeared over a broad period band and the particular resonance that develops with pulse-type motions is not captured. For example, the contribution for a Magnitude-Distance bin centered at 6 km (Figure 7a) increases from 4.1% to 10.3% when considering time-domain analyses (the comparison is with the Enhanced-Broadband model that considers pulse motions through $S_a(T_1)$). Equally important, the contribution of more distant earthquake increases significantly. For example, the time-domain PSDA predicts a small contribution to hazard of low magnitude earthquakes for distances up to 15 km (up to 5% contribution to hazard), while the Enhanced-Broadband model predicts no contribution to hazard for distances higher than 6 km. The same pattern (e.g. increase in the contribution to hazard of small earthquakes) persists even for distances of 21 km from the fault (Figure 4-9d) but is not present at larger distances. Figure 4-10 plots the magnitude-distance deaggregation of the New-PSDA model separated into the contributions of near-source and far-source events, those with and without pulses, and those with pulses that control structural response. In Figure 4-10, different plots are presented for different hazard components (e.g. near source with dominant pulses (NS-P-in), near source without dominant pulses (NS-P-out), near source with no pulses (NS-NP-in and NS-NP-out, where in and out indicate whether the pulse period is close to the structural period or not, and non near source scenarios). The y-axis is the contribution to total hazard for each bin.Magnitude and pulse-period deaggregation results show that as site-source distance increases, higher magnitudes contribute more in hazard. Note that the contribution of near-source motions with dominant pulses (NS-P-in) dominates the contribution of small to intermediate magnitude earthquakes

to the overall hazard. This makes sense when one considers that a M_w 5.75 earthquake generates a pulse with a period of 1.1 sec, which is close to the period of the structure (1.0 sec). This confirms previous speculation that smaller magnitude earthquakes can contribute more to hazard than large magnitude earthquakes (Somerville 2003).

Figure 4-11 shows a magnitude and pulse-period deaggregation and Figure 4-12 shows a magnitude pulse-amplitude deaggregation plot. At near distances to the fault, lower magnitude events have larger contribution to hazard for shorter periods. As magnitude increases the contribution of longer period increases. At areas close to the fault, events with lower magnitudes generate pulses with shorter period but relatively large amplitudes. These short periods pulses excite higher modes of the structure. Intermediate magnitude events generate pulses whose periods are equal to the elastic or nonlinear fundamental period of the structure. Large magnitude events generate pulses with long periods which do not fall within the range where pulse periods are dominant. At further distances, short period pulses generated with lower magnitude are attenuated and are not as effective as near distances. On the other hand, pulses generated with intermediate magnitude events are still strong enough to excite the structure and have more significant contribution.

These observations have significant relevance for the design of structures in near-fault regions, as they indicate the importance of considering the near-source pulses for smaller magnitude earthquakes. For these cases, it is necessary to consider pulse-like motions in evaluating hazards. For these cases, a deaggregation of pulse period and pulse amplitude can guide the selection of design ground motions. Figure 4-13 shows a deaggregation of pulse-period and pulse-amplitude for a site-to-fault distance of 6 km. This plot can be used directly

to select simplified pulses that contribute the most to hazard. In this particular case, it is obvious that pulse periods between 0.75 sec and 1.5 sec control design, and the dominant pulse amplitude is centered around 30 cm/sec. Simplified pulses with these characteristics can be selected for the design of this particular structure.

Figure 4-14 shows contours of variations between pseudo-acceleration of period 1.0 sec exceeding an arbitrary value (0.5 g) predicted by the Traditional-PSHA and the Broadband-PSHA models. Note that, in Figure 4-14 there are cases that the Broadband-PSHA predicts an intensity measure hazard level lower than the traditional-PSHA. These cases are associated to the situation that the first factor of directivity (defined by Somerville et al., which accounts for the change in the shaking intensity in the average horizontal component) becomes negative. Consequently, the Traditional-PSDA model underestimates EDP hazard (λ_{EDP}) when compared to the Broadband-PSDA, the Enhanced-Broadband-PSDA, and the New-PSDA models (respectively Figure 4-15, Figure 4-16, and Figure 4-17). The variation between the hazard curves of the aforesaid methods decreases when site-source distance is increased as shown in Figure 4-15, Figure 4-16, and Figure 4-17. Note that, λ_{EDP} was calculated for MIDD with intervals equal to 1. Therefore, IMs with small differences (for example 2%) predicted from the Traditional-PSHA and the Broadband-PSHA may result in MIDDs which fall in the same interval. Although the Broadband-PSDA and the Enhanced-Broadband-PSDA models account for forward-directivity effects and result in higher hazard compared to the Traditional-PSDA, they underestimate the hazard for higher EDPs compared to the New-PSDA model. For larger distance from the fault, where there is no directivity, the

variation between the New-PSDA and the other PSDA predictive models decrease and the λ_{EDP} predicted by all the models are in close agreement.

Higher MIDDs are associated with a narrower band of periods roughly equivalent to the fundamental period of the structure. This is not captured by broadband directivity models where the response spectrum of a structure will increase monotonically with respect to moment magnitude for all structural periods and hence the EDPs increase monotonically with an increase in the response spectra. On the other hand, the New-PSDA model provides more reasonable IMs utilized within the specified range. Within this range, forward-directivity pulses control structural response and result in higher demand. It is for this reason that in vicinity of the fault, predicted hazard based on the proposed New-PSDA model at higher EDPs is greater than those predicted from the both Broadband-PSDA models.

4.11. Conclusion

A new PSDA model was developed to include forward-directivity effects for near-fault zones. Events were classified as being near-source or not. Near-source events were separated to two categories; events with and without forward-directivity pulses. Near-source faults with pulses were divided into two different cases as events with pulses whose periods are roughly equal to the fundamental period of the structure and those that are not. For events with pulses in the vicinity of the fundamental period of the structure, rather than using a spectral based intensity measure, the EDP was computed using time-domain analyses with an equivalent pulse model. For other events, response spectra pseudo-acceleration was used as the Intensity Measure to predict the structural response using a statistical model.

Results of the New-PSDA model were compared with the results obtained from a PSDA model which does not account for forward-directivity and a PSDA model that accounts for forward directivity through a broadband model (Somerville et al. 1997, Abrahamson 2000). Results showed that even though the Broadband-PSDA models accounts for forward-directivity and predicts larger hazard for near-fault scenarios, it still underestimates the hazard compared to the proposed PSDA model. When a separate function is used to predict structural response for pulse-like motions, the computed hazard increases to nearly the level predicted by the proposed methodology. Nonetheless it still fails to fully capture the hazard levels computed by the new time-domain methodology. The increase in computed hazard in the time-domain methodology results from the different treatment of pulse-like motions: whereas existing methodologies consider near-fault hazard through average increase in response spectral estimates, the proposed methodology captures its narrowband nature. Moreover, by performing structural analyses for each realization of the pulse-type motions, the resonant nature of the structural response to pulse-like motions is captured and introduced into the hazard computation.

Analysis with the proposed methodology indicated that near-source structures with structural periods close to about 1.0 seconds can be affected by smaller magnitude earthquakes that generate ground motion pulses with periods close to the structural period. Traditional, spectral acceleration-based PSDA analysis do not capture this effect and underestimate the contribution to hazard from small magnitude earthquakes and can lead to errors in ground motion selection for design.

Although the example selected in this report corresponds to an idealized MDOF structure and an idealized fault, both the fault model and the structural model were selected to represent realistic conditions and the results shown would very likely be reproduced for actual structures located near active faults. The proposed methodology not only computes a more adequate hazard from existing faults, but also provides, through pulse-period and pulse-amplitude disaggregation, a tool for selecting ground motions for design of such structures.

4.12. Figures

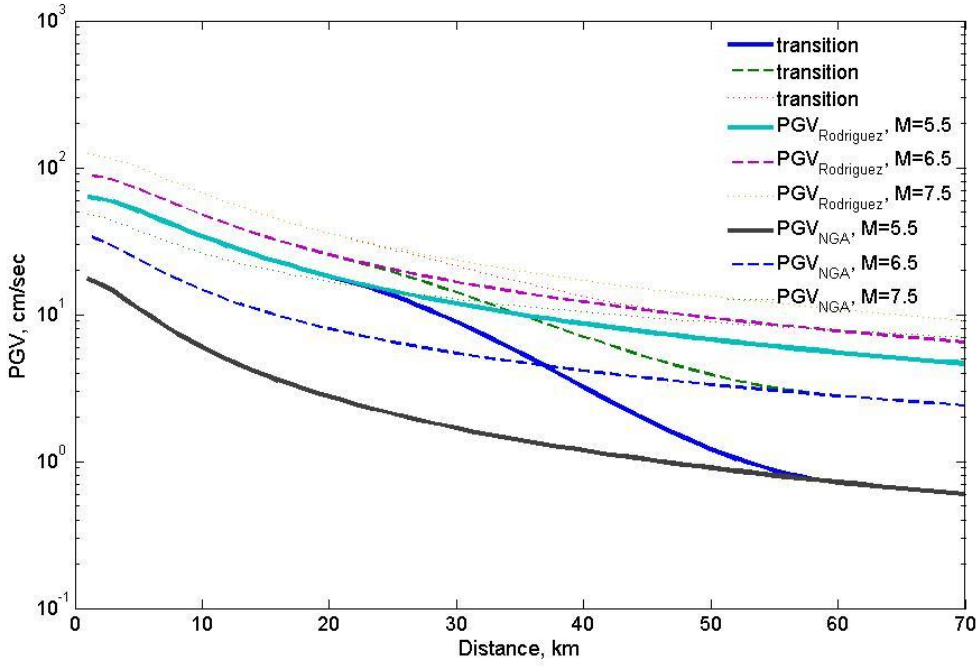

Figure 4-1: Transition from PGV estimated by Bray and Rodriguez-Marek (2004) to PGV estimated by Abrahamson and Silva (2007) for distances between 20 and 60 km.

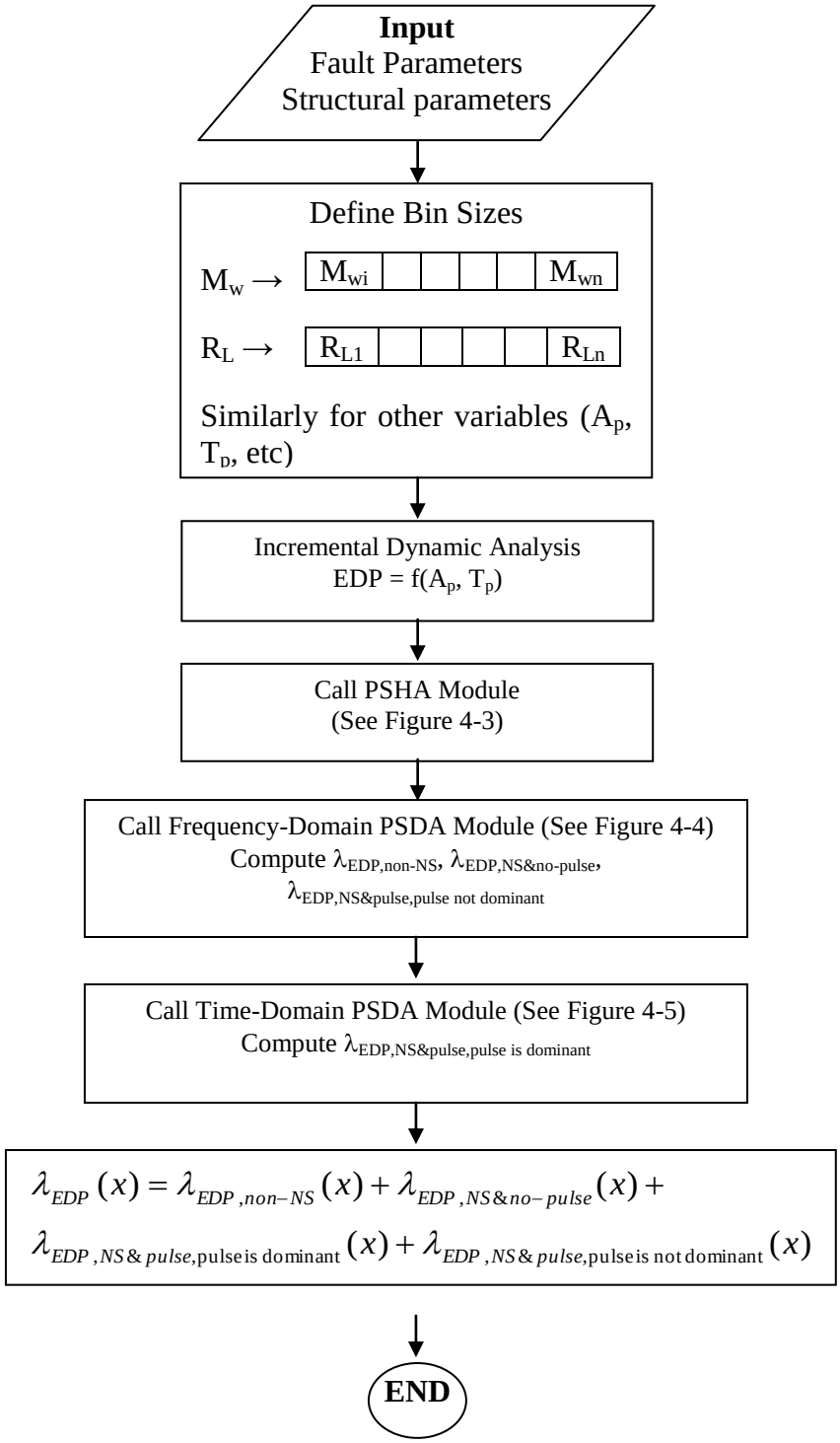

Figure 4-2: Flow chart for the main module.

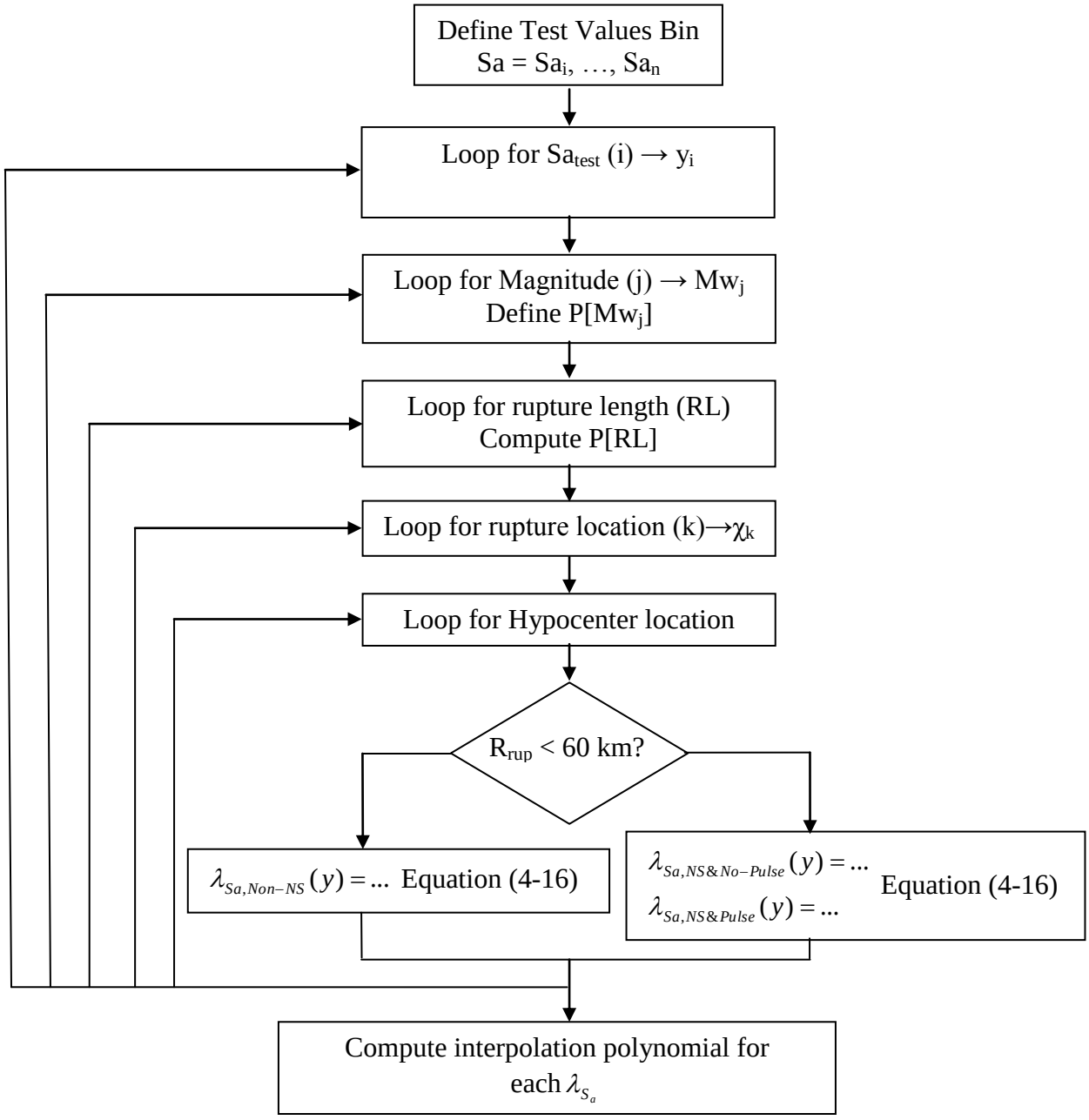

Figure 4-3: Flow chart for the PSHA module.
Note that this module is used to compute the hazard curve for the intensity measure, $S_a(T_1)$.

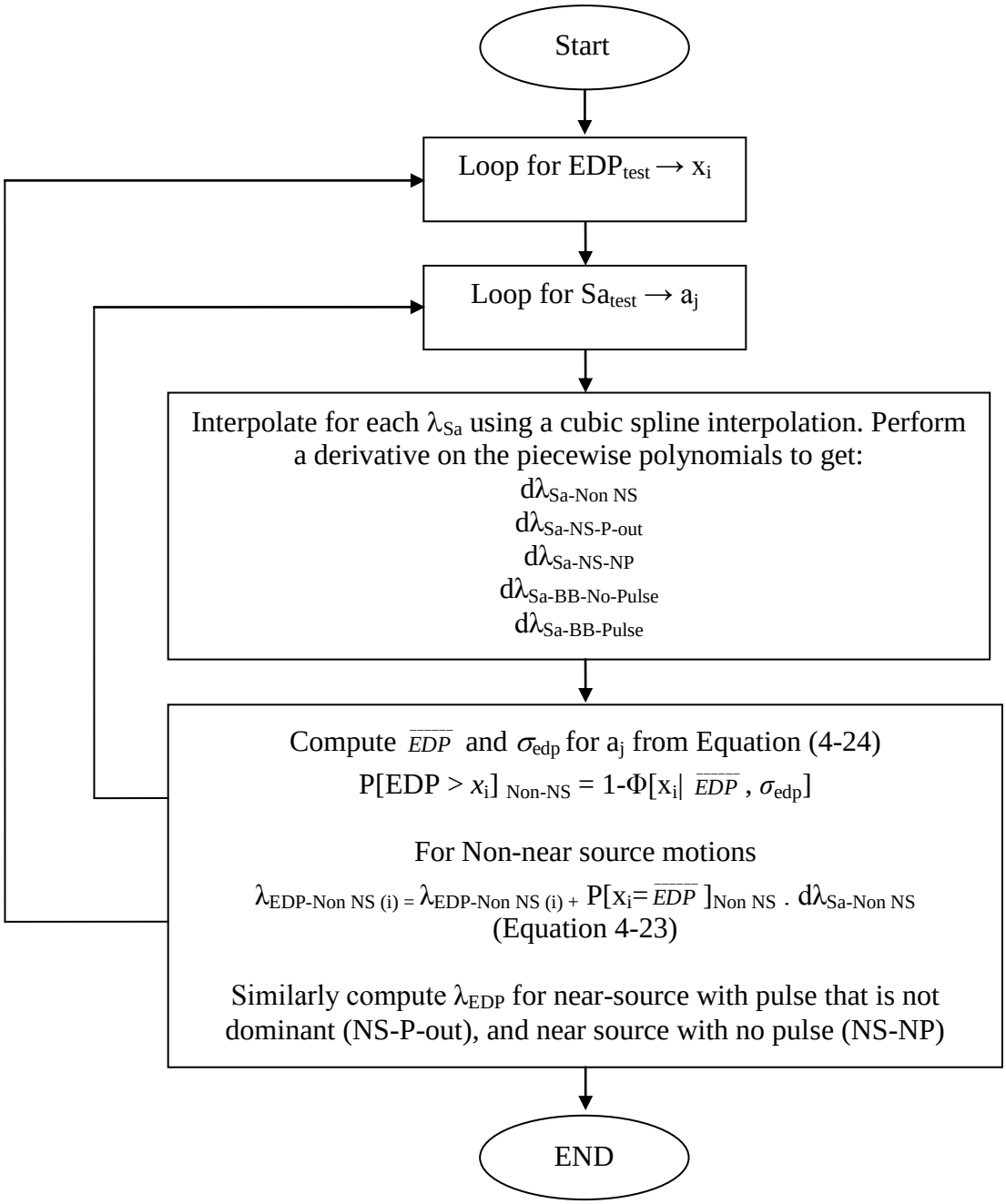

Figure 4-4: Frequency-Domain PSDA Module

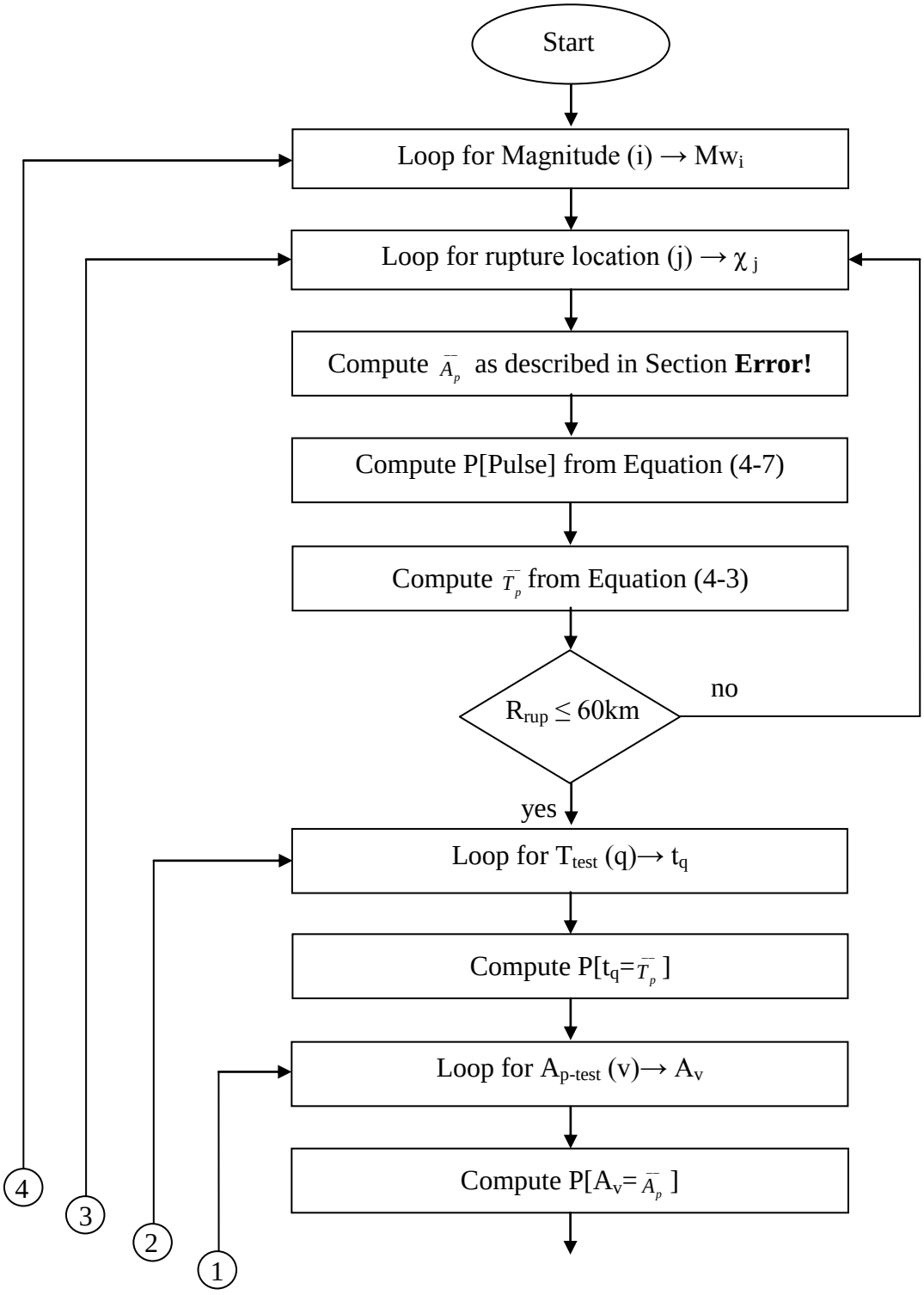

Figure 4-5a: Time-Domain PSDA Module

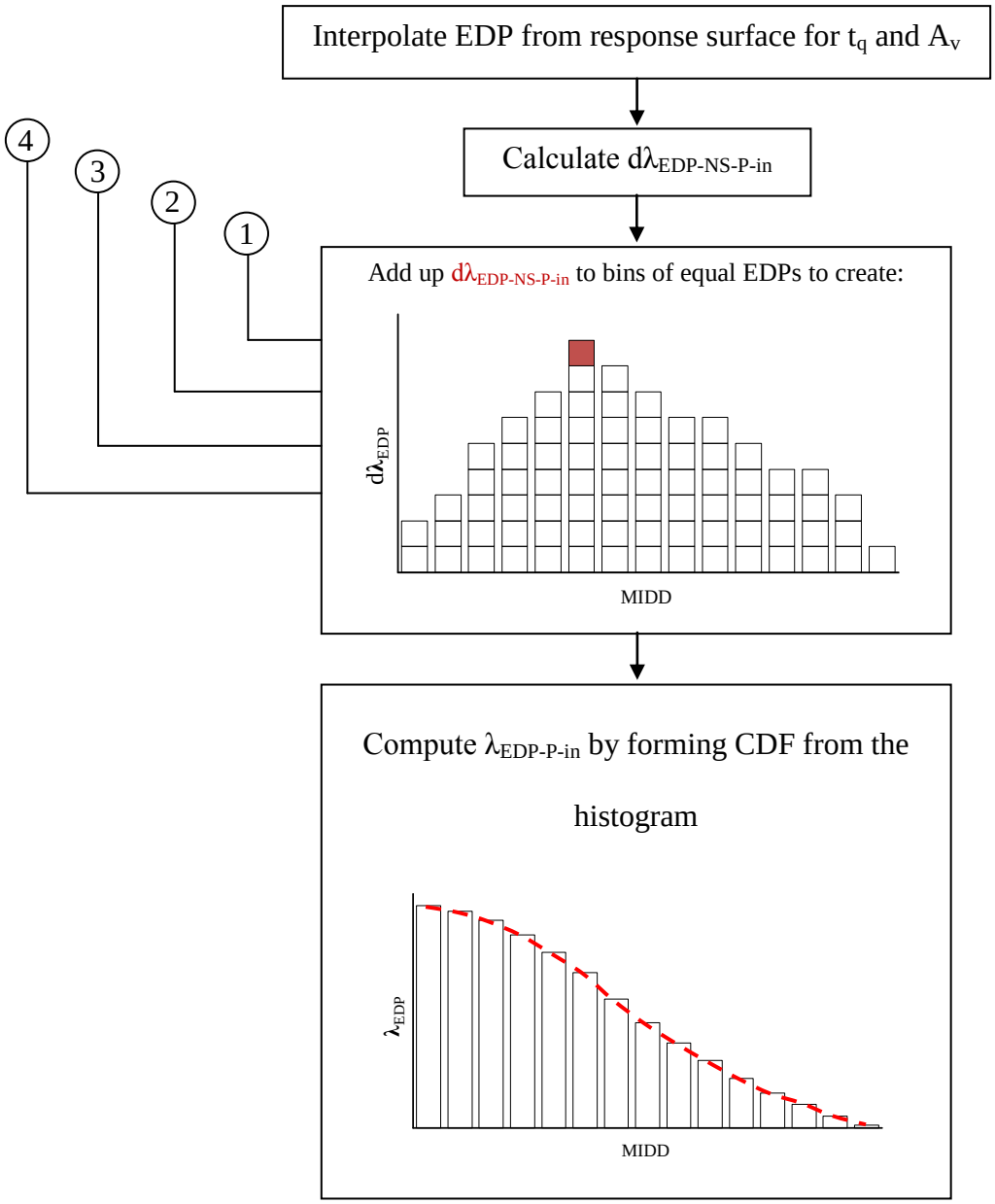

Figure 4-5b: Time-Domain PSDA Module

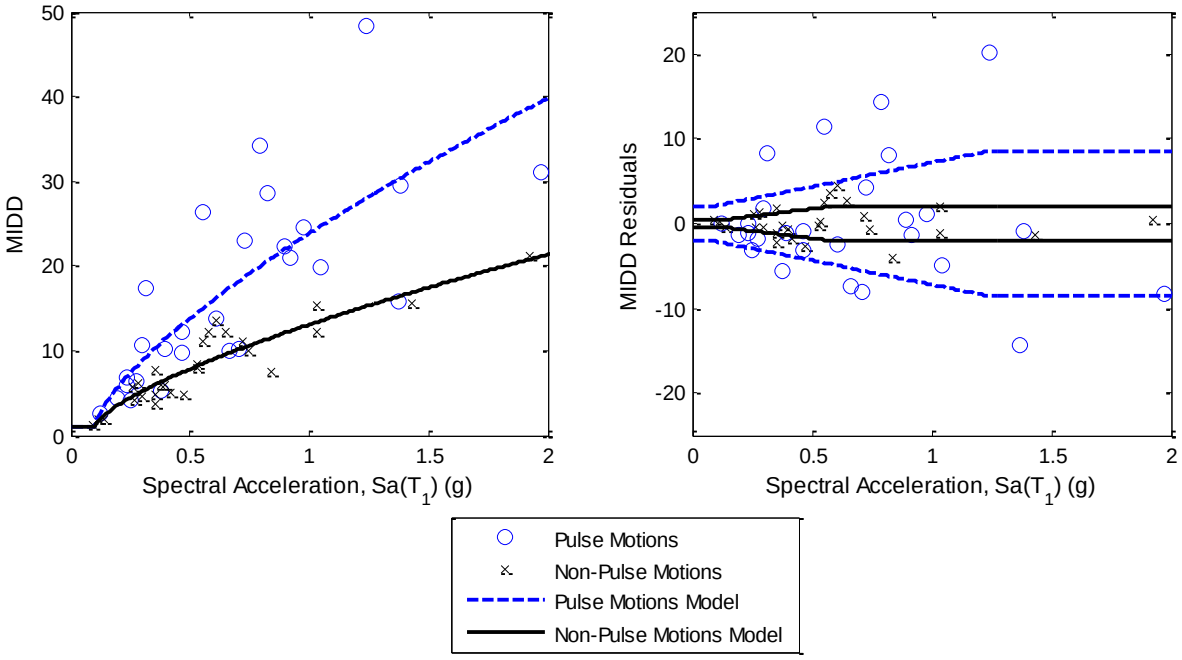

Figure 4-6: Predictive model for Maximum Inter-story Ductility Demand (MIDD) as a function of spectral acceleration at the first mode period of the structure. The figure on left shows the mean predictions (Equations 4-24a and 4-25) along with MIDD computed from dynamic analyses. The figure on the right shows the residuals (MIDD computed for each record minus the predicted MIDD for each record) and the model for standard deviation (Equation 4-24b).

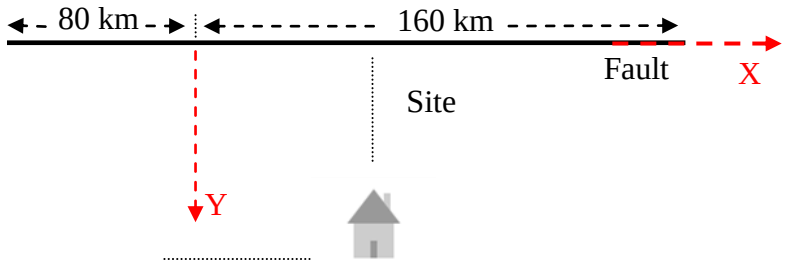

Figure 4-7: Fault and site geometry.

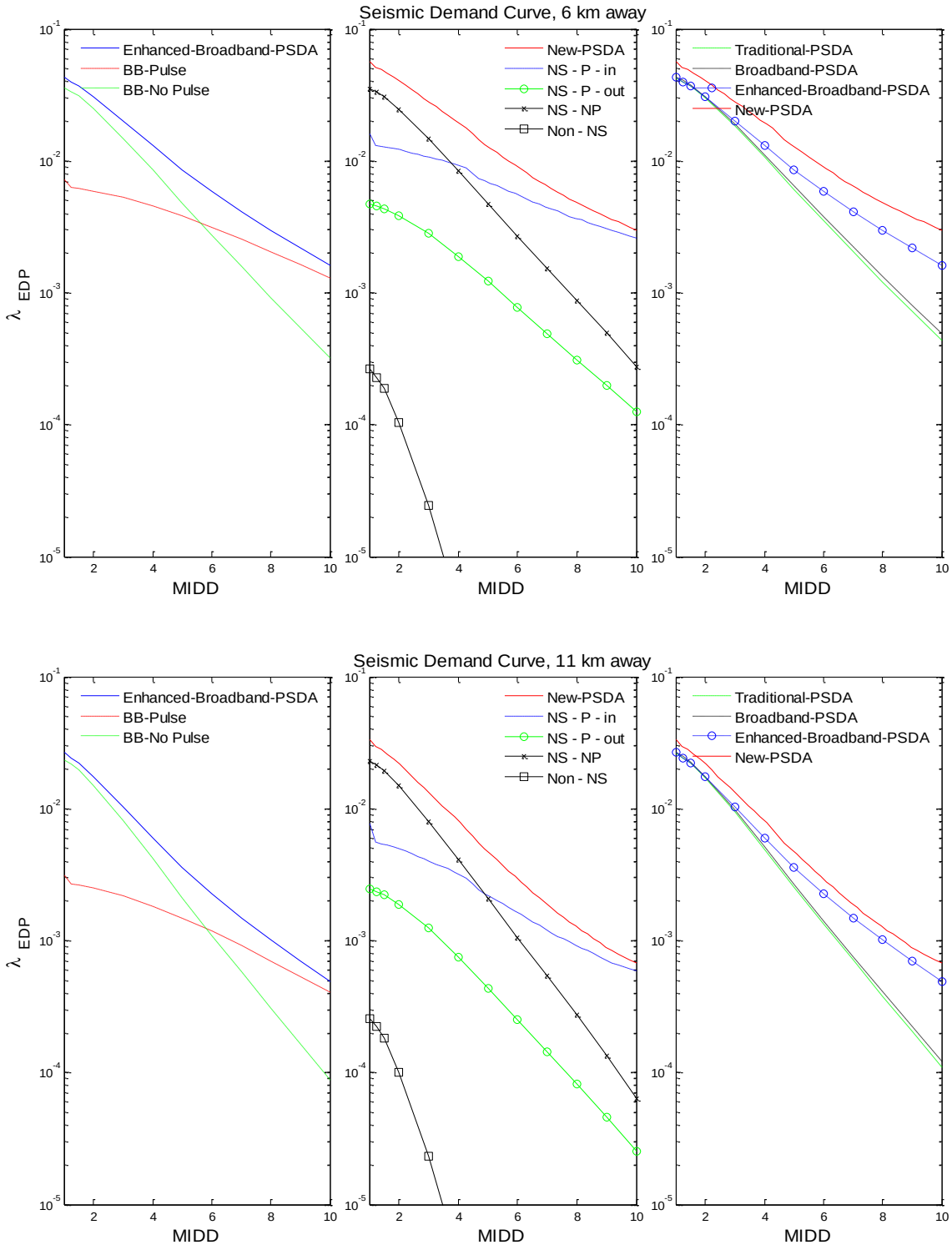

Figure 4-8a: MAF of EDP for sites located along the centerline of the fault at 6 and 11 km from the fault.

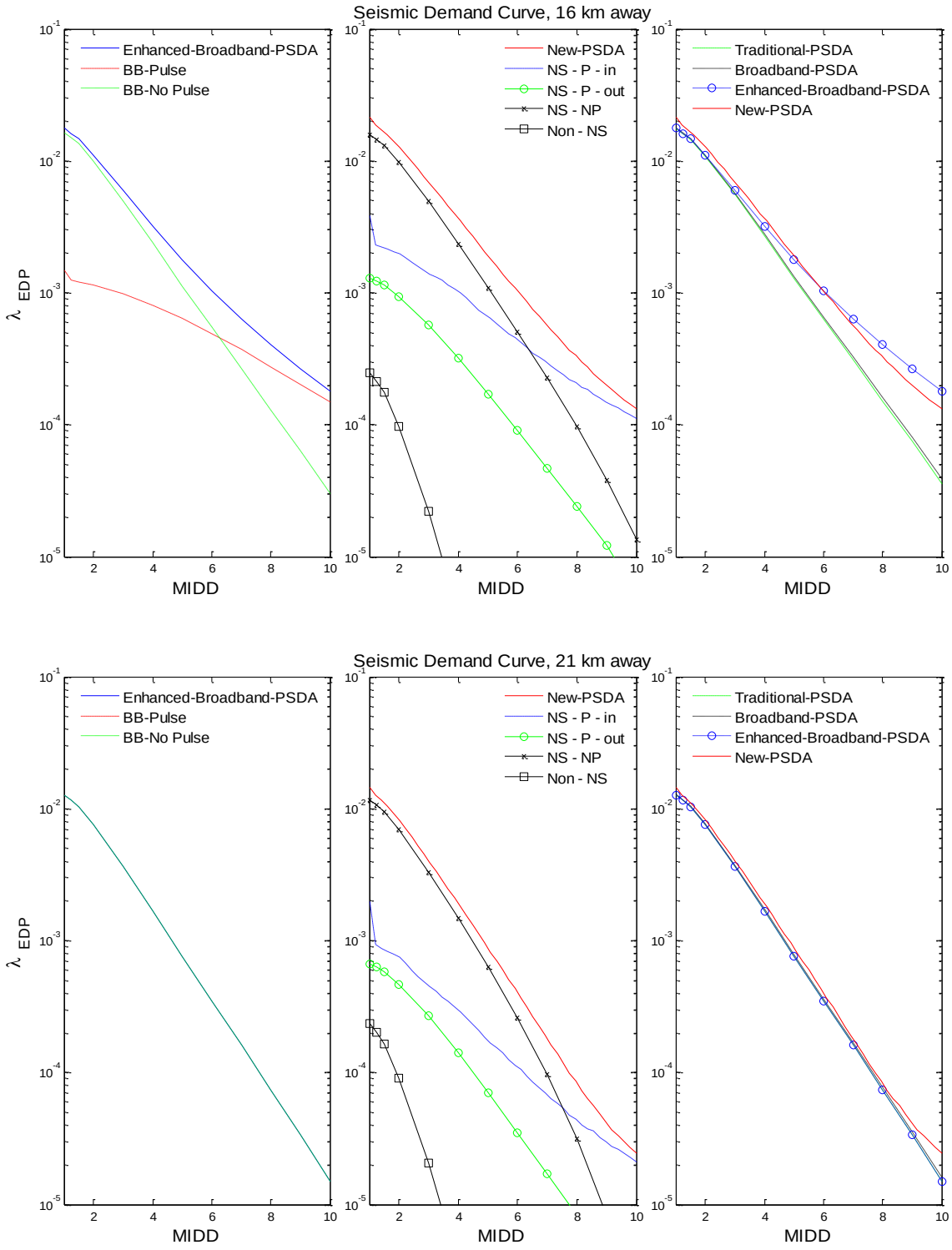

Figure 4-8b: MAF of EDP for sites located along the centerline of the fault at 16 and 21 km from the fault.

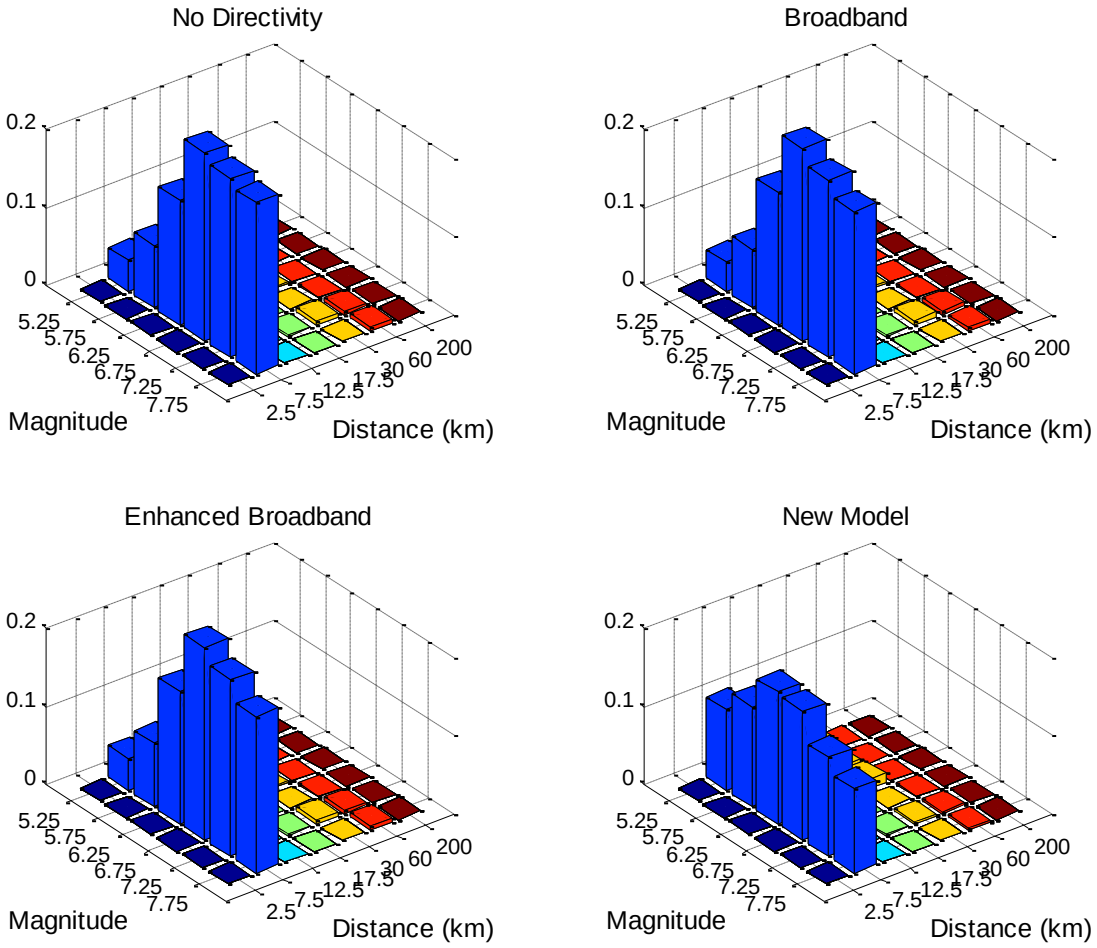

Figure 4-9a: Magnitude and distance deaggregation of λ_{EDP} when EDP = 5
for four different PSDA models and for a site located at 6 km from the fault along its centerline. The y-axis shows percentage contribution to risk for each PSDA model.

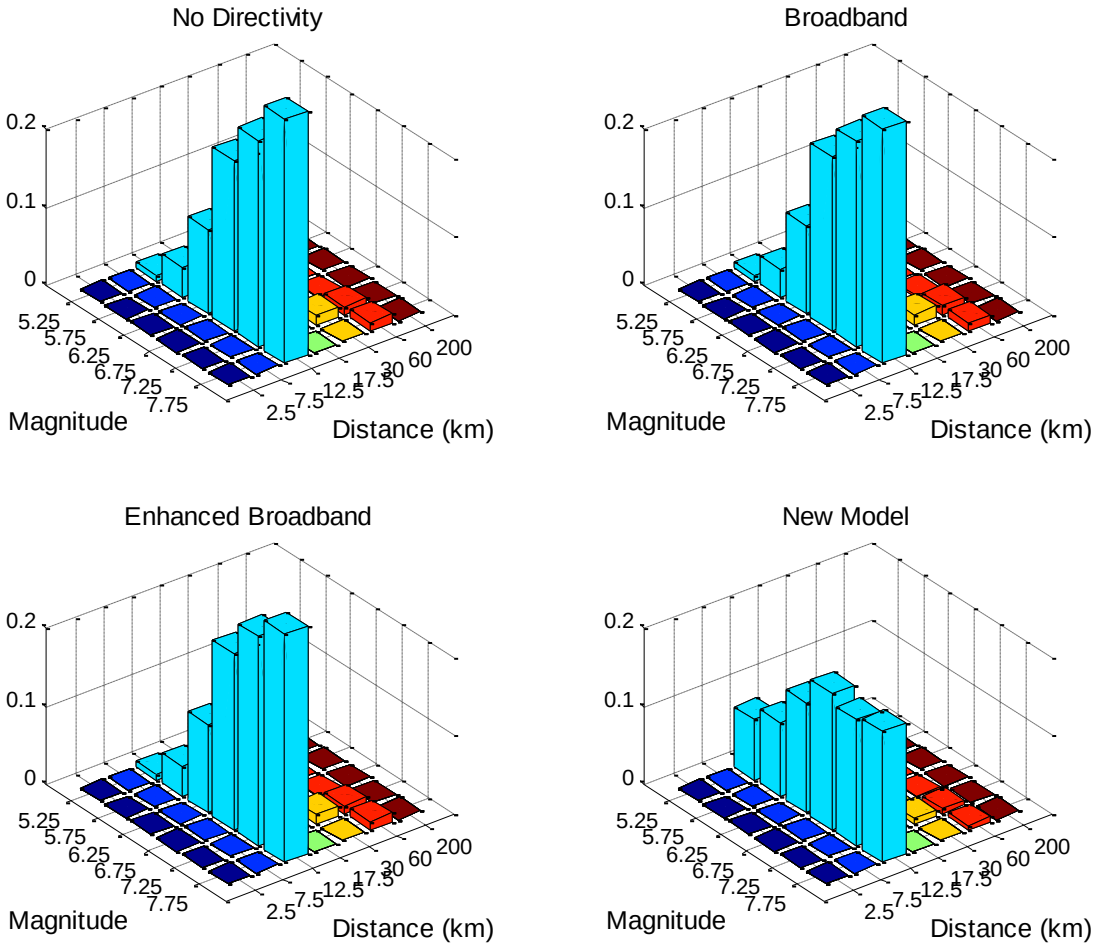

Figure 4-9b: Magnitude and distance deaggregation of λ_{EDP} when EDP = 5
for four different PSDA models and for a site located at 11 km from the fault along its centerline. The y-axis shows percentage contribution to risk for each PSDA model.

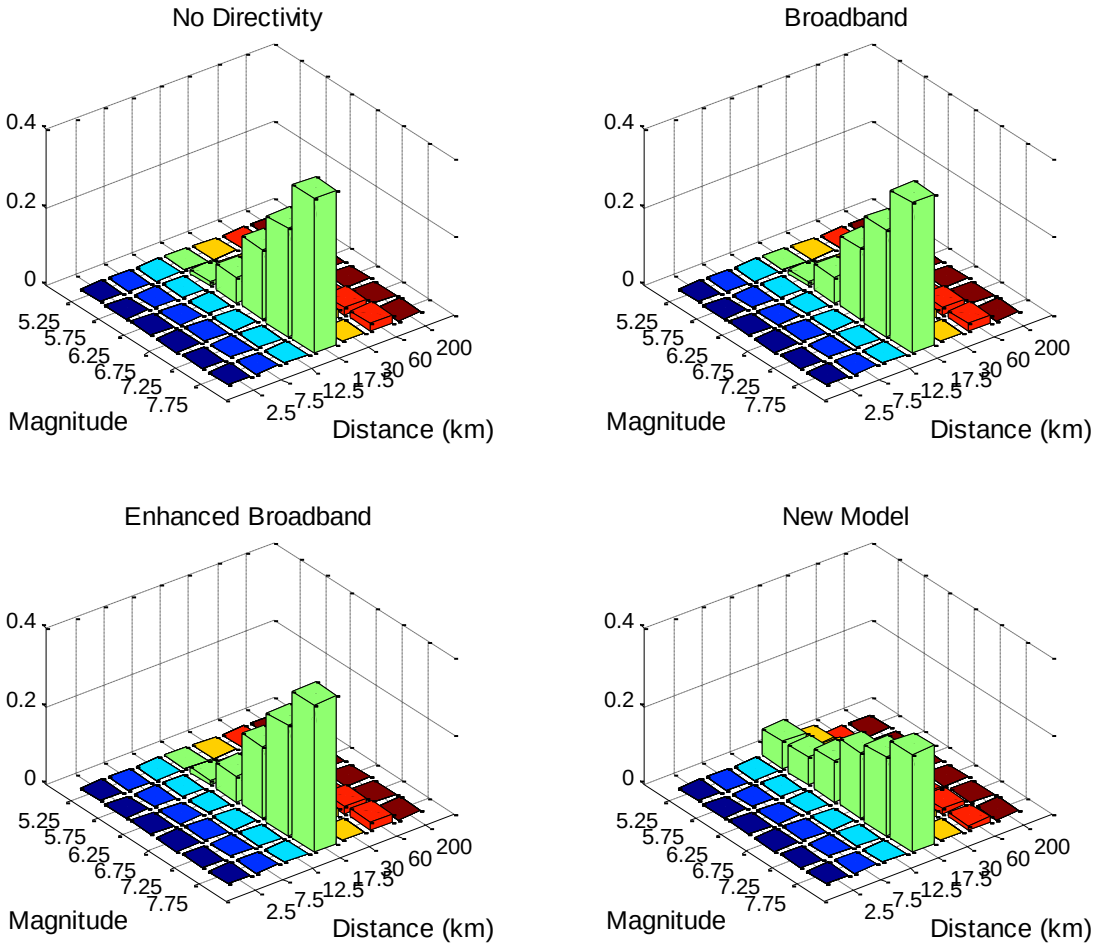

Figure 4-9c: Magnitude and distance deaggregation of λ_{EDP} when EDP = 5
for four different PSDA models and for a site located at 16 km from the fault along its centerline. The y-axis shows percentage contribution to risk for each PSDA model.

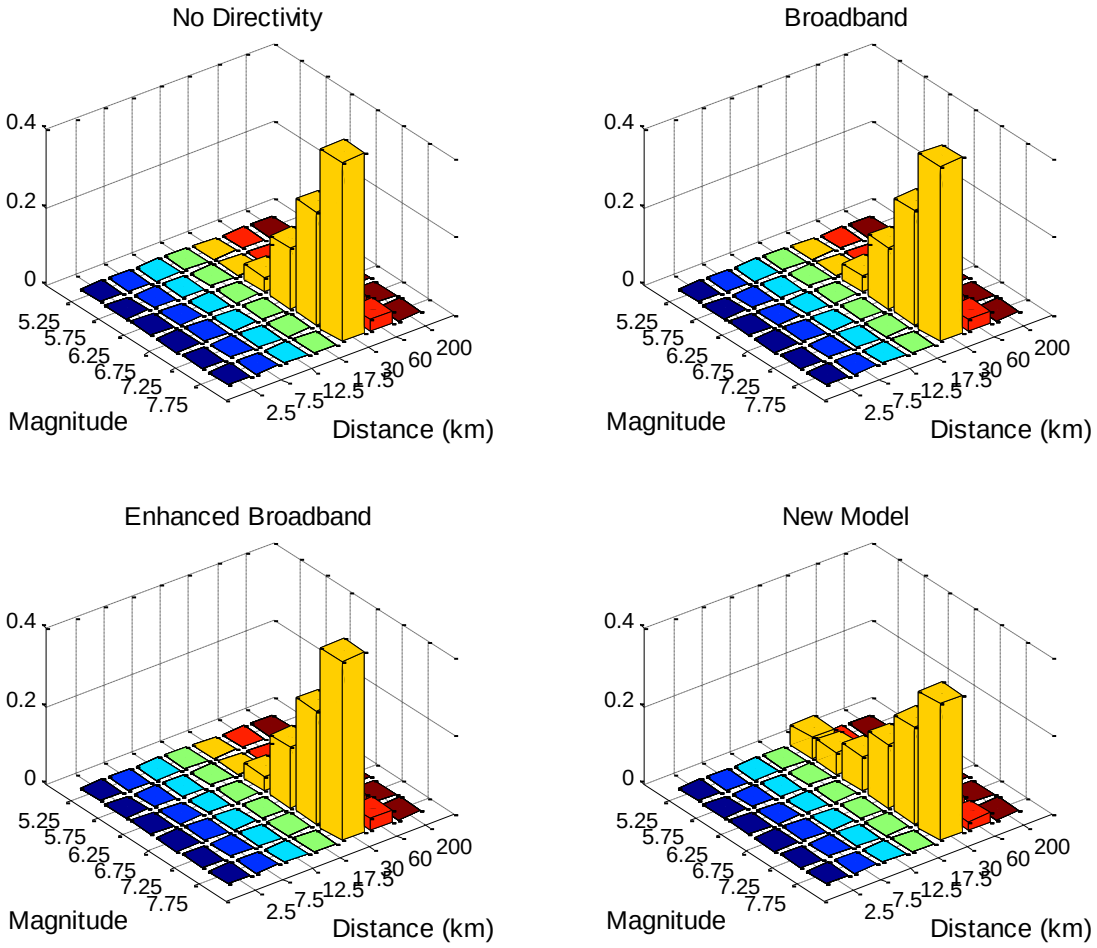

Figure 4-9d: Magnitude and distance deaggregation of λ_{EDP} when EDP = 5
for four different PSDA models and for a site located at 21 km from the fault along its centerline. The y-axis shows percentage contribution to risk for each PSDA model.

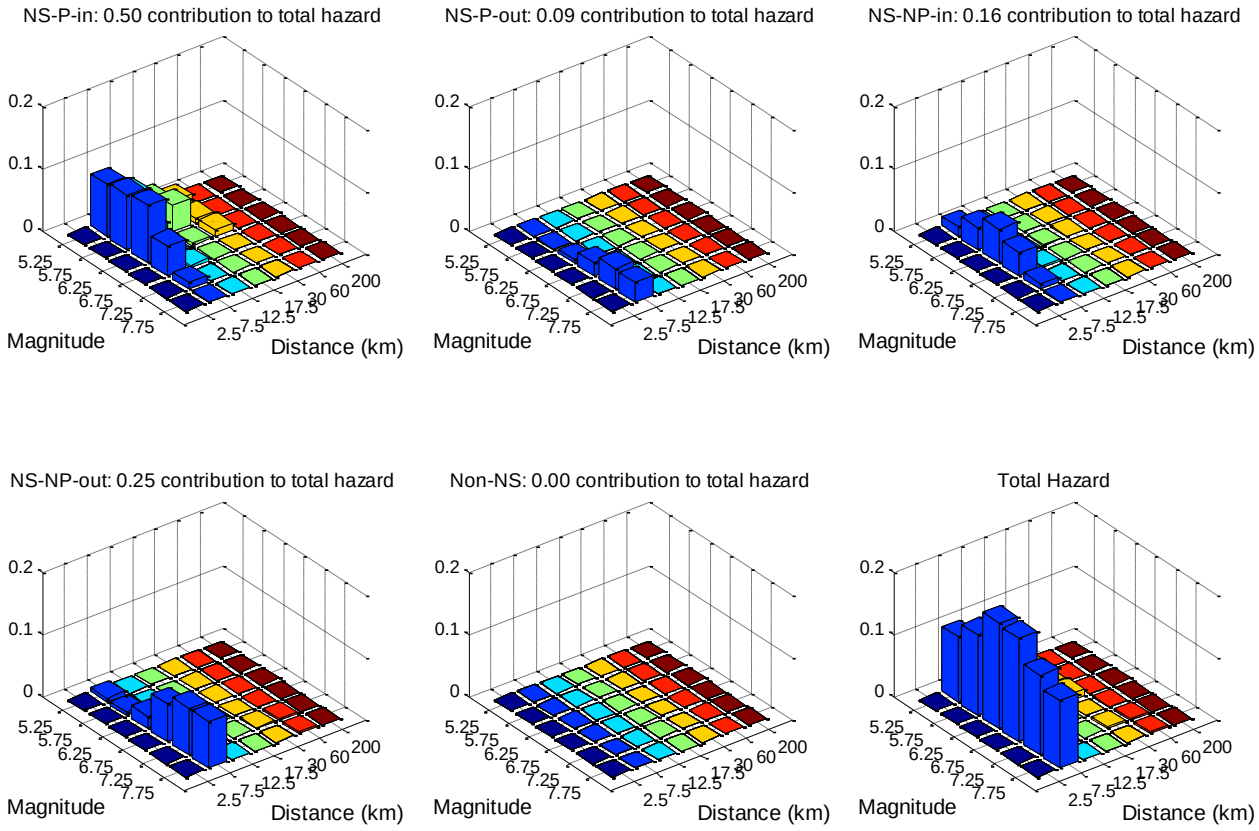

Figure 4-10a: Magnitude and distance deaggreagation of λ_{EDP} when EDP = 5 for a site at 6 km from the fault along its centerline.

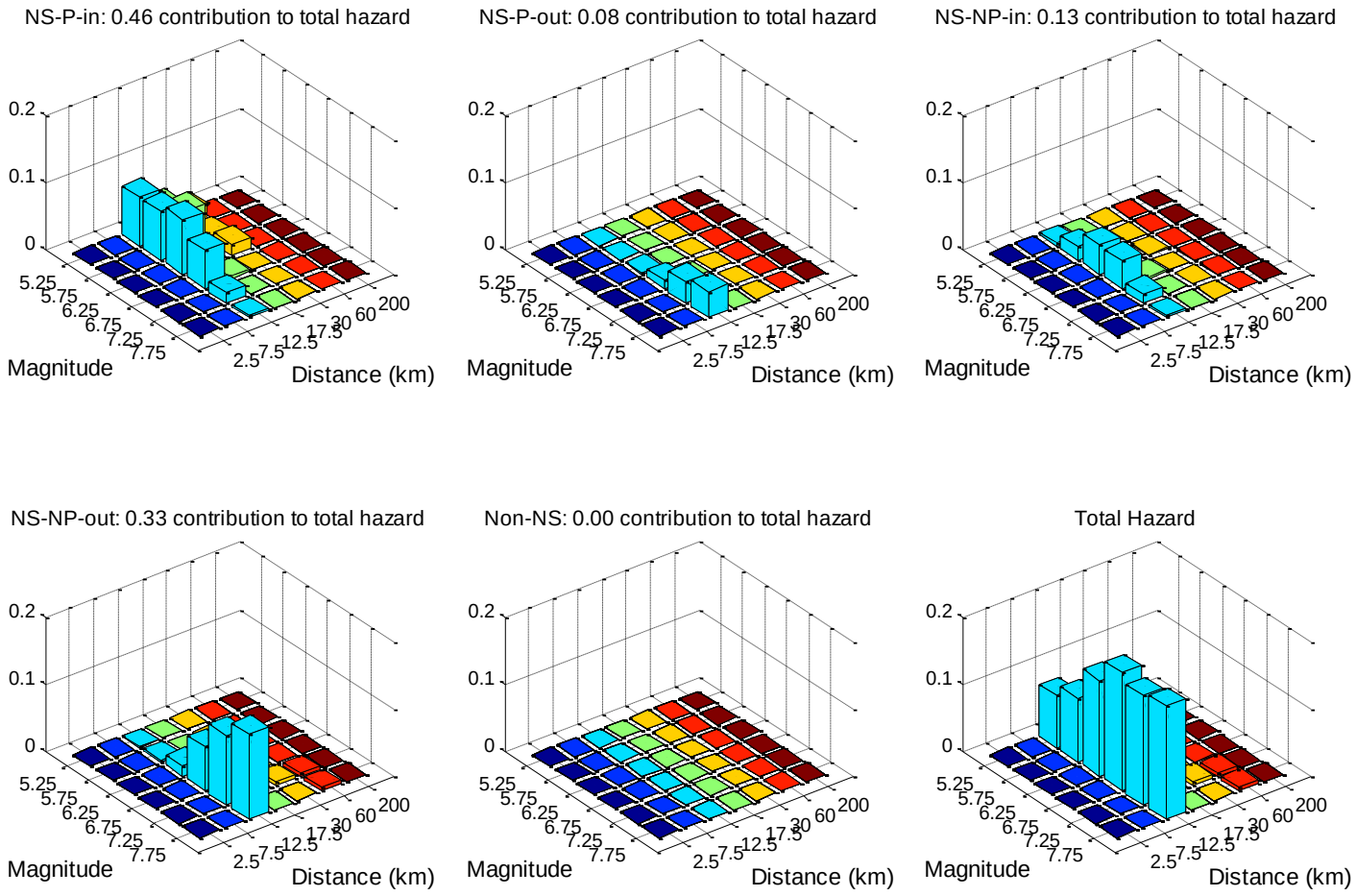

Figure 4-10b: Magnitude and distance deaggreagation of λ_{EDP} when EDP = 5 for a site at 11 km from the fault along its centerline.

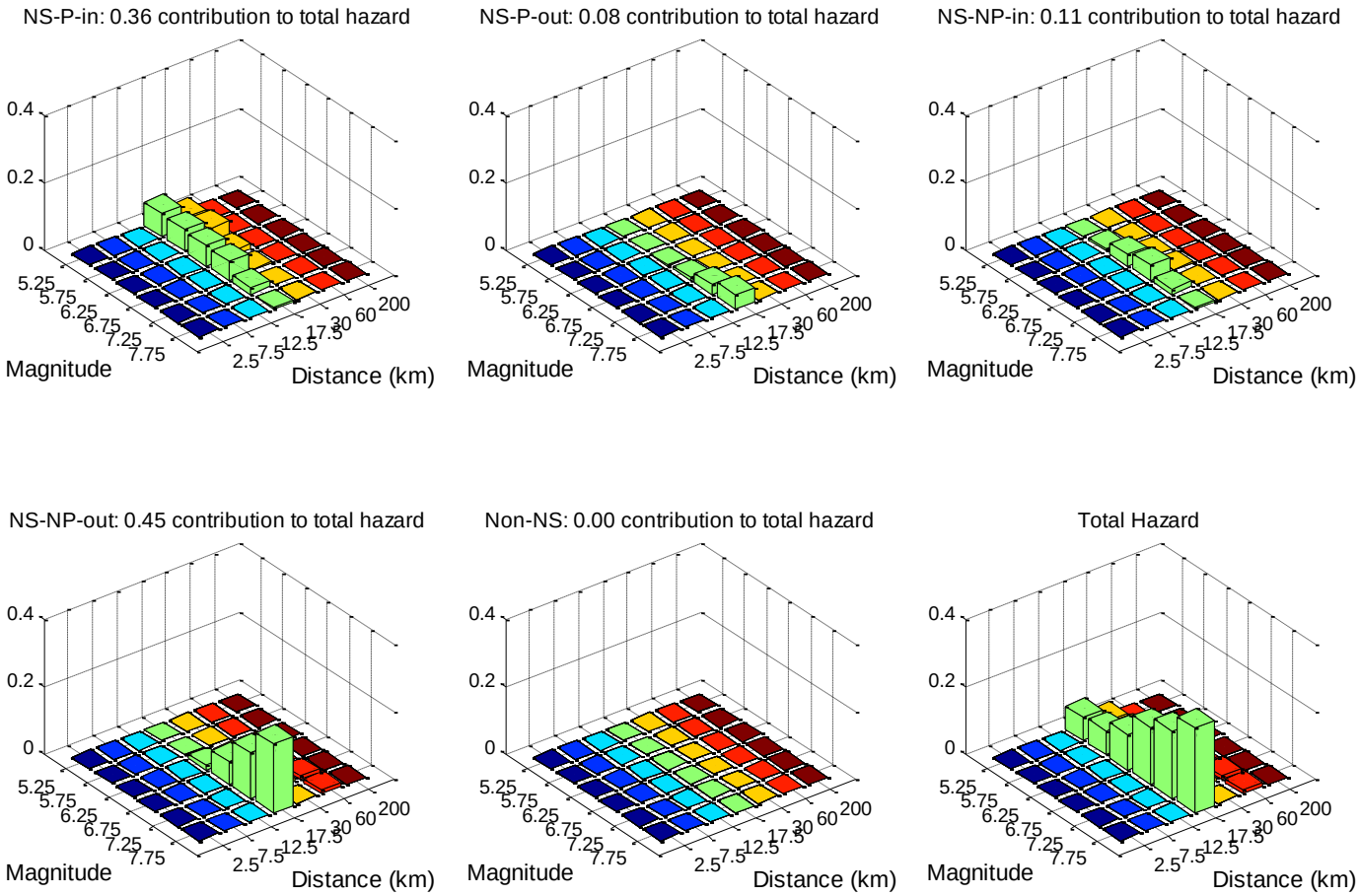

Figure 4-10c: Magnitude and distance deaggreagation of λ_{EDP} when EDP = 5 for a site at 16 km from the fault along its centerline.

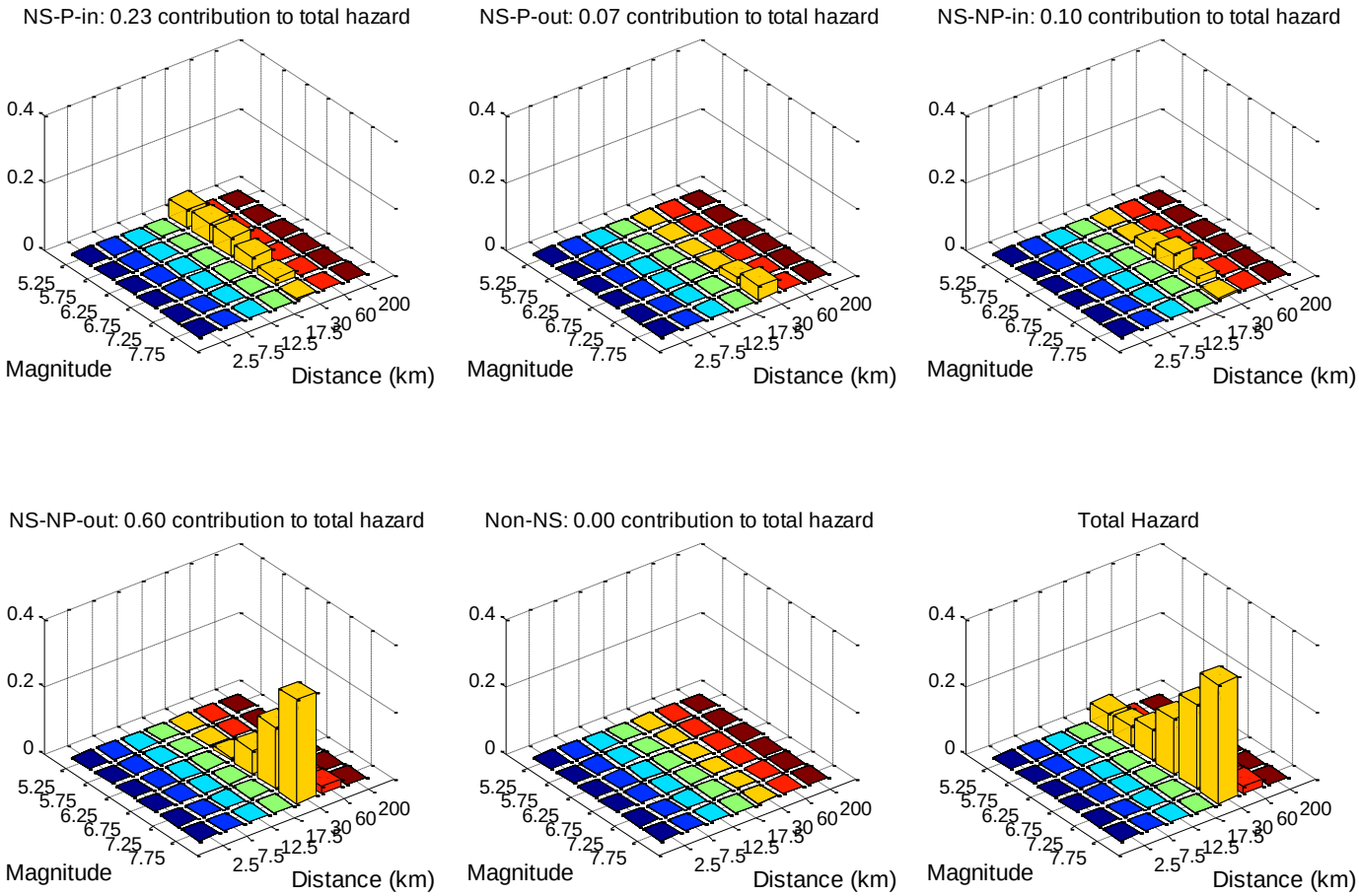

Figure 4-10d: Magnitude and distance deaggreagation of λ_{EDP} when EDP = 5 for a site at 21 km from the fault along its centerline.

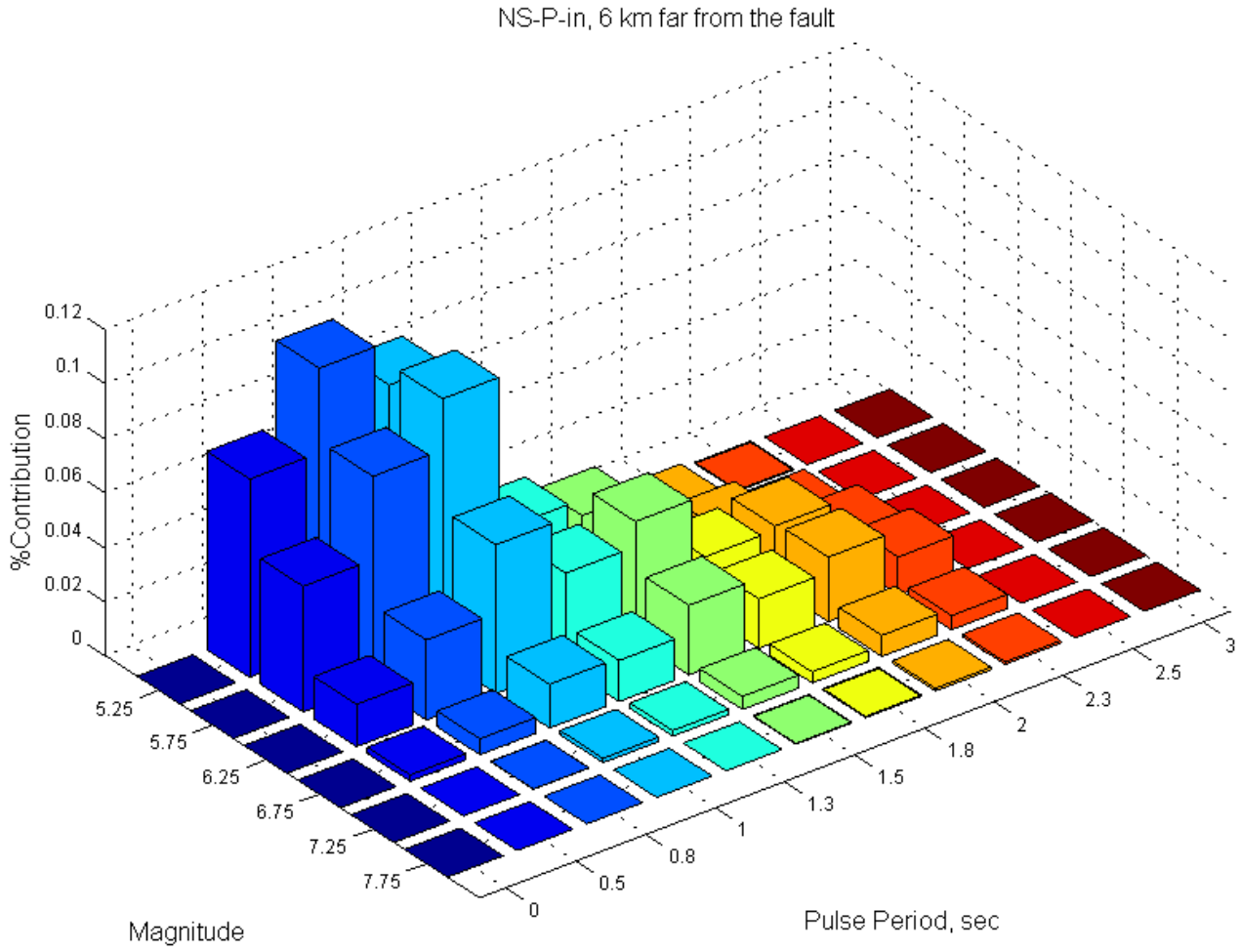

Figure 4-11a: Pulse period and magnitude deaggreagation of λ_{EDP} when EDP = 5 for a site located at 6 km far from the fault along its centerline.

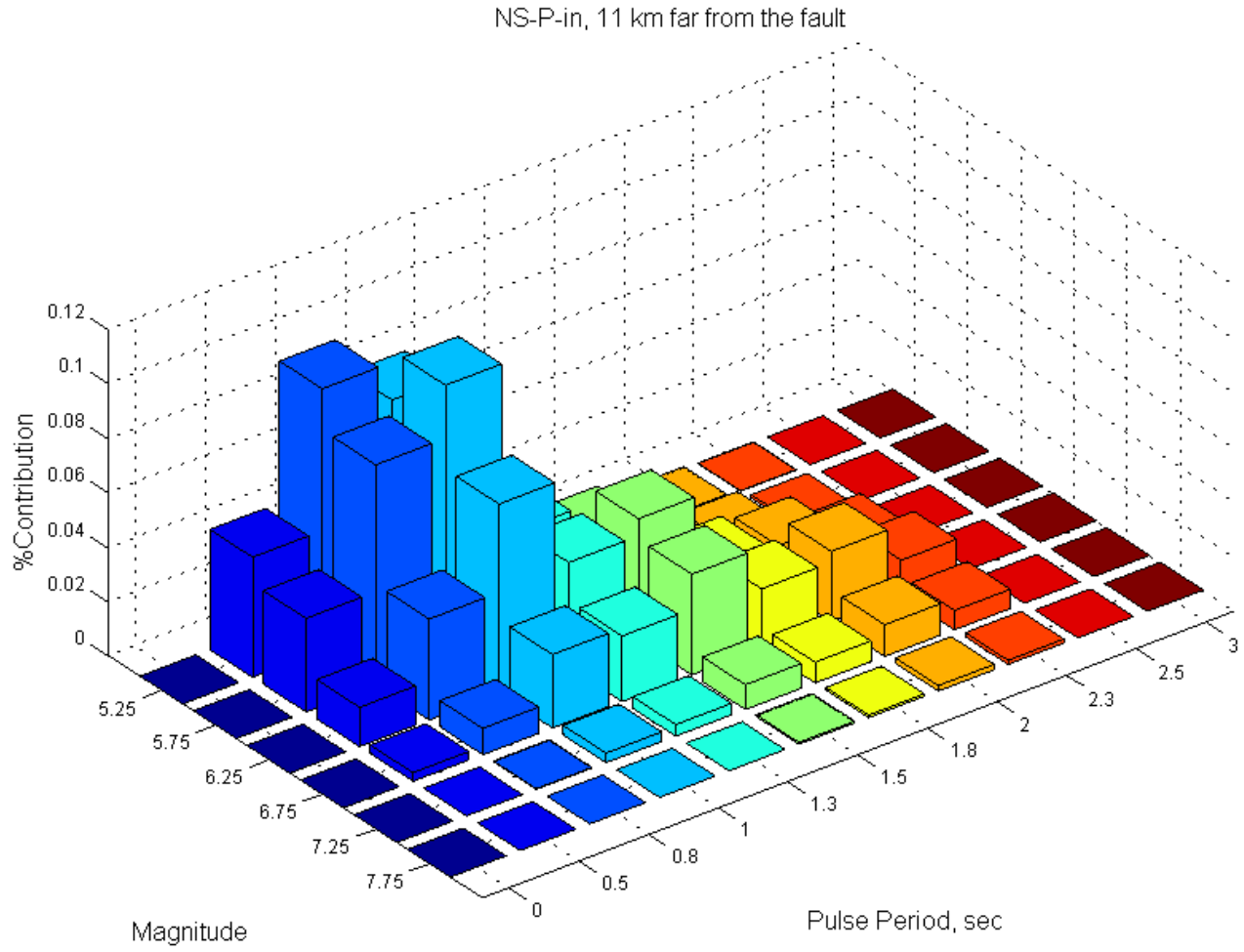

Figure 4-11b: Pulse period and magnitude deaggreagation of λ_{EDP} when EDP = 5 for a site located at 11 km far from the fault along its centerline.

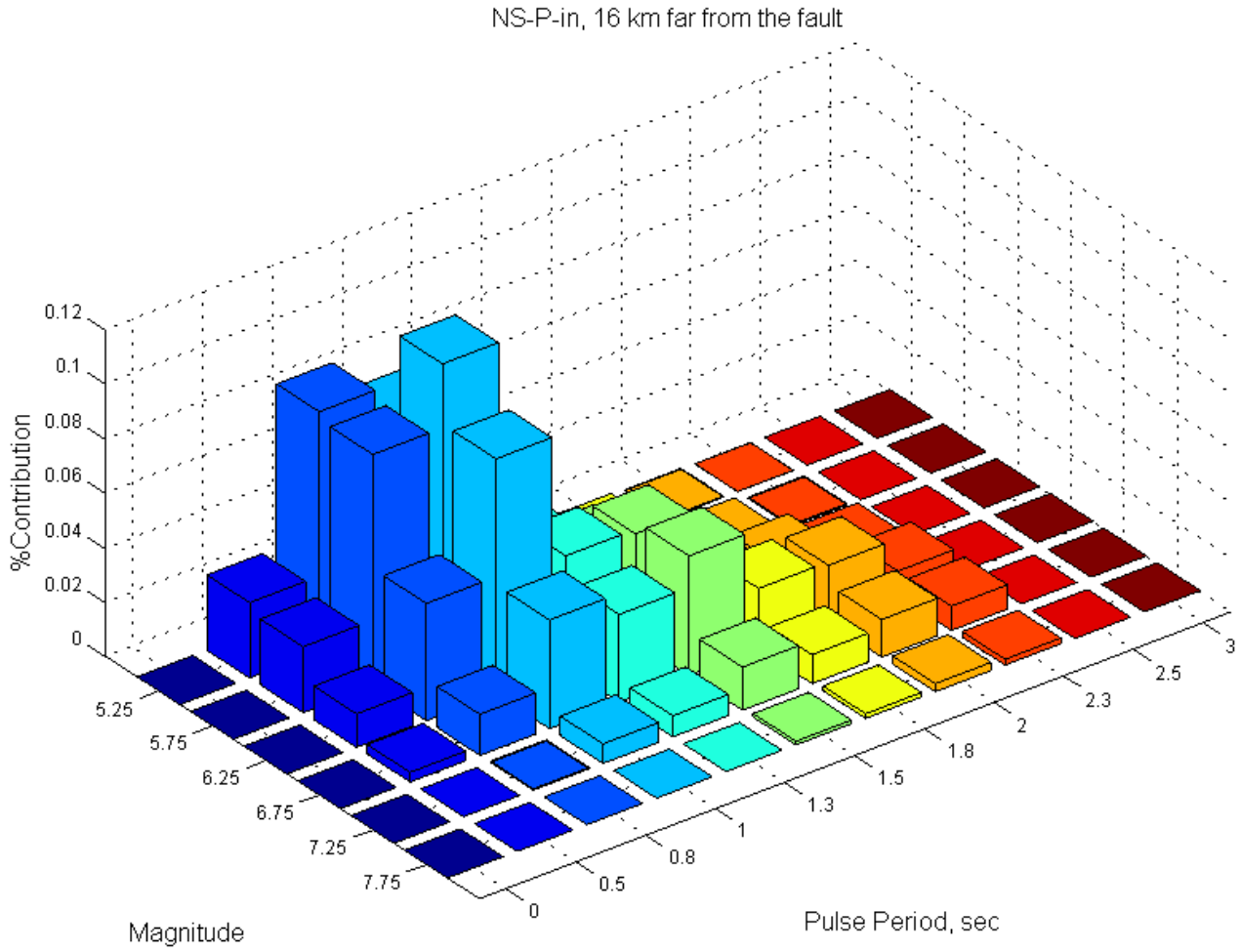

Figure 4-11c: Pulse period and magnitude deaggreagation of λ_{EDP} when EDP = 5 for a site located at 16 km far from the fault along its centerline.

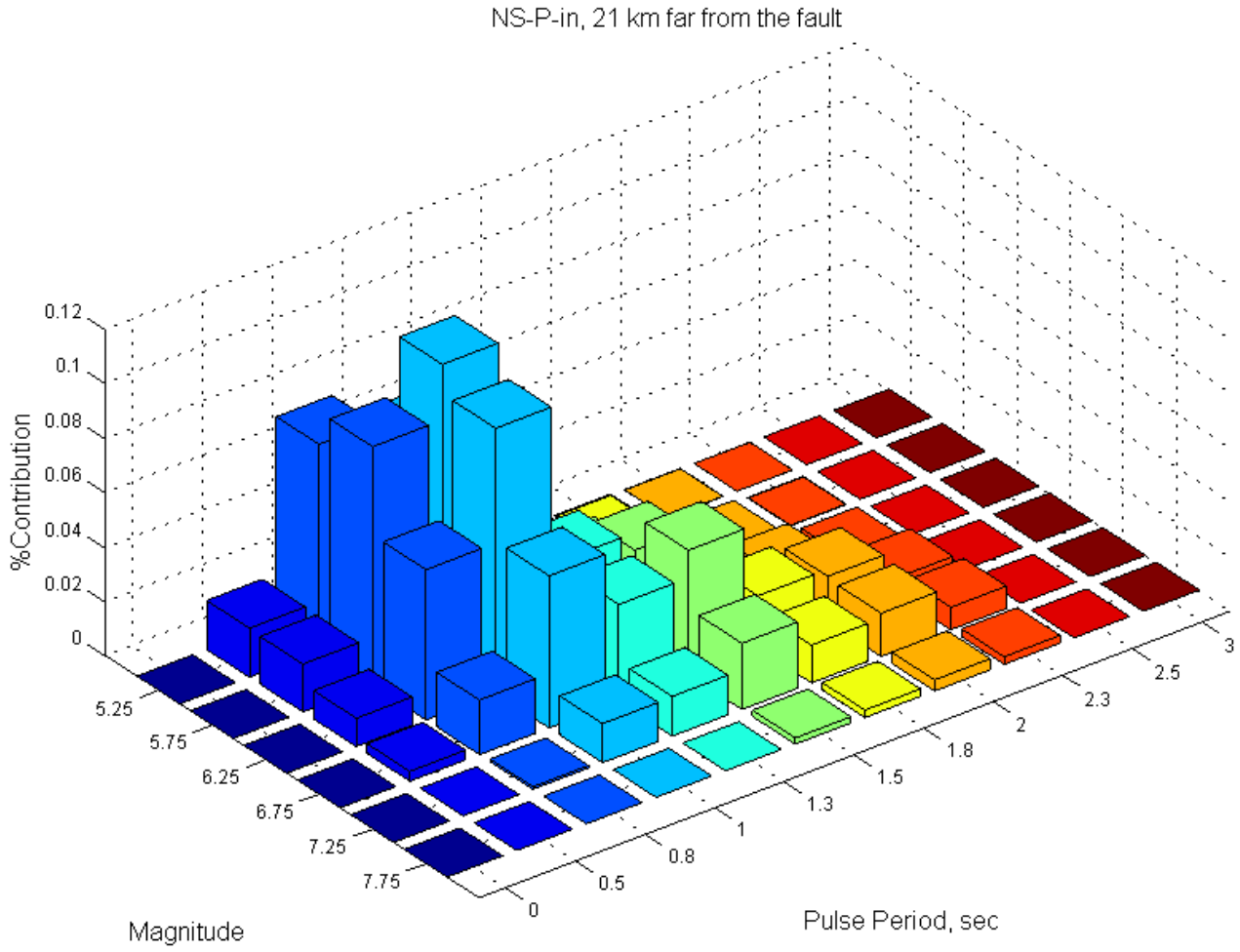

Figure 4-11d: Pulse period and magnitude deaggreagation of λ_{EDP} when EDP = 5 for a site located at 21 km far from the fault along its centerline.

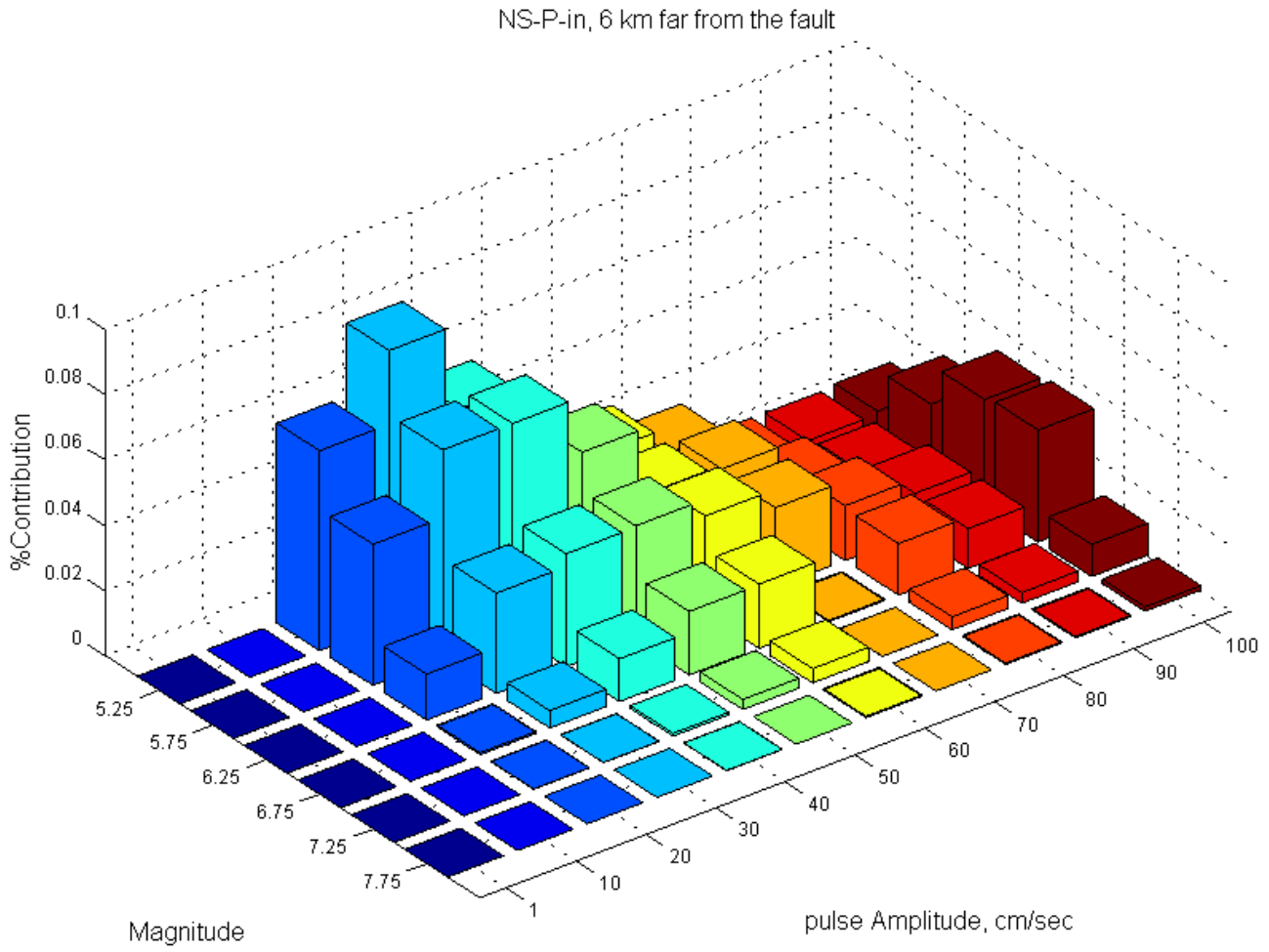

Figure 4-12a: Magnitude and pulse amplitude deaggreagation of λ_{EDP} when EDP = 5 for a site located 6 km far from the fault along its centerline.

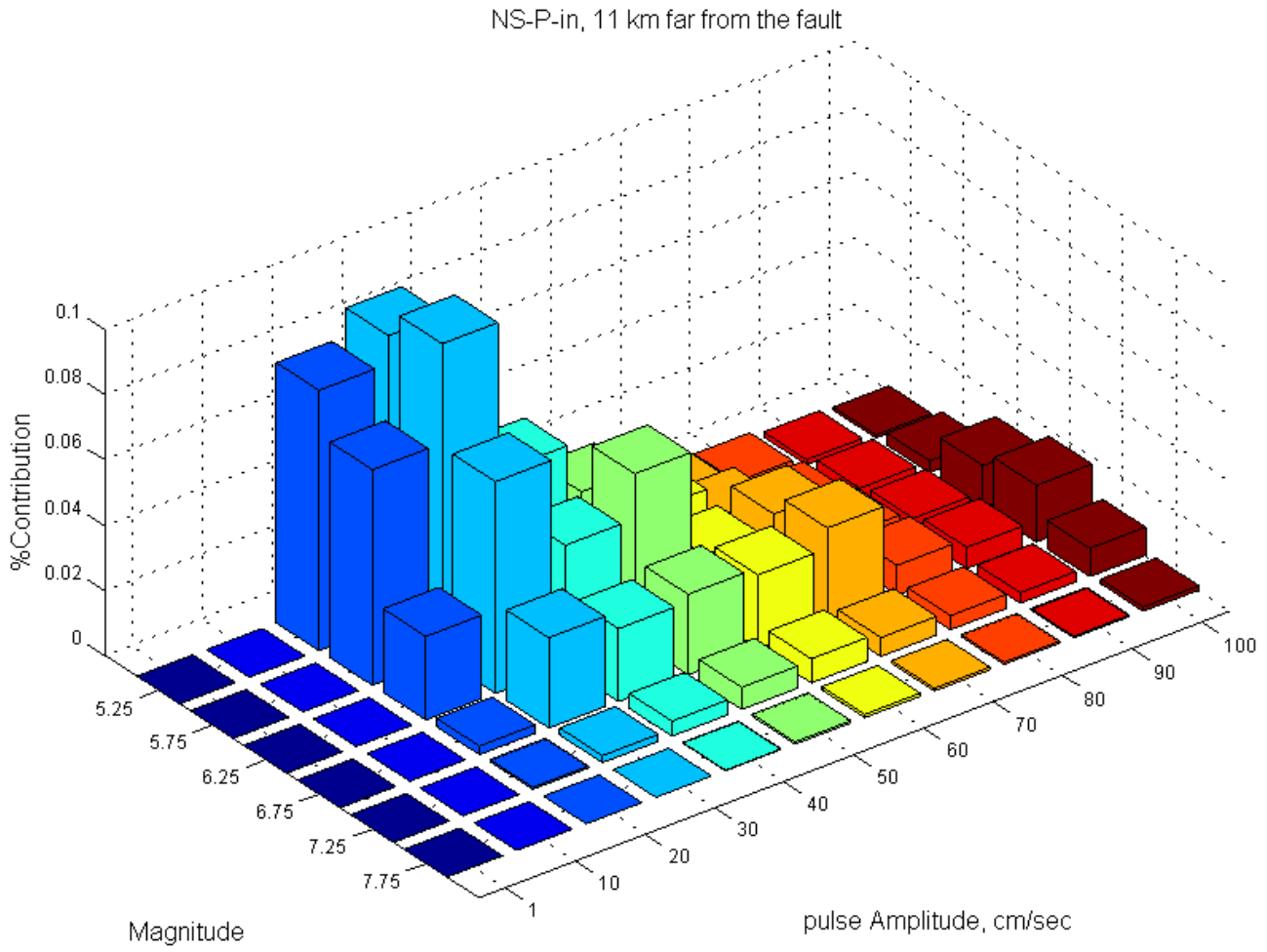

Figure 4-12b: Magnitude and pulse amplitude deaggreagation of λ_{EDP} when EDP = 5 for a site located 11 km far from the fault along its centerline.

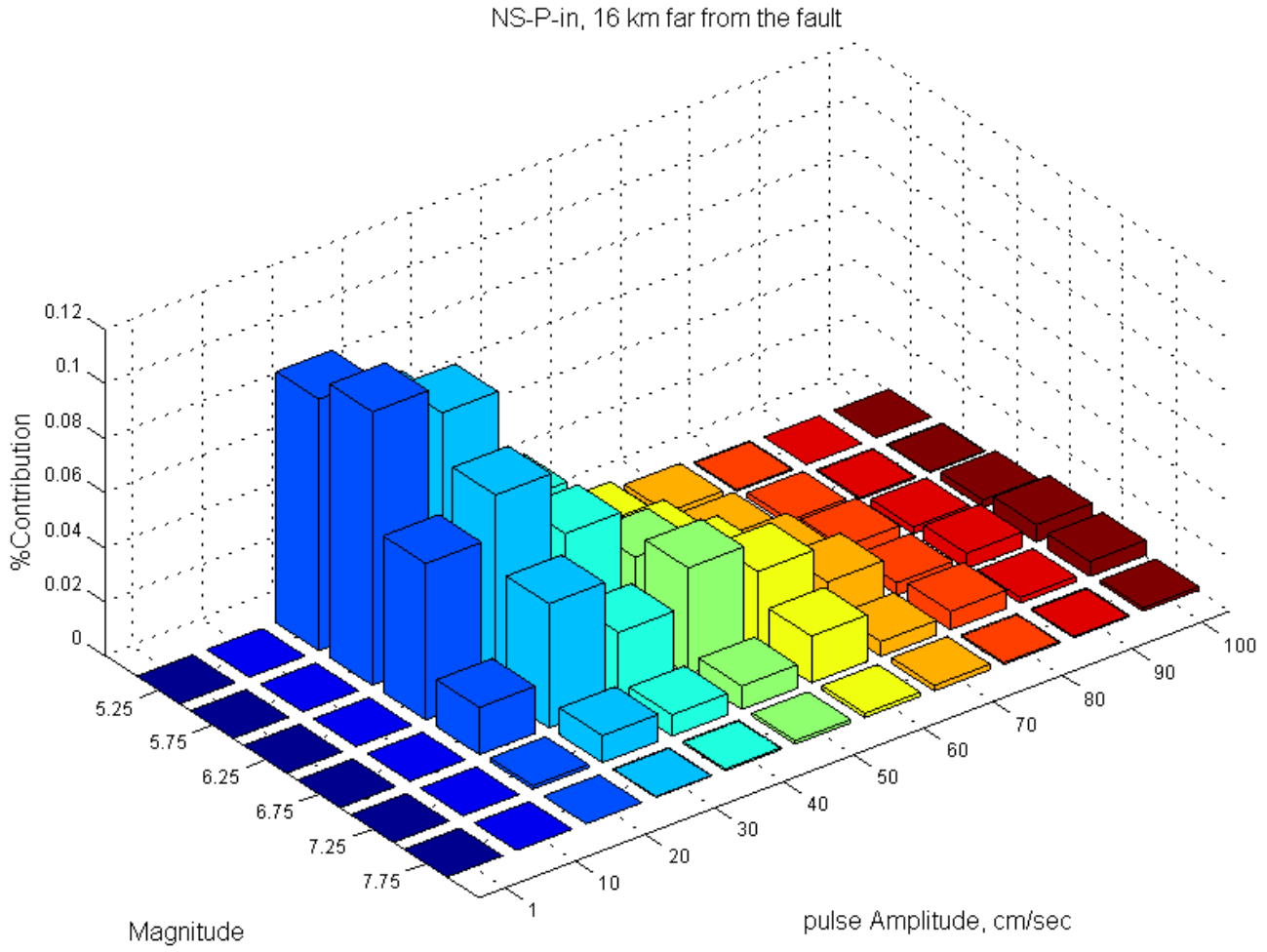

Figure 4-12c: Magnitude and pulse amplitude deaggreagation of λ_{EDP} when EDP = 5 for a site located 16 km far from the fault along its centerline.

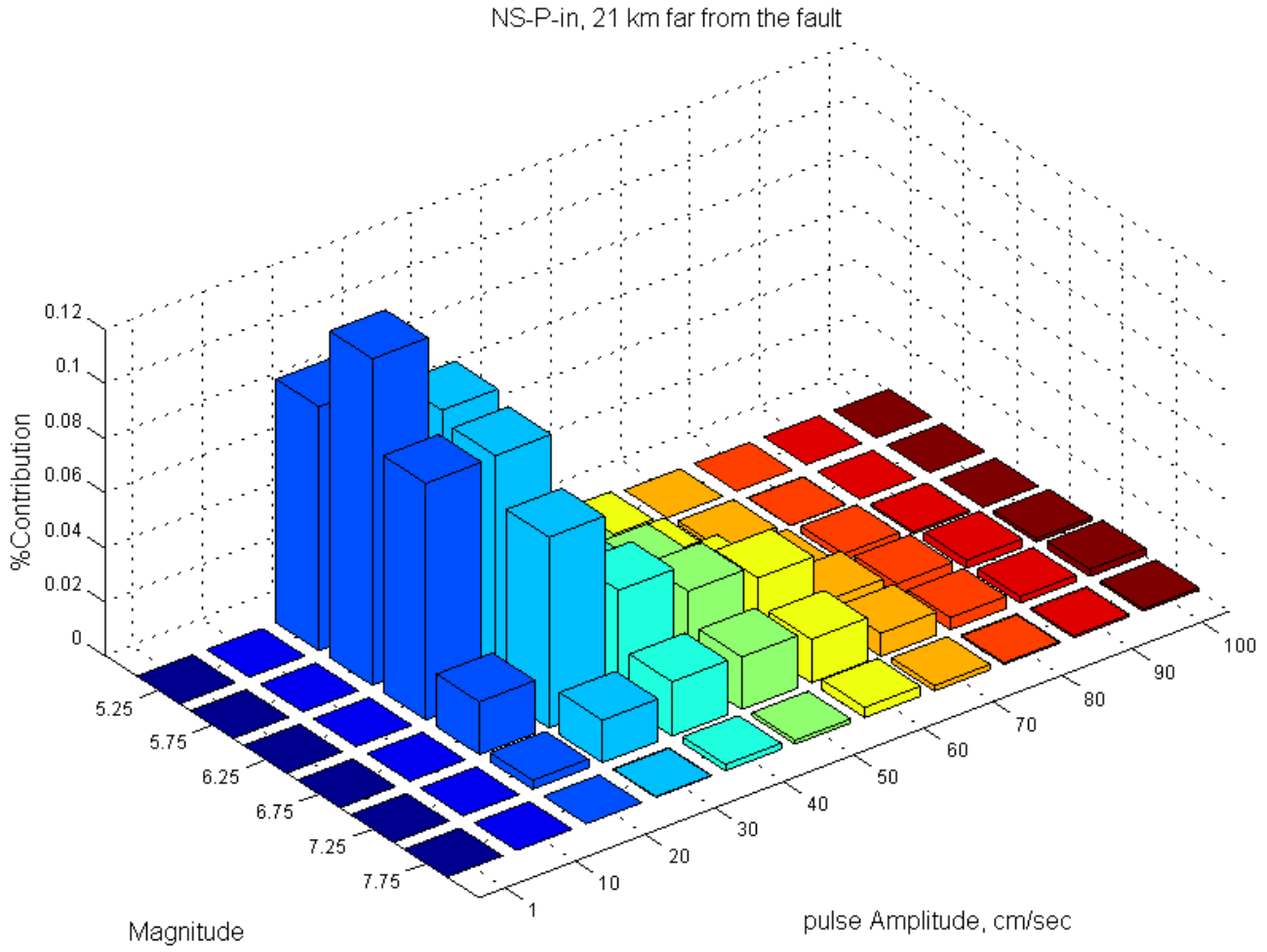

Figure 4-12d: Magnitude and pulse amplitude deaggreagation of λ_{EDP} when EDP = 5 for a site located 21 km far from the fault along its centerline.

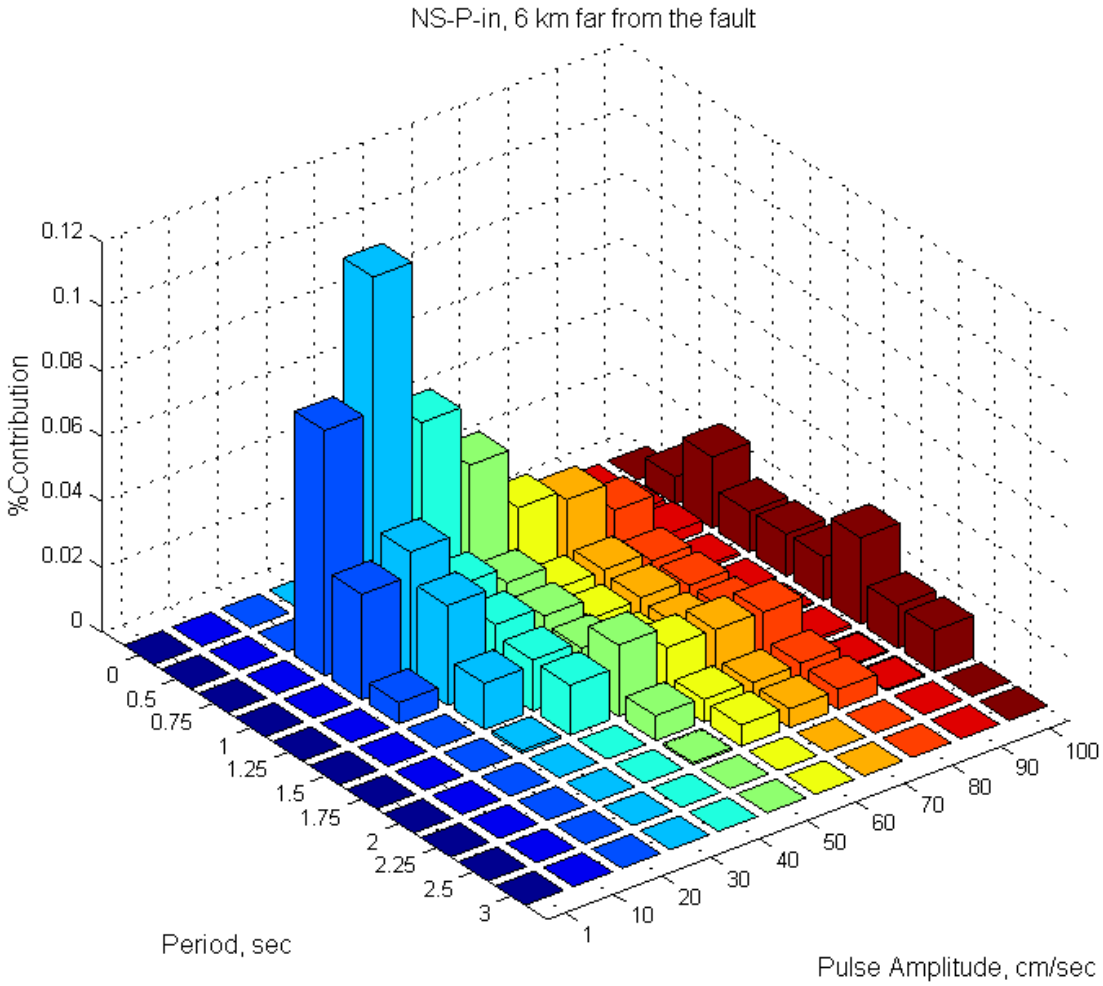

Figure 4-13: Period and Amplitude deaggreagation of λ_{EDP} when EDP = 5 for sites located 6 km far from the fault and between two ends of the fault

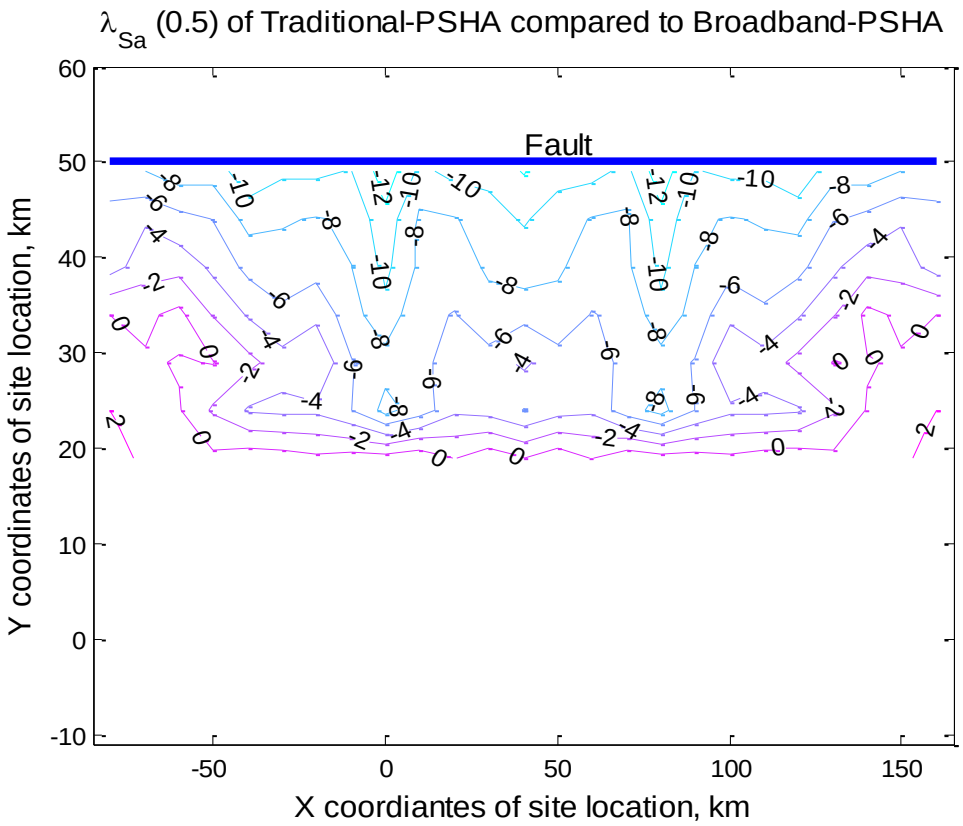

Figure 4-14: Contours of percentage change of spectral acceleration hazard estimated by Traditional-PSHA versus the Broadband-PSHA.

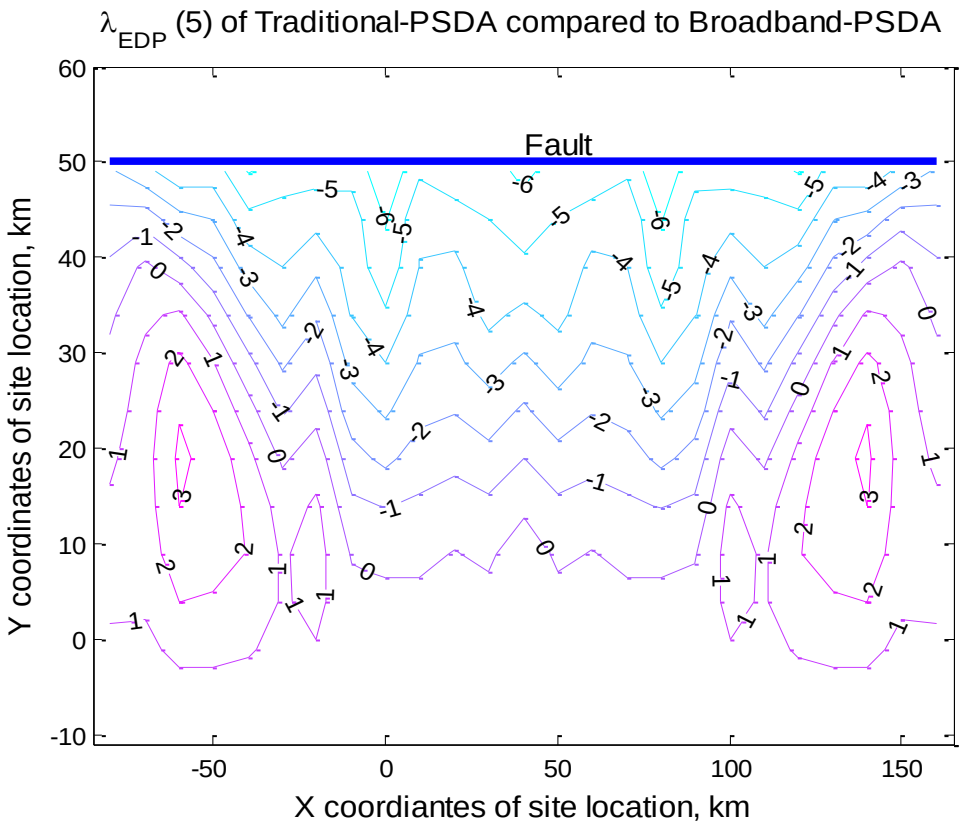

Figure 4-15: Contours of percentage change of λ_{EDP} when EDP = 5 predicted by the Traditional-PSDA versus the Broadband-PSDA.

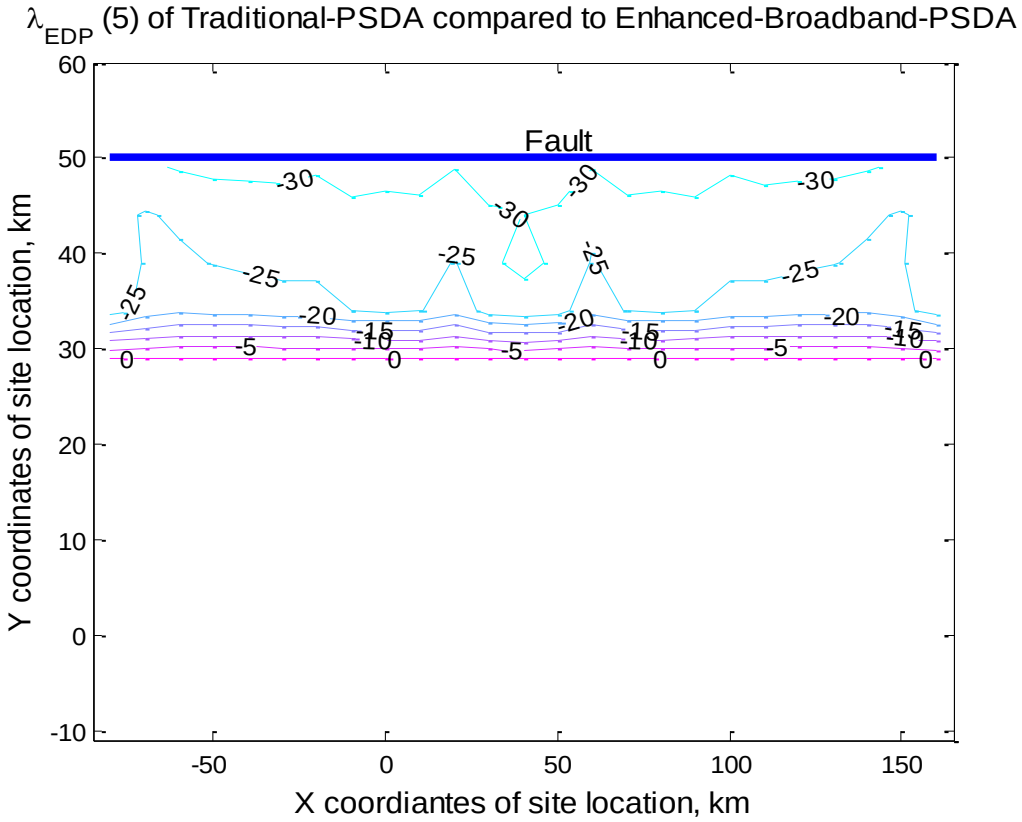

Figure 4-16: Contours of percentage change of λ_{EDP} when EDP = 5 predicted by the Traditional-PSDA versus the Enhance-Broadband-PSDA.

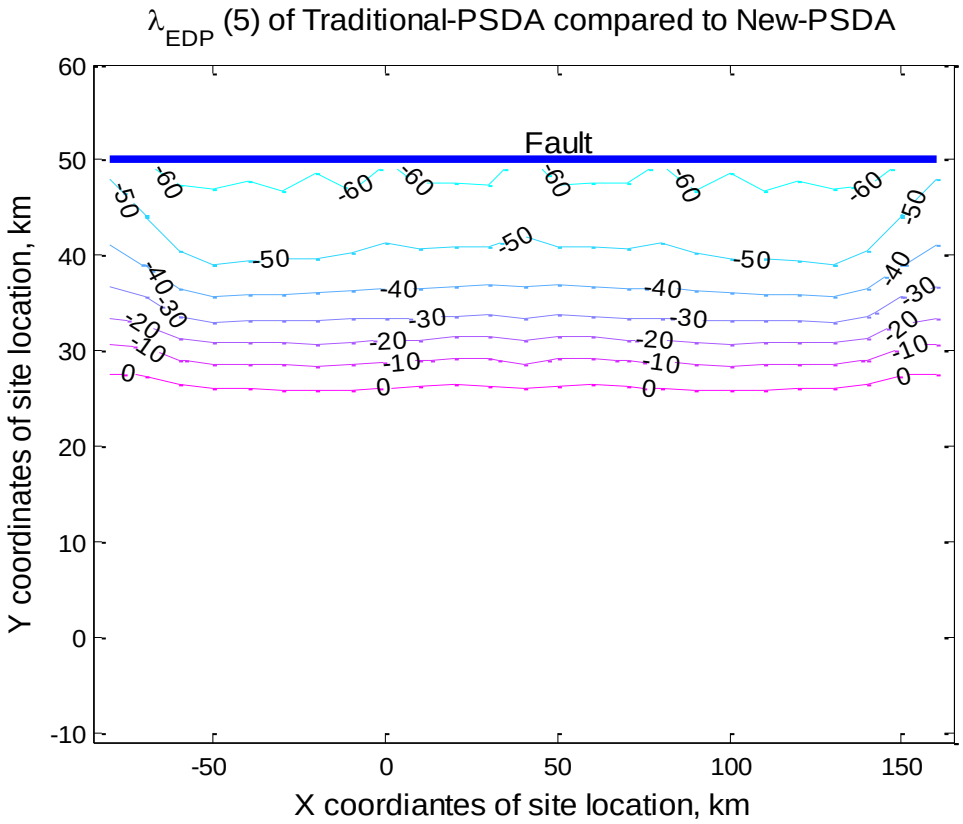

Figure 4-17: Contours of percentage change of λ_{EDP} when EDP = 5 predicted by the Traditional-PSDA versus the New-PSDA model.

4.13. Tables

Table 4-1: Ground motions with forward-directivity effects; selected from Gillie (2005).

Station	Agency	Station #	Event[a]	R[b] (km)	Site[c]	PGA (g)	PGV (cm/s)	$T_{v\text{-}p}$ [e](s)	$(T_p)_{Baker}$ [f] (s)	$(A_p)_{Baker}$ [g] (cm/s)
Cabazon Post Office	USGS	5073	PS	8.4	s	0.23	17.5	0.22	2.81	5.56
Desert Hot Springs	CSMIP	12149	PS	6.8	s	0.34	26.8	0.40	1.65	14.01
N. Palm Springs Pst. Off.	USGS	5295	PS	3.4	s	0.71	73.2	1.10	1.32	48.53
PS10	TAPS	10	DE	3.0	s	0.33	108.0	2.80	8.81	47.24
Bam	BHRC	BAM	SS	4.8	s	0.81	134.0	1.50	2.00	96.33
Coalinga - Slack Canyon	CSMIP	CE46175	B	10.0	r	0.33	42.1	0.69	0.76	40.37
Fault Zone 9	CSMIP	CE36443	B	1.1	r	0.14	26.1	1.00	1.15	23.81
Fault Zone 12	CSMIP	CE36138	B	1.2	s	0.25	57.4	1.00	1.20	55.75
Fault Zone 14	CSMIP	CE36456	B	0.1	s	0.99	84.7	0.66	0.62	86.90
Fault Zone 15	CSMIP	CE36445	B	0.6	s	0.21	28.1	1.10	1.51	19.88
Middle Mountain	USGS	MFU	B	2.0	s	0.32	32.3	0.31	3.28	13.47
Vineyard Canyon 1E	CSMIP	CE36455	B	6.5	r	0.32	34.6	0.38	1.26	22.63
Vineyard Cyn 1W	CSMIP	CE36448	B	2.1	r	0.14	21.1	0.38	1.12	18.93
Vineyard Cyn 2W	CSMIP	CE36447	B	17.0	r	0.61	30.2	0.34	0.36	24.66
Cholame #2	CDMG	1013	PF	0.1	s	0.47	75.0	0.66	0.36	8.57
Temblor	CDMG	1438	PF	9.9	r	0.29	17.5	0.40	1.88	7.68
Pacoima Dam	CDMG	279	SF	2.8	r	1.47	114.0	1.15	1.58	86.22
Brawley Airport	USGS	5060	IV	8.5	s	0.21	36.1	3.11	4.03	25.45
EC County Center	CDMG	5154	IV	7.6	s	0.22	54.5	3.44	4.52	39.44
EC Meloland Overpass	CDMG	5155	IV	0.5	s	0.38	115.0	2.86	3.35	78.47
El Centro Array #10	USGS	412	IV	8.6	s	0.23	46.9	3.82	4.49	33.03

Station	Agency	Station #	Event[a]	R[b] (km)	Site[c]	PGA (g)	PGV (cm/s)	$T_{v\text{-}p}$ [e](s)	$(T_p)_{Baker}$ [f] (s)	$(A_p)_{g}^{Baker}$ (cm/s)
El Centro Array #3	USGS	5057	IV	9.3	s	0.27	45.4	4.27	5.24	27.24
El Centro Array #4	USGS	955	IV	4.2	s	0.47	77.8	4.00	4.61	62.86
El Centro Array #5	USGS	952	IV	1.0	s	0.53	91.5	3.25	4.05	76.81
El Centro Array #6	USGS	942	IV	1.0	s	0.44	112.0	3.41	3.84	89.94
El Centro Array #7	USGS	5028	IV	0.6	s	0.46	109.0	3.31	4.23	69.98
El Centro Array #8	USGS	5159	IV	3.8	s	0.59	51.9	4.00	5.39	35.31
El Centro Diff Array	USGS	5165	IV	5.3	s	0.44	59.6	3.02	5.86	33.94
Holtville Post Office	USGS	5055	IV	7.5	s	0.26	55.1	4.20	4.69	39.37
Westmorland Fire Sta.	CDMG	5169	IV	15.1	s	0.10	26.7	4.71	5.02	17.62
Coyote Lake Dam	CDMG	57217	MH	0.1	r	1.00	68.7	0.71	0.97	59.14
Gilroy Array #6	CDMG	57383	MH	11.8	r	0.61	36.5	1.16	1.23	33.13
El Centro Imp Co. Cent.	CDMG	1335	SH	13.9	s	0.31	51.9	1.25	7.31	20.74
Lucerne	SCE	24	L	1.1	r	0.78	147.0	4.30	5.12	72.30
LA Dam	USGS	–	N	2.6	r	0.58	77.0	1.30	1.65	50.25
Pacoima Dam (upper left)	CDMG	24207	9	8.0	r	1.47	107.0	0.73	0.90	79.23
KJMA (Kobe)		–	10	0.6	r	0.85	96.0	0.86	0.95	100.16
Kobe University	CEOR	–	10	0.2	r	0.32	42.2	1.33	2.06	40.59
OSAJ		–	10	8.5	s	0.08	19.9	1.18	5.52	8.89

[a] See Table 1. [b] Closest distance to the fault plane. [c] Soil (s) or rock (r).

[e] Period corresponding to the peak in the velocity response spectrum.

[f] Pulse period determined using the procedure of Baker (2007).

[g] Pulse amplitude determined using the procedure of Baker (2007).

[h] The fault normal direction for these records was assumed to be the direction oriented with the largest velocity pulse (N122º for TCU052 and N199º for TCU068).

[i] The fling step was removed by the procedure described in Bray and Rodriguez-Marek (2004).

Table 4-2: synopsis of fault seismicity

M_w	$P(M_w)$	R_L (km)	$P[R_L]$
5.25	0.604	2.1	0.032
		3.2	0.242
		4.8	0.452
		7.3	0.242
		11.1	0.032
5.75	0.241	4.3	0.032
		6.5	0.242
		9.9	0.452
		15	0.242
		22.6	0.032
6.25	0.096	8.8	0.032
		13.3	0.242
		20.2	0.452
		30.5	0.242
		46.2	0.032
6.75	0.038	18	0.032
		27.2	0.242
		41.2	0.452
		62.4	0.242
		94.4	0.032
7.25	0.015	36.7	0.032
		55.6	0.242
		84.1	0.452
		127.4	0.242
		192.8	0.032
7.75	0.006	75	0.032
		113.5	0.242
		171.8	0.452
		260	0.242
		393.6	0.032

CHAPTER FIVE

SUMMARY AND CONCLUSIONS

5.1 Summary and main findings

A methodology for probabilistic seismic demand analysis that includes the effects of forward directivity through time domain analysis has been proposed. First, the structural response of three multi-degree of freedom structures to both pulse-like forward-directivity and non-pulse-like near-fault ground motions was studied. It was observed that the structural demands resulting from pulse-like ground motions exceed those resulting from non-pulse ground motions. In particular, when MIDD is used as the EDP and elastic response spectra is used as the IM, the structures under study consistently showed higher demands when subjected to pulse-like ground motions compared to non-pulse-like ground motions. Moreover, the dispersion around the median prediction for pulse-like ground motions was higher than that for non-pulse ground motions, indicating that elastic response spectra are not good intensity measure for pulse-like forward-directivity ground motions.

As an alternative to the use of elastic response spectra, simplified mathematical representations for pulse-type forward-directivity ground motions were proposed. Intensity Measures for forward directivity ground motions were then proposed based on the proposed equivalent pulses. Results of incremental dynamic analyses showed that whenever the pulse period of forward-directivity ground motions is close to the first-mode structural period, structural response is controlled by forward-directivity pulses. For these cases, structural response can be predicted using pulse-period and pulse-amplitude as intensity measures.

The principles of Probabilistic Seismic Demand Analysis were then extended to consider the effect of forward-directivity within a probabilistic framework. Structural response to pulse-type forward-directivity ground motions was quantified by means of time-domain analysis of simplified pulses that comprehensively represent all possible pulse-type ground motion scenarios. The hazard due to pulse-type motions was coupled with conventional spectral domain seismic demand analyses for non-pulse-type ground motions.

Hazard computations with the proposed methodology resulted in higher computed hazard for MIDD for the selected structures for sites located near the fault. This increase results from the different treatment of pulse-like motions: whereas existing methodologies consider near-fault hazard through the average increase in response spectral estimates, the proposed methodology captures its narrowband nature. Moreover, by performing structural analyses for each realization of the pulse-type motions, the resonant nature of the structural response to pulse-like motions is captured and introduced into the hazard computation.

Analysis with the proposed methodology indicated that near-source structures with structural periods close to about 1.0 seconds can be affected by smaller magnitude earthquakes that generate ground motion pulses with periods close to the structural period. Traditional, spectral acceleration-based PSDA analyses do not capture this effect and underestimate the contribution to hazard from small magnitude earthquakes and can lead to errors in ground motion selection for design.

Although the example selected in this dissertation corresponds to an idealized MDOF structure and an idealized fault, both the fault model and the structural model were selected

to represent realistic conditions and the results shown would very likely be reproduced for actual structures located near active faults. Therefore, it is recommended that the proposed methodology be used for the design of infrastructure located near faults. The proposed methodology not only computes a more adequate hazard from existing faults, but also provides, through pulse-period and pulse-amplitude disaggregation, a tool for selecting ground motions for the design of such structures.

5.2. Consideration of Forward-Directivity in Building Codes and Provisions

The velocity pulses that can occur in forward-directivity ground motions are associated with severe loads which can impose a larger demand to structures when compared to loads resulting from ordinary ground motions. The subsequent dynamic displacements resulting from forward-directivity ground motions are considerable on long period structures (such as bridges). Moreover, when such structures straddle the fault, large static displacement may occur due to tectonic displacement across the fault. Seismic guidelines and codes, such as, UBC 1997, IBC 2006, and NEHRP 2007 have recognized the possibility of rupture directivity and its effect on near-fault buildings, but none of the aforementioned codes consider this effect in design. In light of the results shown in this thesis, the paragraphs below review the existing literature to consider recommendations for improving current design practices.

Near-fault ground motions had been considered as a special case meriting site-specific analysis (site specification) by NEHRP in the editions before that of 2007. For the 2007 update, NEHRP discussed the inclusion of directivity in the ground motions by means of a

10 percent (distance dependence) increase to the mapped value of the Maximum Considered Earthquake spectral response acceleration at a period of 1 second, S_1, obtained from a combination of the various USGS probabilistic seismic hazard maps and deterministic hazard maps. However, this approach was still under discussion (USGS 2007).

None of the aforementioned building codes has yet considered the effects of pulse-like ground motion on the dynamic response of structures. For example, current building codes do not consider the redistribution of story shear, nor do they account for changes in level of story ductility demand due to variations in frequency, amplitude, and type of pulse (Alavi and Krawinkler 2004b). Redistribution of story ductility demand caused by inelastic behavior of the structure cannot be captured through an elastic or spectral analysis. Moreover, small modifications of a near-fault time history that have no significant effect on the response spectrum can have a major effect on the response of a structure when subjected to non-linear time history analysis (Alavi and Krawinkler 2004b).

As discussed in Chapter 3, the response of a structure to pulse-like ground motions is different than that to ordinary ground motions. It was shown that the location of the critical story changes depending on the frequency content of ground motions. The maximum story ductility demand occurs in the upper stories for ground motions with forward-directivity pulses with short periods. As the period of forward-directivity pulses increase, the maximum demand migrates to the bottom portion of the structure, where it grows rather rapidly with further increase in the pulse period. In the medium-period range, code-compliant frame structures may experience excessive ductility demands associated with a level of structural damage that is not expected by present code provisions. Ductility demand distribution over

the height of frame structures leads to large variations of required story shear strength. Therefore, the design of near-fault structures should be improved to consider the effects of rupture directivity.

Alavi and Krawinkler (2004b), realizing the severe demand imposed to structures subjected to pulse-like ground motions, proposed strengthening techniques with the objective of reducing maximum drift demands. One technique is to modify the code-based SRSS distribution of story shear strength over the height by strengthening of the lower stories of the frame. The modified distribution reduces the maximum story ductility demand, particularly for weak and flexible structures. However, this strengthening technique is less effective for stiff structures, and is almost ineffective for cases in which the maximum demand occurs in the upper stories, i.e. strong and flexible structures. The other technique proposed by Alavi and Krawinkler (2004b) is to add walls that are either fixed or hinged at the base (as shown in Figure 5-1). They found that strengthening with hinged walls is very effective in reducing drift demands for structures with a wide range of periods and at various performance levels. Based on their study, walls with inelastic behavior only slightly reduce the benefits of strengthening with hinged walls.

In addition to the aforementioned methods, there are many potential ways to improve structural design for buildings subjected to forward-directivity ground motions and some of these are addressed in the following section.

5.3. Some Thoughts to Improve Structural Design:

We strongly recommend that more adequate Intensity Measures, such as those proposed in this study, be employed for the analysis of structures subjected to near-fault ground motions rather than the conventional Intensity Measure, $S_a(T_1)$. To predict ground motions hazard for near-fault locations, site-specific analyses should be performed rather than relying on the hazard maps provided by the USGS. The use of PSHA modified for forward-directivity will provide deeper insight into the expected ground motion hazard. Furthermore, performance based analysis can be conducted using the methodology presented in this work in order to better account for the near-fault hazard.

In a force-based design procedure, forces are computed based on the elastic response of a single degree of freedom and reduced by a response modification coefficient (R factor) to account for nonlinear behavior of the structure. The philosophy of the response modification coefficient is based on the well known "equal-displacement" approximation, which has dubious validity (Priestley et al. 2007). Since near-fault structures are subjected to large displacement, inaccuracy of the "equal-displacement" approximation becomes a significant concern. Therefore, the R factor should be selected with more care for structures subjected to near-fault ground motions. This may require modification of the R factor provided by building codes. A preferred solution would be the use of displacement-based design. Displacement-based design procedures yield more reliable results compared to those of the force-based design procedures.

Furthermore, a seismic evaluation of structural performance is necessary. Seismic evaluation of structures is often done through static nonlinear analysis, known as pushover analysis. However, pushover analysis may fall short in evaluating the performance of multi-mode dominated structures, which is true for some near-fault cases. In pushover analyses, the structure is subjected to a certain distribution of lateral forces over its height, which increases monotonically until a target displacement is reached. The main assumption in pushover analysis is that the response is controlled by the fundamental mode and that the mode shape remains unchanged after the structure yields. However, this assumption is inconsistent with dynamics of structures. Therefore, adaptive pushover analyses can improve the seismic evaluation of multi-mode dominated structures.

Since the fundamental period of structures becomes a more sensitive issue for near-fault ground motions, its calculation should not be base on the approximate equation $T=C(h)^n$ introduced by building codes but based on exact methods.

5.4. Recommendations for further study

While the work in this thesis has increased the understanding of the treatment of forward directivity ground motions for structural analysis, it also identified a number of issues that warrant further investigation:

- Some of the components of the model presented herein have not yet been fully developed. For example, the computation of near-fault hazard for non-pulse-type motions should be performed using a complete ground motion database that excludes non-pulse near-source motions. Such a task is beyond the scope of this

research, yet it can be achieved thanks to the recent compilation of the NGA database. Other components that need to be improved are the predictive models for PGV and pulse period. These models, understandably, are poorly constrained by existing data. Additional constraints from modeling or possibly with data collected from future earthquakes are necessary to generate more robust models.

- The model presented herein should be applied to actual structures located near actual faults.
- The analyses presented herein assumed that the structure has a weak axis aligned with the fault normal direction. While theory predicts that forward-directivity pulses are aligned with the fault normal direction, actual recordings have indicated that the orientation of these pulses is a random variable. This variability should be considered when making estimates of hazard to structures.

5.5. Figures

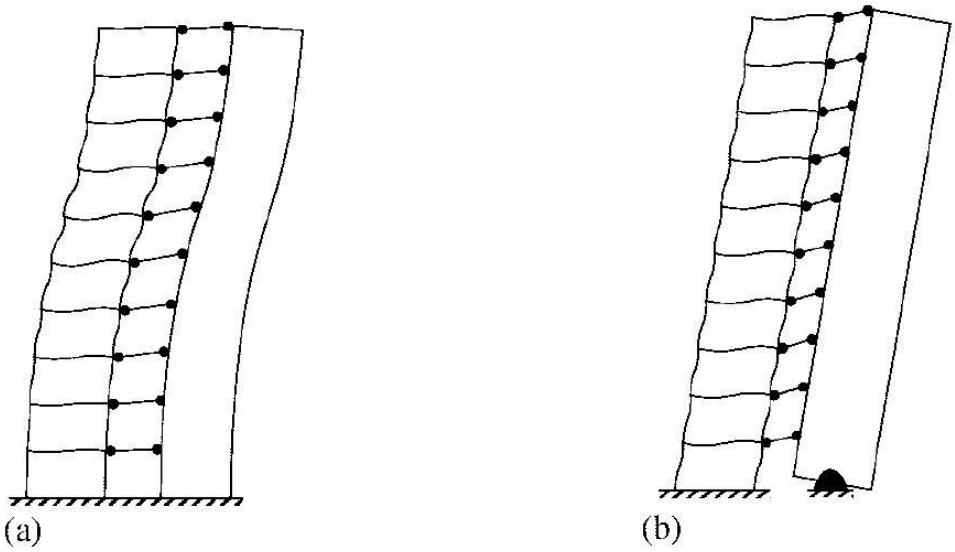

Figure 5-1: Typical elastic deflected shape of dual systems: (a) fixed wall; and (b) hinged wall (Krawinkler et al. 2003b)

6. APPENDIX A

Incremental Dynamic Analysis (IDA) is an emerging analysis method that offers thorough seismic demand and capacity prediction capability by using a series of nonlinear dynamic analyses under a multiply scaled suite of ground motion records. Realization of its opportunities requires several innovations, such as choosing suitable ground motion Intensity Measures (IMs) and representative Damage Measures (DMs). In addition, proper interpolation and summarization techniques for multiple records need to be employed, providing the means for estimating the probability distribution of the structural demand given the seismic intensity. Limit-states, such as the dynamic global system instability, can be naturally defined in the context of IDA, thus allowing annual rates of exceedance to be calculated. Finally, the data gathered through IDA can provide intuition for the behavior of structures and shed new light on the connection between the Static Pushover (SPO) and the dynamic response (Vamvatsikos and Cornell 2004).

7. REFERENCES

Abrahamson, N., and Silva, W. (2007). "NGA Ground Motion Relations for the Geometric Mean Horizontal Component of Peak and Spectral Ground Motion Parameters." Pacific Earthquake Engineering Research Center College of Engineering, University of California, Berkeley.

Abrahamson, N. A. (1993). "Non-stationary spectral matching program RSPMATCH." User Manual.

Abrahamson, N. A. (1998a). "Probabilistic Seismic Hazard Assessment." *CE 524 Notes*, Probabilistic Seismic Hazard Assessment.

Abrahamson, N. A. (1998b). "Seismological aspects of near-fault ground motions."

Abrahamson, N. A. "Effects of rupture directivity on probabilistic seismic hazard analysis." *Sixth International Conference on Seismic Zonation*, Palm Springs.

Abrahamson, N. A., and Silva, W. J. (1997). "Empirical response spectral attenuation relations for shallow crustal earthquakes." *Seismological Research Letters*, 68(1), 94-127.

Agrawal, A. K., and He, W.-L. "A closed-form approximation of near-fault ground motion pulses for flexible structures." *15th ASCE Engineering Mechanics Conference*, Columbia University, New York, NY.

Alavi, B., and Krawinkler, H. "Consideration of near-fault ground motion effects in seismic design." *Proceedings, 12th World Conference on Earthquake Engineering*, New Zealand, 1-8.

Alavi, B., and Krawinkler, H. (2001). "Effects of near-fault ground motions on frame structures." Dept. of Civil Engrg., Stanford University, Stanford, CA.

Alavi, B., and Krawinkler, H. (2004a). "Behavior of moment-resisting frame structures subjected to near-fault ground motions." *Earthquake Engineering and Sturctural Dynamics*, 33, 687-706.

Alavi, B., and Krawinkler, H. (2004b). "Strengthening of moment-resisting frame structures against near-fault ground motion effects." *Earthquake Engineering Structural Dynamics*, 33, 707-722.

Anderson, J. C., and Bertero, V. V. (1987). "Uncertainties in establishing design earthquakes." *ASCE Journal of Structural Engineering*, 113(8), 1709-1724.

ATC-3-06. (1978). "Tentative Provisions for the Development of Seismic Regulations for Buildings." Applied Technology Council.

ATC-40. (1996). "Seismic Evaluation and Retrofit of Concrete Buildings." Applied Technology Council, Redwood City, California.

ATC-58. (2004). "Engineering Demand Parameters for Structural framing System." Project Task Report, Applied Technology Council, Redwood City, CA.

Baker, J. (2007a). "Quantitative classification of near-fault ground motions using wavelet analysis." *Bulletin of the Seismological Society of America*, 97(5), 1486-1501.

Baker, J., and Cornell, A. (2008). "Vector-valued intensity measures for pulse-like near-fault ground motions." *Engineering Structures 2008*, 30, 1048-57.

Baker, J. W. (2007b). "Probabilistic Structural Response Assessment Using Vector-Valued Intensity Measures." *Earthquake Engineering Structural Dynamic*(36), 1861–1883.

Baker, J. W., and Cornell, A. (2005). "Vector-Valued Ground Motion Intensity Measure Consisting of Spectral Acceleration and Epsilon." *Earthquake Engineering and Structural Dynamics*, 34(10), 1193-1217.

Bazzurro, P. (1998). "Probabilistic Seismic Demand Analysis," Ph.D. thesis, Stanford University, California.

Bazzurro, P., and Cornell, C. (1994a). "Seismic Hazard Analysis of Nonlinear Structures I: Methodology." *Journal of Structural Engineering, ASCE*, 120, 3320–3344.

Bazzurro, P., and Cornell, C. (1994b). "Seismic hazard analysis of nonlinear structures II: Applications." *Journal of Structural Engineering, ASCE*, 120, 3345-3365.

Bertero, V. V., Mahin, S. A., and Herrera, R. A. (1978). "Aseismic design implications of near-fault San Fernando earthquake records." *Earthquake Engineering & Structural Dynamics*, 6, 31-42.

Bouchon, M., and Vallee, M. (2003). "Observation of long supershear rupture during the magnitude 8.1 Kunlunshan earthquake." *Science*, 301(5634), 824-826.

Bray, J. D., and Rodriguez-Marek, A. (2004). "Characterization of forward-directivity ground motions in the near-fault region." *Soil Dynamics and Earthquake Engineering*, 24, 815-828.

Chopra, A. (1995). *Dynamics of structures*, Prentice Hall, Englewood Cliffs, NJ.

Chopra, A. K., and Chintanapakdee, C. (2001). "Comparing response of SDF systems to near-fault and far-fault earthquake motions in teh context of spectral regions." *Earthquake engineering and Structural Dynamics*, 30, 1769-1789.

Cornell, C. A., Jalayer, F., Hamburger, R. O., and Foutch, D. A. (2002). "Probabilistic basis for 2000 SAC Federal Emergency Management Agency steel moment frame guidelines." *Journal of Structural Engineering*, 128(4), 526-533.

Dimitrios, V., and Cornell, A. "The incremental dynamic analysis and its application to performance -based earthquake Engineering." *12th European Conference on Earthquake Engineering*.

FEMA-274, and Agency, t. F. E. M. (1997). "NEHRP Guidelines for the Seismic Rehabilitation of Buildings." the Applied Technology Council for the Building Seismic Safety Council, Federal Emergency.

Gabor, D. (1946). "Theory of communication." *IEEE*, 93, 429-41.

Hall, J. F. (1998). "Seismic response of steel frame buildings to near-source ground motions." *Earthquake Engineering and Structural Dynamics*, 27, 1445-1464.

Hall, J. F., Heaton, T. H., Halling, M. W., and Wald, D. J. (1995). "Near-source ground motion and its effects on flexible buildings." *Earthquake Spectra*, 11(4), 569-605.

Hamburger, R. O. (2003). "A Vision for Performance Based Earthquake Engineering, Unpublished report for the ATC-58 project." Applied Technology Council, Redwood City, California.

IBC. (2006). "International Code Council (ICC). International Building Code." Country Club Hills, IL.

Imbsen & Associates Inc. "Xtract version 3.0.5, http://www.imbsen.com/."

Iwan, W., Huang, C.-T., and Guyader, A. C. (1998). "Evaluation of the effects of near-source ground motions." *Report Developed for the PG&E/PEER Program, CalTech, Pasadena, California*.

Kalkan, E., and Kunnath, S. (2006). "Evaluation of two ground motion scaling methods to estimate meanstructural demands." *Centennial Meeting of the Seismological Society of America*.

Kennedy, R., Short, S., Merz, K., Tokarz, F., and Idriss, I. (1984). "Powers M, Sadigh K. Engineering Characterization of Ground Motion-Task I: Effects of Characteristics of Free-Field Motion on Structural Response." *NUREG=CR-3805, U.S. Regulatory Commission, Washington, D.C.*

Kramer, S. L. (1996). *Geotechnical Earthquake Engineering*, Prentice Hall, Upper Saddle River, New Jersey.

Krawinkler, H., and Alavi, B. "Development of Improved Design Procedures for Near Fault Ground Motions." *SMIP 98: Seminar on Utilization of Strong Motion Data*, Oakland, CA, 21- 41.

Krawinkler, H., Medina, R., and Alavi, B. (2003a). "Seismic drift and ductility demands and their dependence on ground motions." *Engineering Structures*, 25, 637-653.

Krawinkler, H., Medina, R., and Alavi, B. (2003b). "Seismic Drift and Ductility Demands and their Dependence on Ground Motions." *Engineering Structures*, 25, 637–653.

Lehmann, E., and D'Abrera, H. (1998). " Non parametrics: Statistical Methods Based on Ranks (Rev. 1st edn). Prentice-Hall:Upper Saddle River, NJ." (463).

Luco, N. (2002). "Probabilistic seismic demand analysis, SMRF connection fractures, and near-source effects," Ph.D. Dissertation, Dept. of Civil Engrg., Stanford University, Stanford, CA.

Luco, N., and Cornell, A. (2001). "Structure-Specific Scalar Intensity Measures for Near-Source and Ordinary Earthquake Ground Motion." *Earthquake Spectra*, 1-29.

Luco, N., and Cornell, C. A. (2007). "Structure-Specific Scalar Intensity Measures for Near-Source and Ordinary Earthquake Ground Motions." *Earthquake Spectra,Earthquake Engineering Research Institute*, 23(2), 357-392.

MacRae, G. A., and Roeder, C. W. (1999). "Near-field ground motion effects on short structures." Dept. of Civil Engineering, University of Washington, Seattle, WA.

Makris, N. (1997). "Rigidity-plasticity-viscocity: can electrorheological dampers protect base-isolated structures from near-source ground motions." *Earthquake Engineering Structural Dynamics*, 26, 571–91.

Makris, N., and Chang, S. (1998). "Effect of Damping Mechanisms on the Response of Seismically Isolated Structures." Pacific Earthquake Engineering Research Center, University of California, Berkeley.

Makris, N., and Chang, S. (2000). "Effect of viscous, viscoplastic and friction damping on the response of seismic isolated structures." *Earthquake Engineering Structural Dynamics*, 29, 85–107.

Malhotra, P. K. (1999). "Response of Buildings to Near-Field Pulse-Like Ground Motions." *Earthquake Engineering and Structural Dynamics*, 28, 1309-1326.

Martinez-Rueda, J. (1998). "Scaling procedure for natural accelerograms based on a system of spectrum intensity scales." *Earthquake Spectra*, 14, 135 –152.

Mavroeidis, G. P., and Papageorgiou, A. S. (2003). "A mathematical representation of near-fault ground motions." *Bulletin of the Seismological Society of America*, 93(3), 1099-1131.

McGuire, R. K. (2004). *Seismic hazard and risk Analysis*, Earthquake Engineering Research Institute, Boulder, Colorado.

Moehle, J. P. " A framework for performance-based earthquake engineering." *Proceedings, Tenth U.S.-Japan Workshop on Improvement of Building Seismic Design and Construction Practices*, Redwood City, California.

Mylonakis, G., and Reinhorn, A. (2001). "Yielding oscillator under triangular ground acceleration pulse." *Journal of Earthquake Engineering*, 5, 225-51.

Nassar, A., and Krawinkler, H. (1991). "Seismic Demands for SDOF and MDOF Systems." Dept. of Civil Engineering, Stanford University, Stanford, CA.

PEER. (1999). "Pacific Earthquake Engineering Research Center, strong motion database. http://peer.berkeley.edu/smcat/search.html."

Priestley, M. J. N., Calvi, G. M., and Kowalsky, M. J. (2007). *Displacement-Based Seismic Design of Structures*, IUSS Press.

Sasani, M., and Bertero, V. V. "Importance of severe pulse-type ground motions in performance-based engineering: historical and critical review." *Proceedings, 12th World Conference on Earthquake Engineering*, New Zealand, 1-7.

SEAOC. (Vision 2000). "performance based seismic engineering for buildings." Structural Engineers Association of California, Sacramento, CA, 1995.

Shome, N., and Cornell, C. "Normalization and scaling accelerograms for nonlinear structural analysis." *Sixth U.S. National Conference on Earthquake Engineering*, Seattle, WA.

Somerville, P. G. "Development of an Improved Representation of Near-Fault Ground Motions." *SMIP 98: Seminar on Utilization of Strong Motion Data*, Oakland, CA, 1-20.

Somerville, P. G. (2003). "Magnitude scaling of the near fault rupture directivity pulse." *Physics of the Earth and Planetary Interiors*, 137, 201-212.

Somerville, P. G., Collins, N., Graves, R., and Pitarka, A. "Development of an engineering model of the amplitude and duration effects of basin generated surface waves." *CSMIP Seminar*, Oakland, CA, 127-145.

Somerville, P. G., Smith, N. F., Graves, R., and Abrahamson, N. A. (1997). "Modification of Empirical Strong Ground Motion Attenuation Relations to Include the Amplitude and Duration Effects of Rupture Directivity." *Seismological Research Letters*, 68(1), 199-222.

Spudich, P., and Chiou, B. (2008). "Directivity in NGA earthquake ground motions: analysis using isochrone theory." *Earthquake Spectra*, 24(1), 279-98.

The MathWorks Inc. "MATLAB Version 7.1.0.246, Revision 14, Service Pack 3, ©1984-2005. http://www.mathworks.com/."

Tothong, P., Cornell, C., and Baker, J. (2007). "Explicit Directivity-Pulse Inclusion in Probabilistic Seismic Hazard Analysis." *Earthquake Spectra, Earthquake Engineering Research Institute*, 23(4), 867–891.

Travasarou, T., Chacko, J., and Vahdani, S. "Observations from Probabilistic Treatment of Rupture Directivity Effects." *8th NCEE, 2006*.

USGS. (2007). "Preliminary Documentation for the 2007 Update of the United States National Seismic Hazard Maps,." *The National Seismic Hazard Mapping Project*.

Vamvatsikos, D., and Cornell, C. A. (2004). "Applied incremental dynamic analysis." *Earthquake Spectra*, 20, 523–553.

Zhang, Y., and Iwan, W. (2002). "Active interaction control of tall buildings subjected to near-field ground motions." *Journal of Structural Engineering*, 128, 69-79.